Effects of Multipath and Oversampling on Navigation Using Orthogonal Frequency Division Multiplexed Signals of Opportunity

THESIS

Christopher M. Schexnayder, B.S.E.E.

AFIT/GE/ENG/08-25

DEPARTMENT OF THE AIR FORCE
AIR UNIVERSITY

AIR FORCE INSTITUTE OF TECHNOLOGY

Wright-Patterson Air Force Base, Ohio

The views expressed in this thesis are those of the author and do not reflect the official policy or position of the United States Air Force, Department of Defense, or the United States Government.

AFIT/GE/ENG/08-25

Effects of Multipath and Oversampling on Navigation Using Orthogonal Frequency Division Multiplexed Signals of Opportunity

THESIS

Presented to the Faculty

Department of Electrical and Computer Engineering

Graduate School of Engineering and Management

Air Force Institute of Technology

Air University

Air Education and Training Command

In Partial Fulfillment of the Requirements for the

Degree of Master of Science in Electrical Engineering

Christopher M. Schexnayder

B.S.E.E.

March 2008

AFIT/GE/ENG/08-25

Effects of Multipath and Oversampling on Navigation Using Orthogonal Frequency Division Multiplexed Signals of Opportunity

Christopher M. Schexnayder
B.S.E.E.

Approved:

/signed/	29 Feb 2008
Dr. John F. Raquet (Chairman)	date
/signed/	29 Feb 2008
Dr. Richard K. Martin (Member)	date
/signed/	29 Feb 2008
Dr. Michael A. Temple (Member)	date

Abstract

The Global Positioning System (GPS) has become the primary system for navigation and precise positioning. GPS has limitations, though, and is not suitable in environments where a line-of-site (LOS) path to multiple satellites is not available. Reliable alternatives need to be developed to provide GPS-like positioning when GPS is unavailable. One such alternative is to use signals of opportunity (SoOP). This concept refers to navigation using signals which inherently exist in the environment and were developed for non-navigation applications.

This research focuses on exploiting the Orthogonal Frequency Division Multiplexed (OFDM) signal for the purpose of navigation. An algorithm was developed to simulate a transmitter, receiver, channel noise, and multipath propagation. A transmitter and reference receiver, both at known locations, and a mobile receiver at an unknown location were used to conduct simulations with a transmitted OFDM signal in a Rayleigh-distributed multipath environment.

The OFDM signal structure was exploited by using its cyclic prefix in a correlation process to find the first symbol boundary in each received signal. Each receiver calculates statistical features about each symbol in the received signal. These two sets of data are then correlated in order find the difference in symbol arrival times. The simulations were run for varying levels of oversampling in an effort to gain more accurate results by decreasing the sample period. Results show that oversampling the signal only slightly reduces errors in the symbol boundary correlation process, while multipath has a significant impact on correlation performance. It was also found that increasing the window size significantly improved feature correlator performance and yielded promising results even in the presence of high multipath environments.

Acknowledgements

First and foremost, I would like to thank everyone who enabled me to make the transition back to academia and to complete this thesis. It was a humbling experience and I couldn't have done it without your support.

I would especially like to thank my thesis advisor, Dr. Raquet. Your guidance throughout this process has helped me stay on course. I appreciate everything that you have done for me. I also wish to thank my committee members, Dr. Temple and Dr. Martin. Your guidance and expertise were crucial to the completion of this research. You all have really gone above and beyond to make this transition as painless as possible.

I would also like to express my gratitude to my fellow students. Your friendship, guidance, and countless hours of study group will not be forgotten. Remember, sometimes unforseen events can happen which will alter the course of your life. You must be able to adapt and press onward. Thank you for your friendship.

Next, I thank my beautiful wife. Without you, I wouldn't have been able to complete this task. I am truly grateful to have you in my life.

Finally, I thank the Air Force for affording me this great opportunity to enhance my education.

Christopher M. Schexnayder

Table of Contents

Page

Abstract iv

Acknowledgements v

List of Figures viii

List of Tables xii

List of Abbreviations xiii

I. Introduction 1
1.1 Problem Statement 2
1.2 Assumptions 3
1.3 Related Research 4
1.3.1 Radionavigation Systems 4
1.3.2 Navigation Using SoOP Other Than OFDM . . 6
1.3.3 Navigation Systems Using OFDM Signals . . . 10
1.4 Thesis Overview 15

II. Background 16
2.1 OFDM System Structure 16
2.1.1 Coding 18
2.1.2 Interleaving 19
2.1.3 Constellation Mapping 20
2.1.4 Pilot Tones 20
2.1.5 OFDM Modulation Using IFFT 23
2.1.6 Cyclic Prefix 24
2.2 Multipath 25
2.3 TDOA Positioning 26
2.3.1 TDOA Calculation 27
2.4 Summary 31

III. Simulation Development 32
3.1 OFDM Model 32
3.1.1 OFDM Signal Generator 33
3.2 Oversampling Algorithm 33
3.3 Multipath Model 36
3.3.1 OFDM Receiver 38

3.3.2 Symbol Features 40
3.3.3 Symbol Feature Correlator 44
3.4 TDOA Calculations 45
3.5 Summary 46

IV. Simulation Results and Analysis 47
4.1 Simulation Specifications 47
4.1.1 Signal Parameters 47
4.1.2 Oversampling Parameters 48
4.1.3 Multipath Parameters 48
4.2 Types of Errors 49
4.2.1 Measurement Noise 49
4.2.2 Non-LOS Error 50
4.2.3 Ambiguity Resolution Failure 50
4.2.4 Receiver Sampling Algorithm Error 51
4.3 Baseline Setup: One Receiver 51
4.3.1 Transmitter - Mobile Receiver 52
4.3.2 Transmitter - Reference Receiver 63
4.4 Test Setup: Two Receivers 64
4.4.1 Raw Data Analysis 64
4.4.2 Error Analysis 68
4.4.3 Key Observations 71
4.5 Mean vs. Mini-mean 75
4.6 Summary 75

V. Conclusions and Recommendations 80
5.1 Conclusion 80
5.1.1 Symbol Boundary Correlator 80
5.1.2 Feature Correlator 81
5.2 Future Work 83

VI. Complete Simulated Results 85

Bibliography 107

List of Figures

Figure		Page
1.1.	The HIPERLAN/2 Network Structure.	12
1.2.	MAC frame structure for HIPERLAN/2.	13
1.3.	Access Point-based TOA geolocation method.	14
2.1.	FDMA vs. OFDM (Frequency Domain)	17
2.2.	Block Diagram of OFDM System	18
2.3.	Interleaving Process	21
2.4.	QAM/PSK Constellations	22
2.5.	DVB Pilot Tone Constellation.	23
2.6.	Pilot Tone Constellation Used for Research.	23
2.7.	Cyclic Prefix Extension.	25
2.8.	Multipath.	26
2.9.	System Model.	27
2.10.	Time Difference of Arrival Technique.	28
3.1.	3× Signal Oversampling: Upsampled Signal and Sinc Function	35
3.2.	3× Signal Oversampling: Oversampled Signal	36
3.3.	Delay Profile.	37
3.4.	Symbol Boundary Correlator Results	41
4.1.	Baseline $P_{e_{symbol}}$ Graph for $L = 1$ at Low SNRs.	53
4.2.	Baseline $P_{e_{symbol}}$ Graph for $L = 1$ at High SNRs.	54
4.3.	$P_{e_{symbol}}$ Graph for $L = 1$ With No Error Threshold for $SNR = 10$ dB.	55
4.4.	Baseline $P_{e_{symbol}}$ Graphs for $L = 3, 9$ for $SNR =$ -20 dB.	57
4.5.	Histograms Sample Errors for $L = 1$ and $SNR = 10$ dB.	58
4.6.	Graph of Standard Deviation of Errors (meters) for $L = 1$.	59
4.7.	Graph of Standard Deviation of Errors (meters) for $L = 3$.	60
4.8.	Graph of Standard Deviation of Errors (meters) for $L = 9$.	60

Figure Page

4.9. Graph of Mean of Errors (meters) for $L = 1$. 61

4.10. Graph of Mean of Errors (meters) for $L = 3$. 62

4.11. Graph of Mean of Errors (meters) for $L = 9$. 63

4.12. $P_{e_{feature}}$ of All Features for SNR = 10 dB, $L = 1$, and $K = 10$ symbols. 65

4.13. $P_{e_{feature}}$ of All Features for SNR = 10 dB and $L = 1$ Separated by Delay Size. 66

4.14. $P_{e_{feature}}$ Graphs for $L = 3, 9$ for Feature Correlator. 67

4.15. Test Setup: $P_{e_{feature}}$ Graph for $L = 1$. 69

4.16. Feature $P_{e_{feature}}$ For Correct Symbol Boundary Correlation. . . 70

4.17. Feature $P_{e_{feature}}$ For Correct Symbol Boundary Correlation With Oversampling. 72

4.18. Feature $P_{e_{feature}}$ For Correct Symbol Boundary Correlation With $K = 100$ Symbols. 73

4.19. Feature $P_{e_{feature}}$ For Correct Symbol Boundary Correlation With Oversampling and $K = 100$ Symbols. 74

4.20. Comparison of $P_{e_{feature}}$ for Mean vs. Mini-mean with no multipath and $K = 10, 100$ Symbols. 76

4.21. Test Setup: $P_{e_{feature}}$ Graph for $L = 1$ and $K = 10$. 77

4.22. Test Setup: $P_{e_{feature}}$ Graph for $L = 1$ and $K = 100$. 78

F.1. Baseline Setup: $P_{e_{symbol}}$ Graph for $L = 1$ With $SNR = -20$ dB. 85

F.2. Baseline Setup: $P_{e_{symbol}}$ Graph for $L = 1$ With $SNR = -10$ dB. 86

F.3. Baseline Setup: $P_{e_{symbol}}$ Graph for $L = 1$ With $SNR = 0$ dB. . 86

F.4. Baseline Setup: $P_{e_{symbol}}$ Graph for $L = 1$ With $SNR = 10$ dB. . 87

F.5. Baseline Setup: $P_{e_{symbol}}$ Graph for $L = 3$ With $SNR = -20$ dB. 87

F.6. Baseline Setup: $P_{e_{symbol}}$ Graph for $L = 3$ With $SNR = -10$ dB. 88

F.7. Baseline Setup: $P_{e_{symbol}}$ Graph for $L = 3$ With $SNR = 0$ dB. . 88

F.8. Baseline Setup: $P_{e_{symbol}}$ Graph for $L = 3$ With $SNR = 10$ dB. . 89

F.9. Baseline Setup: $P_{e_{symbol}}$ Graph for $L = 9$ With $SNR = -20$ dB. 89

Figure Page

F.10. Baseline Setup: $P_{e_{symbol}}$ Graph for $L = 9$ With $SNR = -10$ dB. 90

F.11. Baseline Setup: $P_{e_{symbol}}$ Graph for $L = 9$ With $SNR = 0$ dB. . 90

F.12. Baseline Setup: $P_{e_{symbol}}$ Graph for $L = 9$ With $SNR = 10$ dB. . 91

F.13. Baseline Setup: $P_{e_{symbol}}$ Graph for $L = 1$ With $SNR = 40$ dB. . 91

F.14. Baseline Setup: $P_{e_{symbol}}$ Graph for $L = 1$ With No Error Threshold. 92

F.15. Test Setup: $P_{e_{feature}}$ Graph for $L = 1$ With $SNR = -20$ dB and $K = 10$ Symbols. 93

F.16. Test Setup: $P_{e_{feature}}$ Graph for $L = 1$ With $SNR = -10$ dB and $K = 10$ Symbols. 93

F.17. Test Setup: $P_{e_{feature}}$ Graph for $L = 1$ With $SNR = 0$ dB and $K = 10$ Symbols. 94

F.18. Test Setup: $P_{e_{feature}}$ Graph for $L = 1$ With $SNR = 10$ dB and $K = 10$ Symbols. 94

F.19. Test Setup: $P_{e_{feature}}$ Graph for $L = 1$ With $SNR = 20$ dB and $K = 10$ Symbols. 95

F.20. Test Setup: $P_{e_{feature}}$ Graph for $L = 1$ With $SNR = 50$ dB and $K = 10$ Symbols. 95

F.21. Test Setup: $P_{e_{feature}}$ Graph for $L = 3$ With $SNR = -20$ dB and $K = 10$ Symbols. 96

F.22. Test Setup: $P_{e_{feature}}$ Graph for $L = 3$ With $SNR = -10$ dB and $K = 10$ Symbols. 96

F.23. Test Setup: $P_{e_{feature}}$ Graph for $L = 3$ With $SNR = 0$ dB and $K = 10$ Symbols. 97

F.24. Test Setup: $P_{e_{feature}}$ Graph for $L = 3$ With $SNR = 10$ dB and $K = 10$ Symbols. 97

F.25. Test Setup: $P_{e_{feature}}$ Graph for $L = 9$ With $SNR = -20$ dB and $K = 10$ Symbols. 98

F.26. Test Setup: $P_{e_{feature}}$ Graph for $L = 9$ With $SNR = -10$ dB and $K = 10$ Symbols. 98

F.27. Test Setup: $P_{e_{feature}}$ Graph for $L = 9$ With $SNR = 0$ dB and $K = 10$ Symbols. 99

F.28. Test Setup: $P_{e_{feature}}$ Graph for $L = 9$ With $SNR = 10$ dB and $K = 10$ Symbols. 99

F.29. Test Setup: $P_{e_{feature}}$ Graph for $L = 1$ With $SNR = -20$ dB and $K = 100$ Symbols. 100

F.30. Test Setup: $P_{e_{feature}}$ Graph for $L = 1$ With $SNR = -10$ dB and $K = 100$ Symbols. 100

F.31. Test Setup: $P_{e_{feature}}$ Graph for $L = 1$ With $SNR = 0$ dB and $K = 100$ Symbols. 101

F.32. Test Setup: $P_{e_{feature}}$ Graph for $L = 1$ With $SNR = 10$ dB and $K = 100$ Symbols. 101

F.33. Test Setup: $P_{e_{feature}}$ Graph for $L = 3$ With $SNR = -20$ dB and $K = 100$ Symbols. 102

F.34. Test Setup: $P_{e_{feature}}$ Graph for $L = 3$ With $SNR = -10$ dB and $K = 100$ Symbols. 102

F.35. Test Setup: $P_{e_{feature}}$ Graph for $L = 3$ With $SNR = 0$ dB and $K = 100$ Symbols. 103

F.36. Test Setup: $P_{e_{feature}}$ Graph for $L = 3$ With $SNR = 10$ dB and $K = 100$ Symbols. 103

F.37. Test Setup: $P_{e_{feature}}$ Graph for $L = 9$ With $SNR = -20$ dB and $K = 100$ Symbols. 104

F.38. Test Setup: $P_{e_{feature}}$ Graph for $L = 9$ With $SNR = -10$ dB and $K = 100$ Symbols. 104

F.39. Test Setup: $P_{e_{feature}}$ Graph for $L = 9$ With $SNR = 0$ dB and $K = 100$ Symbols. 105

F.40. Test Setup: $P_{e_{feature}}$ Graph for $L = 9$ With $SNR = 10$ dB and $K = 100$ Symbols. 105

F.41. Comparison of $P_{e_{feature}}$ for Mean vs. Mini-mean with no multi-path and $K = 10, 100$ Symbols. 106

List of Tables

Table		Page
2.1.	IEEE Std 802.11a Rate Dependent Convolutional Rates.	19
4.1.	OFDM Simulation Input Parameters.	47

List of Abbreviations

Abbreviation		Page
GPS	Global Positioning System	1
NAVWAR	Navigation Warfare	1
LOS	Line-of-Sight	1
SoOP	Signals of Opportunity	2
EM	Electromagnetic	2
OFDM	Orthogonal Frequency Division Multiplexed	2
AWGN	Additive White Gaussian Noise	2
TDOA	Time Difference of Arrival	2
WLAN	Wireless Local Area Network	2
DAB	Digital Audio Broadcast	2
DVB-T	Digital Video Broadcast-Terrestrial	2
LORAN	Long Range Navigation	4
AMES	Air Ministry Experimental Station	4
LF	Low Frequency	5
RMS	Root-Mean-Squared	5
VLF	Very Low Frequency	5
PRN	Pseudo-Random Noise	6
DGPS	Differential GPS	6
NTSC	National Television Systems Committee	7
ATSC	Advanced Television Systems Committee	7
VHF	Very High Frequency	7
UHF	Ultra High Frequency	7
COFDM	Coded OFDM	10
HIPERLAN	HIgh PErformance Radio LAN	11
MAC	Media Access Control	11

Abbreviation		Page
TDMA/TDD	Time Division Multiple Access/Time Division Duplex	12
SNR	Signal-to-Noise Ratio	14
PAPR	Peak-to-Average Power Ratio	15
FDM	Frequency Division Multiplexing	16
BER	Bit-Error Rate	19
FEC	Forward Error Correction	19
QAM	Quadrature Amplitude Modulation	20
PSK	Phase-Shift Keying	20
QPSK	Quadrature Phase-Shift Keying	22
BPSK	Binary Phase-Shift Keying	22
FFTs	Fast Fourier Transforms	23
IFFTs	Inverse Fast Fourier Transforms	23
ISI	Inter-Symbol Interference	24

Effects of Multipath and Oversampling on Navigation Using Orthogonal Frequency Division Multiplexed Signals of Opportunity

I. Introduction

The Global Positioning System (GPS) has become the primary source for precision navigation, positioning and timing applications for military and civilian users. Its popularity has skyrocketed because it is highly accurate and easy to use. GPS requires no monthly subscription and the only cost to users is the purchase of a GPS receiver, of which there are many affordable models. It is used for applications ranging from dropping precise munitions on enemy targets to guiding automated farming equipment to land surveying. Even though civilian users far outnumber military users, GPS is still a military system and must be protected. The military's role is to ensure that the signal is readily available for military use, thus, the three tenets of Navigation Warfare (NAVWAR) must be adhered to [1]:

1. Protection of military service in a theater of operation.
2. Prevention of adversarial exploitation of GPS services.
3. Preservation of civil service outside a theater of operations.

Currently, the signal structure is designed such that the civil signal in a theater of operation cannot be jammed to prevent enemy use without partially jamming the coded signal. This means that the military cannot prevent adversarial use of the system without degrading its own use. This dilemma has driven the modernization of GPS, resulting in plans to add a new carrier frequency with only a civil signal and to add civil and military-only signals (not to be confused with the encrypted signal used now) to the existing carriers [2]. Even with modernization plans, however, the capabilities are degraded in areas where a line-of-sight (LOS) path to multiple satellites is not present, such as in a jungle, indoors, or in an outdoor urban environment.

This degraded service, along with the threat of enemy jamming or exploitation, brings about the need to develop alternative methods of navigation.

One potential solution to this problem is navigation using signals of opportunity (SoOP). These signals are electromagnetic (EM) signals which were designed to serve another purpose, but can be exploited for navigation purposes. Examples of SoOP include broadcast television signals, AM and FM radio, and cellular communications signals. These systems have a readily available infrastructure. The challenge is to be able to collect the signal, manipulate it, and take advantage of its properties in order to determine a position estimate.

1.1 Problem Statement

The focus of this research is to evaluate the impact of multipath and oversampling on an Orthogonal Frequency Division Multiplexed (OFDM) signal in an effort to determine its potential as a navigation source. This research expands upon the proof of concept conducted by Jamie Velotta [3] which exploits the OFDM signal by correlating symbol statistics which characterize each symbol instead of correlating the entire symbol. While Velotta's research analyzed a signal on an Additive White Gaussian Noise (AWGN) channel, this research adds multipath effects as well as noise. Also, signal oversampling is performed in order to try and reduce error magnitude by reducing the sample period and, thus, the error resulting from an individual sample. Lastly, Time Difference of Arrival (TDOA) measurements can be calculated to determine the position accuracy of the system.

Applications which use this type of signal are wireless local area networks (WLAN), digital broadcast television, HD Radio, terrestrial repeaters for satellite radio, and the European standards for the digital audio broadcast (DAB) system and digital video broadcast-terrestrial (DVB-T) [4]. The signal investigated here is based on the IEEE 802.11a/g standards for WLANs. The navigation potential of this signal is tested by transmitting the simulated signal over a channel which adds varying levels of multipath effects and noise. The signal is transmitted to a reference

and a mobile receiver over unique multipath channels. The data from each receiver is correlated to determine the TDOA. The correlation calculation is implemented using Velotta's feature correlation method (described in Section 1.3.3) [3]. This method involves correlating statistical features of each symbol of the received data instead of the data itself, which reduces back channel bandwidth needed to complete the correlation between the receivers. Then, a method for calculating the TDOA measurements is given to determine a position estimate. In order to increase position accuracy, a method for oversampling is implemented and analyzed for effectiveness and various oversampling values are tested. This should decrease position errors since the sample period is shorter. Essentially, this research aims to determine whether or not this system is accurate enough to even be considered as a viable alternative to GPS. If it is not viable in its current state, some techniques will be identified which could improve the accuracy of the system.

1.2 Assumptions

During the course of this research, certain assumptions were made in order to limit the scope of the work being performed. First, the SoOP has an existing infrastructure with known transmitter locations. For some civilian infrastructures, such as the terrestrial repeaters for satellite radio or HD Radio broadcast towers, a simple web query can produce the locations of all operational transmitters [3]. The transmitter and the reference receiver simulated here are at known locations while the mobile receiver is at an unknown location. Also, the transmitter has a LOS path to both receivers.

The 802.11a/g signal of interest is known to use OFDM with a defined data length, cyclic prefix length, and data rate. Receivers are not limited by processing capability and can perform any operations necessary. Also, the sampling synchronization algorithm in the receivers work perfectly with no errors. This means that the receivers sample the incoming signal at a precise sample rate and the received samples are the attenuated original samples. This assumption is made to control the

number of error sources since the sampling algorithm inside the actual receiver is not being tested here. It is, however, recognized as an error source and addressed as such in Section 4.2.

Finally, a secure data link is established between the two receivers which allows for real-time, error-free communication in order to perform the correlation calculations [5]. This also limits the types of errors to multipath and channel noise. The reason for limiting errors is to determine the position accuracy with propagation effects only.

1.3 Related Research

This section presents some current and historical examples of radionavigation systems. General radionavigation approaches are detailed first and are followed by SoOP based navigation systems.

1.3.1 Radionavigation Systems. Radionavigation is the practice of navigation by exploiting radio waves [6]. The systems covered here are the GEE Navigation System, the Long Range Navigation (LORAN) system, the Omega Navigation System, and GPS.

1.3.1.1 GEE Navigation System. The GEE navigation system, or Air Ministry Experimental Station (AMES) Type 7000, was a British navigation system used by the Royal Air Force during World War II to improve aircraft navigation accuracy. It consisted of a master station and two slave stations which all transmitted precisely timed pulses. The master station sent a pulse which was followed by a double pulse two milliseconds later. The first slave station sent a single pulse one millisecond after the master station's single pulse. The second slave sent a single pulse one millisecond after the master station's double pulse and the cycle repeated every four milliseconds. The signals from the three stations were then received on board the aircraft and the slaves' signals would show up as blips on an oscilloscope type display.

The pulses from the master station controlled the display timing and the display equipment gave the difference in reception time of the pulses. This yielded the relative distance from the master and each slave. The aircraft carried a chart with hyperbolae plotted on it where each hyperbolic line represented a line of constant time difference for the master and one slave station. The navigator would find the intersection of the two hyperbolae representing the two slave stations to get a position estimate. This system was accurate to within 150 m at short distances and up to 1.6 km at longer ranges over Germany [7].

1.3.1.2 LORAN. LORAN is a terrestrial navigation system which was designed as a high-power hyperbolic system used primarily to guide ships. It was initially developed as a military system. The current version, LORAN-C, was a military system until 1974 when it was made available for civil marine use in U.S. coastal areas. It is comprised of a set of chains of transmitters. Each chain typically consists of a master and two to three slave transmitting stations separated by about 1000 km. Each station transmits at about 1 MW of peak power and operates in the Low Frequency (LF) band at 90 to 110 kHz. The stations of each chain are synchronized and transmit a series of pulses. The receiver measures the time difference of arrival of the pulses from the master and secondary stations. Each measurement defines a hyperbolic line of position for the user such that the intersection of two lines of position will define the 2-D user position. This system provides 2-D Root-Mean-Squared (RMS) positioning accuracy of around 250 m [6].

1.3.1.3 OMEGA Navigation System. OMEGA was the first global, continuously available radionavigation system. It was originally developed by the United States Navy, the United States Coast Guard, and six partner nations in the early 1960's. OMEGA consisted of eight ground-based transmitters, two of which were located in the United States. Each station operated in continuous-wave mode and transmitted synchronized time-shared signals at five frequencies in the Very Low Frequency (VLF) band at about 10 kW. Four of the frequencies are common to all

stations and one of the frequencies is unique to each station in order to identify that particular station. The signals propagated around the world in a "duct" between the ground and ionosphere. OMEGA was a hyperbolic navigation system also, but it measured the phase difference between the signals instead of the time difference of arrival. These measurements yield lines of position by which the user can determine a position estimate. This provided a 2-D RMS positioning accuracy of about 2-4 km [6].

1.3.1.4 GPS. The development of GPS began in 1973 by the United States Department of Defense, in conjunction with several defense contractors. Even though the first satellite was launched in 1978, the system wasn't declared operational until 1995. GPS consists of a constellation of 24-36 satellites, with 30 being used as of October 15, 2007. The satellites are placed in one of six different orbital planes, with each plane oriented at a 55° inclination angle. All satellites currently transmit on two carrier frequencies. The L1 carrier frequency operates at 1575.42 MHz and transmits the coarse-acquisition, unclassified code for civilian use and the encrypted precise code for military use. The L2 carrier frequency operates at 1227.6 MHz and transmits only the precise code. Each satellite transmits a unique pseudo-random noise (PRN) code by which it is identified. GPS receivers require a LOS to four satellite signals to accurately estimate a position in three dimensions and estimate the receiver clock bias. The receiver calculates a pseudorange from each received signal which measures the difference in time between signal transmission and reception and converts it to a distance. This distance is defined as the true range plus the distance error which is caused by the receiver clock error. The pseudorange equations are then linearized using least-squares estimation. The accuracy of this system is about 10 m for standard civilian receivers. Differential GPS (DGPS) receivers range from 1 mm to 2 m accuracy depending on how the measurements are calculated [2, 6].

1.3.2 Navigation Using SoOP Other Than OFDM. Recent research has been conducted on signals of opportunity to determine their potential as navigation sources. Some of the signals exploited include the National Television Systems Committee

(NTSC) broadcast television signal, the Advanced Television Systems Committee (ATSC) digital television signal, and the AM radio signal.

1.3.2.1 NTSC Broadcast Television Signal. Eggert collected NTSC broadcast signals in high and low multipath environments to determine position by using TDOA multilateration techniques [5]. He collected signals from eight local television stations using a reference receiver, which has a known position, and a mobile receiver. The signals were collected using different types of receivers. A simulated signal was also developed to validate his algorithm. He used three data reduction algorithms to estimate the TDOA measurements and used a locally fabricated antenna to mitigate the effects of multipath. His research revealed position errors ranging from 1 m to 200 m, with the most typical errors being around 10 m to 40 m. Eggert attributed much of the position errors to multipath and hardware configurations [5,8].

1.3.2.2 Rosum Corporation. The Rosum Corporation has developed a commercially available radionavigation system using the ATSC digital television signal. The synchronization signals which are part of the standard for digital television are exploited. Consequently, this system requires no changes to the television broadcast stations. The signal can be used for robust indoor positioning where the GPS fails. This is due to the fact that received television synchronization signals typically have a power advantage over GPS of more than 40 dB. The wide bandwidth of roughly 6 MHz, combined with the power advantage, greatly reduces the effects of multipath. Also, the system has a substantially superior geometry for determining lateral position to that which GPS can typically provide in high multipath environments. A wide range of Very High Frequency (VHF) and Ultra High Frequency (UHF) channels have been allocated to television stations and, consequently, there is redundancy built into the system to protect against deep fades on particular channels. In addition, unlike GPS, the synchronization signals are not affected by Doppler, ionospheric propagation delays, or data that is modulated onto the signals [9].

Rosum's system exploits the Digital TV infrastructure to achieve more reliable, accurate, and rapid positioning than can be achieved with existing technologies. Since the transmitters positions are known, their locations can be stored at the receiver or at a reference/monitor station. The receiver determines pseudoranges to a subset of the visible transmitters. Three transmitters are required to resolve the latitude, longitude and clock error. Monitor stations at known positions are used to independently monitor the TV station clock offsets. These offsets can be applied to the receiver position calculation at the station, which receives position data from the receiver, or at the receiver itself after it receives the offset data. The transmitters can also broadcast the clock offset information, in which case the receiver does not need an independent communication channel to the monitor station. The mean errors associated with this system range from 3.2 m in an open outdoor, low multipath environment to 23.3 m inside of an office building [9].

1.3.2.3 AM Radio Signal. Some studies of the AM signal are presented here. McEllroy created a simulation environment to model real-world AM signal characteristics [8]. The model simulated AM transmission sources, receivers, propagation effects, inter-receiver frequency errors, noise addition, and multipath effects. He also developed four methods for estimating the cross-correlation peak within a sampled portion of the cross-correlation data for use in TDOA measurement generation. The raw max peak estimate selects the maximum value of the correlated data within a window of one wavelength. The quad-sample linear fit peak estimate uses data which is resampled at four times the sample rate. Then, four points around each zero crossing around the peak in the same window of one wavelength are selected. A least-squares fit is used to calculate a line passing through each set of four points. The peak estimate is the intersection of the two lines. The raw sine wave fit estimate fits a sine wave to the correlated data and determines the peak based on the fitted sine wave. The high-sample max peak estimate uses data sampled at 100 times the normal sample rate to get better resolution when finding the maximum correlation

value. Results showed that the raw sine wave fit estimate worked best. Position estimates were determined by using TDOA-based multilateration techniques and show the potential for position accuracy of about 20 m [8].

Kim evaluated the correlation characteristics of AM and FM radio signals for the purpose of navigation [10]. He considered two correlation receiver methods with the goal of producing auto-correlation peaks between the received signals of the reference and mobile receivers. He used a reference signal with known characteristics to design a model. He conducted simulations for different combinations of correlation methods (fixed or varying), modulation types (AM or FM), and signal types (song or voice). These options yielded eight possible combinations of systems of which only two provided promising results for the purpose of navigation. The correlation methods used either a fixed or varying reference signal of a user-specified window size in order to determine peaks. The FM voice and FM song signals exhibit distinct auto-correlation peaks using the fixed reference correlation method. However, results for both FM signal types using the varying reference correlation method and all of the AM signals considered yielded relatively limited potential for navigation [10].

Hall developed a radiolocation system based on AM radio signals [8, 11]. His system used an analog front-end for pre-filtering and amplification and a software radio running on a personal computer. This system used carrier phase measurements to determine position estimates. The results showed the error in open areas outdoors was generally smaller than 15 m for relative distances up to 35 km [8, 11]. He determined that the accuracy of the system is affected by how well one can model signal propagation characteristics. In subsequent research, Hall attempted to model groundwave propagation effects, skywave interference, phase perturbation caused by nearby conductors, and phase variation caused by directional transmitter antennas in an effort to improve the accuracy of the positioning system. Results show that a far-field, directional antenna model reduces the errors caused by phase variation in directional antennas. Groundwave errors were reduced using a model developed from Numerical Electromagnetics Code (NEC-4) simulations. The effects due to nearby conductors

and skywave propagation on the received signal can be detected by observing the maximal ambiguity function value [12].

1.3.3 Navigation Systems Using OFDM Signals. There has been limited research into using OFDM signals as a navigation source. Some recent research, as detailed below, describes the use of OFDM as a source for both indoor and outdoor navigation. Since the focus of this research is navigation using OFDM signals also, the systems presented here will be described in more detail than the previous systems.

1.3.3.1 Precision Indoor/Multipath Geolocation System. Cyganski, Orr, and Michalson present a novel means for precise and multipath-compatible geolocation in an indoor environment [13]. Since this system was designed as a personnel locator for first responders, this research is only concerned about a position relative to a reference station instead of an absolute position. Super-resolution location solutions can be obtained for one or more signal sources in a high multipath environment by applying a matrix decomposition-based multi-carrier range recovery algorithm. This technique allows for the separation of LOS signals from the multipath reflections without requiring wideband signals. The signal structure is easily adapted to conform to spectral allocations and is compatible with Coded OFDM (COFDM) communications. This signal structure is shown in Equation (1.1) and operates about carrier frequency f_0 using M sinusoidal carriers, frequency spacing Δf, and arbitrary phases ϕ_m [13].

$$s(t) = \sum_{m=0}^{M-1} A e^{j[2\pi(f_0+m\Delta f)t+\phi_m]} \tag{1.1}$$

This signal is received at the reference receivers with distances d_k and yields propagation delays of $\tau_k = d_k/c$. The received signals are expressed in the form describe in Equation (1.2) and simplified into that of Equation (1.3).

$$s_k(t) = \sum_{m=0}^{M-1} A_k e^{j[2\pi(f_0+m\Delta f)(t+t_0-\tau_{k0})+\phi_m]} \tag{1.2}$$

$$s_k(t) = \sum_{m=0}^{M-1} A_k e^{j[2\pi(f_0+m\Delta f)t+\Phi_{mk}]} \tag{1.3}$$

It is assumed that the reference receivers have synchronized clocks while the source clock has an unknown offset t_0 which induces the phase shift $\psi_m = 2\pi(f_0 + m\Delta_f)t_0$. Then, the phase difference between adjacent carriers for signal $s_k(t)$ is corrected for the known phases ϕ_m using:

$$\Delta\Theta_k = -2\pi\Delta f\tau_{k0} \tag{1.4}$$

Finally, the phase difference of a carrier at two reference receivers is calculated using Equation (1.5) and is used to find the TDOA of the signal at those receivers. This is done using Equation (1.6).

$$\Theta_{qr} = \Delta\Theta_r - \Delta\Theta_q \tag{1.5}$$

$$\Delta\tau_{qr} = \frac{-\Theta_{qr}}{2\pi\Delta f} = \frac{d_2 - d_1}{c} \tag{1.6}$$

Since the signal used is periodic, the solution is affected by a time aliasing ambiguity. If, however, Δf is chosen to be sufficiently small, the TDOA solution will be unambiguous throughout a ranging cell defined by the locus of points within the distance R = $c/\Delta f$ of any reference receiver. The system was tested with an audio signal at wavelengths which matched that of an EM wave with a center frequency of 4.77 GHz and a bandwidth of 5.3 GHz. The experiment yielded promising results and demonstrated that the system works in severe multipath environments and conditions where the LOS signal is small compared to one or more multipath signals [13].

1.3.3.2 Indoor Geolocation Using HIPERLAN/2 WLANs. Li, Pahlavan, Latva-aho, and Ylianttila investigated geolocation methods and system architectures using OFDM signals in High Performance Radio LAN Version 2 (HIPERLAN) [14]. HIPERLAN is a WLAN standard which is the European alternative to the IEEE 802.11 standards. The technique presented here exploits the Media Access Control (MAC) frame structure.

The network shown in Figure 1.1 operates in the 5 GHz band and supports short-range broadband wireless access. The range of the network is 30 m in a typical indoor environment and up to 150 m in a typical outdoor or large, open indoor environment. HIPERLAN/2 protocol basically consists of the Physical (PHY) layer, the Data Link Control (DLC) layer, and the Convergence (CL) layer. The PHY layer defines the basic data transmission functions via a radio channel. The DLC layer consists of the MAC function, the Error Control (EC) function, and the Radio Link Control (RLC) function. The CL layer works as an intermediate component between the DLC layer and a variety of fixed networks to which HIPERLAN/2 is connected. The PHY layer is based on the OFDM multicarrier scheme. The basic signal format on the PHY layer is an RF burst, which starts with a preamble that is followed by the OFDM symbols. The DLC layer constitutes the logical link between the access point and its mobile terminals. It's MAC protocol is based on a dynamic Time Division Multiple Access/Time Division Duplex (TDMA/TDD) scheme with centralized control. Each MAC frame (shown in Figure 1.2) has a duration of 2 ms and is divided into a number of transport channels of varying length [14].

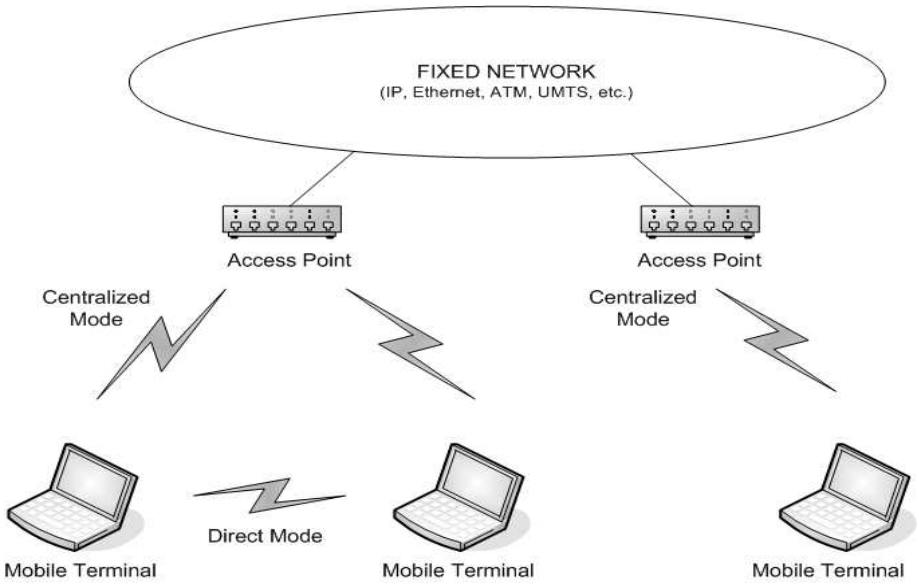

Figure 1.1: The HIPERLAN/2 network structure [14].

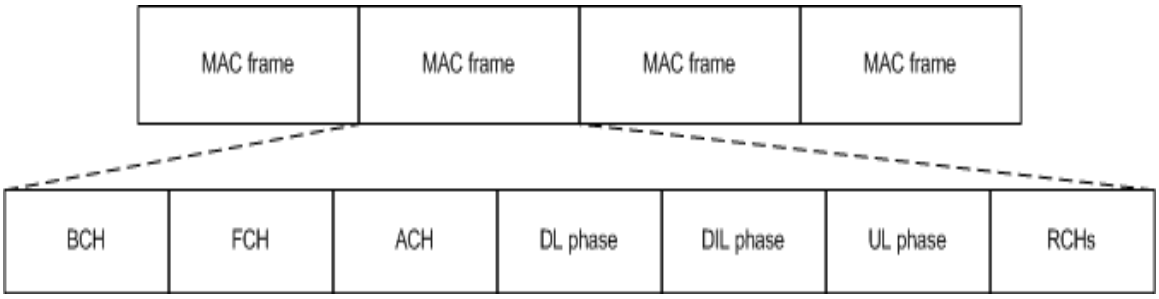

Figure 1.2: MAC frame structure for HIPERLAN/2 [14].

The MAC frame synchronization between the access point and the mobile terminals is established with the aid of a PHY layer Broadcast Burst which is transmitted at the beginning of the Broadcast Channel (BCH). The starting time points of other transport channels are determined with time offsets from the starting point of the MAC frame and they are known to the access point and the mobile terminals. The features of the MAC frame structure can be exploited in measuring TOA and TDOA measurements from OFDM burst signals [14].

The geolocation system architecture addressed is the network-based architecture. More than three Geographic Base Stations (GBS) are needed to geometrically locate the mobile terminal using multiple TOA/TDOA measurements. In network-based architecture the base stations measure radio signals transmitted by the mobile terminal. Then, the GBSs extract geolocation information from the measurements. The functionality of the GBS is implemented in the access point. The TOA from the mobile terminal to the access point (shown in Figure 1.3) can be measured based on round-trip time of propagation where t_0 and t_1 are the times (measured at the access point) of the transmitted Broadcast Burst and the received Uplink Burst from the mobile terminal, respectively, while t_{00} and t_{10} are the times (measured at the mobile terminal) of the received Broadcast Burst from the Access Point and the transmitted Uplink Burst, respectively. The delay τ_{10} is the offset of the Uplink (UL phase) phase within the MAC frame, which is known to both the mobile terminal and the access point. The delay τ_{00} is the TOA to be measured. The mobile terminal determines the starting time t_{00} of the current MAC frame by measuring the received time of the

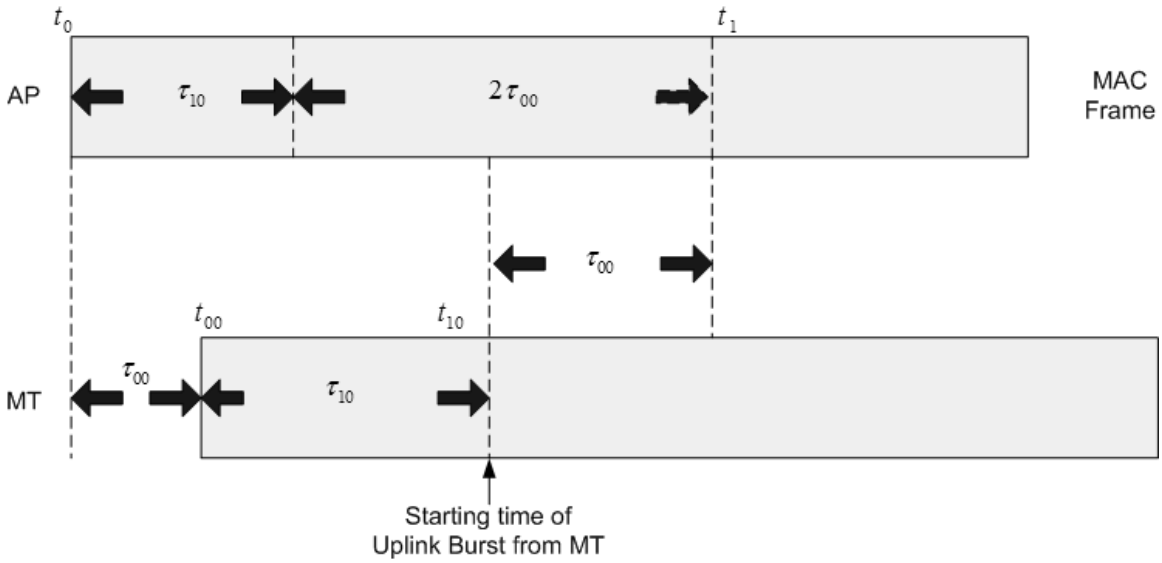

Figure 1.3: Access Point-based TOA geolocation method [14].

Broadcast Burst from the access point. The access point determines t_1 by measuring the receiving time of the Uplink Burst from the mobile terminal. Since the delay τ_{10} is known to both the access point and the mobile terminal, the TOA is calculated at the access point using [14].

$$\tau_{00} = \frac{1}{2}[(t_1 - t_0) - \tau_{10}] \tag{1.7}$$

The signal is oversampled by a factor of 10 at the receiver. Two channel models were used in the simulations, an AWGN channel and a frequency selective channel with an exponential power delay profile. For the frequency selective channel, five paths were chosen with delays of 0, 2, 4, 6, and 8 samples so that the channel impulse response was shorter than the guard interval. Results showed that the mean of ranging errors was around 3 m for the AWGN channel and 7.5 m for the exponential channel when signal-to-noise ratio (SNR) $>$ 9 dB [14].

1.3.3.3 Navigation Using OFDM SoOP. Velotta researched the use of OFDM signals as a source for navigation [3]. Simulations were run on OFDM signals

which were transmitted to a reference receiver and a mobile receiver using an AWGN channel. A correlation calculation was performed on the each of the received signals to determine the boundary of the first OFDM symbol. This process takes advantage of the OFDM symbol structure, where it is known that the cyclic prefix is a copied portion of the data. Then, instead of transmitting the received data between the two receivers in order to calculate the difference of arrival times, statistical "features" from each symbol are transmitted instead. This technique effectively reduces data transmission requirements and, thus, the amount of required backchannel bandwidth. The statistical symbol features include mean, standard deviation, variance, skewness, kurtosis, peak-to-average power ratio (PAPR), RMS, and average symbol phase. Each of these statistics was calculated in the time and frequency domain which yields 16 statistical characteristics about each symbol. The data for the received signals was correlated to determine the number of symbols one signal is delayed from the other. Velotta's results show that time domain statistics perform slightly better in correctly correlating the received signals' statistics, with the mean statistic performing best. This system is the basis for this research and is discussed in more detail in Chapter III [3].

1.4 Thesis Overview

Chapter II presents the background information necessary to understand OFDM signals, signal structure, multipath modeling, and TDOA measurements as they relate to this research. Chapter III describes the computer simulation code and method used to model OFDM signals in a multipath environment. Chapter IV analyzes simulation results to determine the accuracy of the TDOA measurements in positioning. Chapter V gives a summary of the research, the results, and conclusions drawn. It also details recommendations for follow-on research on this topic.

II. Background

This chapter presents the technical background information for the main topics presented in this research. First, a brief discussion of OFDM signals is presented, in which the system structure is detailed. Each component of a transmitter is covered, along with the characteristics of the signal itself. Then, a discussion of multipath effects is provided. Finally, the process of position estimation using TDOA measurements is described. A brief summary follows these topics.

2.1 OFDM System Structure

This section discusses the structure of an OFDM system and closely follows that which is described in [3]. OFDM is a multi-carrier communication method which can be viewed as a modulation technique or a multiplexing technique. In multi-carrier communication systems, a single datastream is transmitted over a number of lower rate subcarriers. OFDM is a special case of Frequency Division Multiplexing (FDM). In a basic FDM system, the subcarriers are spaced so that they don't spectrally overlap and a guard band is inserted to ensure separation. This separation minimizes the interference caused by adjacent subcarriers. This system, however, is an inefficient use of valuable bandwidth. In an OFDM system, the subcarriers spectrally overlap but do not interfere with one another due to orthogonality. The carrier spacing is selected such that each subcarrier is orthogonal to the other subcarriers in frequency [15]. Signals are mathematically orthogonal if the following condition is met:

$$\int_0^{1/T} \chi_1(f) \cdot \chi_2^*(f) \cdot df = 0 \tag{2.1}$$

where T is the OFDM symbol length in time, $\chi_1(f)$ and $\chi_2(f)$ are the Fourier transform of the input signals, and * denotes the complex conjugate of a signal [3]. Since the subcarriers overlap, the OFDM system makes more efficient use of available bandwidth and more subcarriers can be used. Figure 2.1 illustrates the frequency domain structure of the FDMA and OFDM systems. The graphs show the subcarrier separation of FDMA subcarriers and the overlap of the OFDM subcarriers. The overlapping

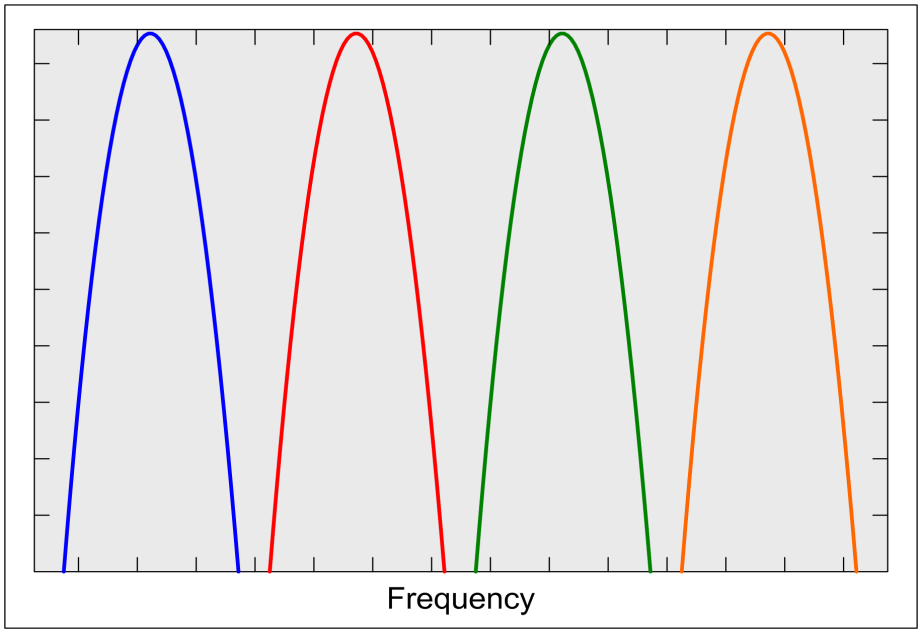

(a) FDMA (Frequency Domain)

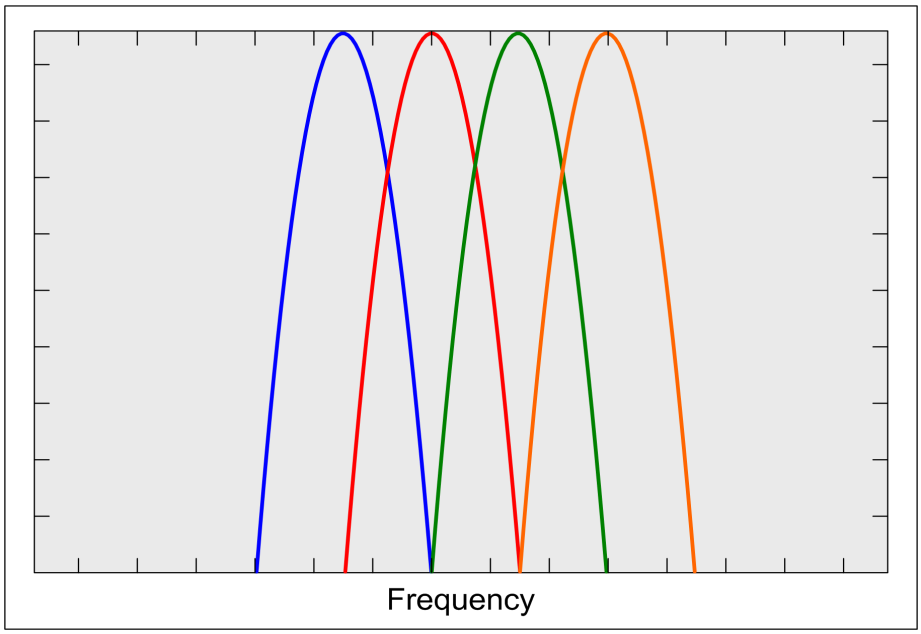

(b) OFDM (Frequency Domain)

Figure 2.1: FDMA vs. OFDM. (a) Four FDMA channels with frequency guard bands. (b) Four OFDM orthogonal channels [3].

subcarriers have null points at the center frequency of the adjacent subcarriers. This is what makes the subcarriers orthogonal. To ensure orthogonality, the subcarriers must be spaced apart by 1/T Hz and comply with Equation (2.1) [15].

Figure 2.2 depicts a block diagram of a typical OFDM system. The transmitter consists of an encoder, interleaver, serial-to-parallel conversion, constellation mapping application, OFDM modulation, parallel-to-serial conversion, a function to add the cyclic prefix, and a RF transmitter. The receiver is made up of a RF receiver, a function to remove the cyclic prefix, synchronization mechanism, serial-to-parallel conversion, OFDM demodulator, constellation demapping application, parallel-to-serial conversion, de-interleaver, and a decoder [3].

2.1.1 Coding. In a multipath fading channel, subcarriers arrive at the receiver with different amplitudes. Some subcarriers may even be completely attenuated

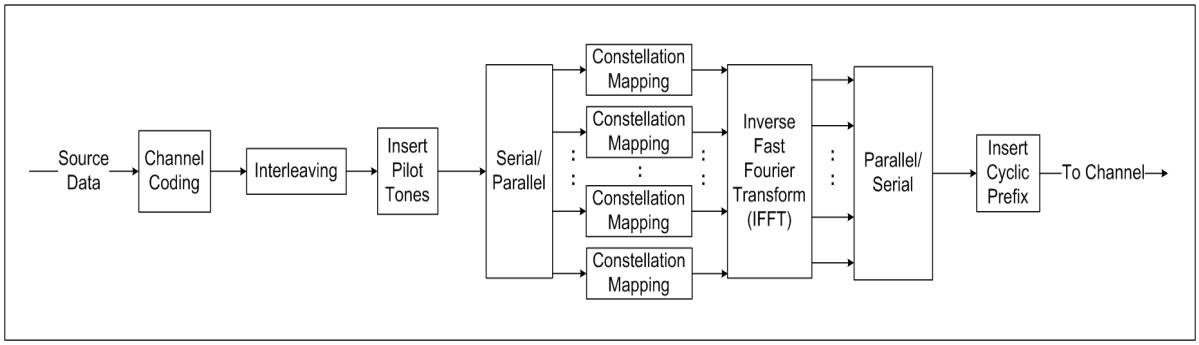

(a) OFDM Transmitter

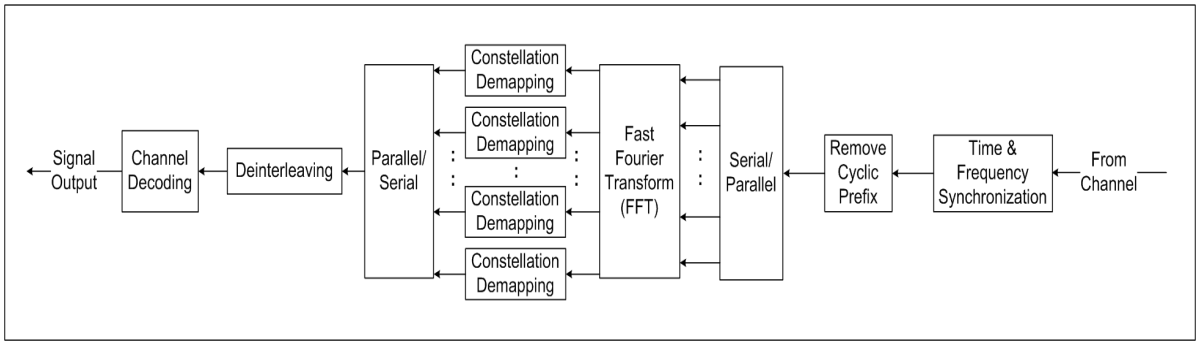

(b) OFDM Receiver

Figure 2.2: Block Diagram of OFDM System [3, 15].

due to deep fades. So even though most subcarriers may be detected without errors, the overall bit-error rate (BER) will be largely dominated by a few weak subcarriers with smaller amplitudes, for which the BER will be close to 0.5. Forward error correction (FEC) coding is essential to avoid this domination by the weakest subcarriers. By using coding across the subcarriers, errors can be detected and corrected up to a certain limit, depending on the strength of the coding scheme. A powerful coding scheme means that the performance of the OFDM link is determined by the average received power instead of the power of the weakest subcarrier [15]. Convolutional, block, and Reed-Solomon coding, along with Trellis coded modulation, are all coding methods that have been recommended for OFDM systems in order to correct bit errors [3]. Table 2.1 displays the IEEE standard 802.11a convolution coding rates. In many cases, multiple types of encoding are performed on a signal at different stages in an OFDM transmitter to improve coding gain at a relatively small implementation cost [15].

2.1.2 Interleaving. Decoders are limited by the strength of the coding scheme as to how many errors can be corrected per codeword. In the case where multipath causes deep fades, errors tend to occur in bursts rather than being randomly scattered [15]. A burst error is a string of successive bit errors. For example, a burst error may cause four bit errors in a row, which may all occur in the same codeword.

Table 2.1: IEEE Std 802.11a Rate Dependent Convolutional Rates [3, 16].

Data Rate (Mbits/s)	**Modulation**	**Coding Rate**
6	BPSK	1/2
9	BPSK	3/4
12	QPSK	1/2
18	QPSK	3/4
24	16-QAM	1/2
36	16-QAM	3/4
48	64-QAM	2/3
54	64-QAM	3/4

Having four bit errors in a codeword is detrimental to a coding scheme that can only correct two errors per codeword. A way to minimize the effects of burst errors is to implement an interleaver. The purpose of the interleaver is to rearrange the order of the bits in order to reduce the effects of burst errors. If a burst error occurs when an interleaver is used, there may be one bit error in four different codewords instead of four bit errors in one codeword. Since the decoder can correct two errors per codeword, all four errors can be corrected and no information will be lost [17]. A block interleaver, shown in Figure 2.3, is one of the more commonly used interleaving schemes. Input bits are written into a matrix column by column and read out into the datastream row by row. The interleaver sequence in the output bit stream shows that the new symbols are made of bits from each of the original symbols [15].

2.1.3 Constellation Mapping. After the interleaving process is completed, the data stream goes through a serial-to-parallel process in which the signal is then demultiplexed into N parallel data streams, where N is also the symbol length. As shown in Figure 2.2, the signal is then mapped to some specified modulation constellation. The main schemes used are quadrature amplitude modulation (QAM) or phase-shift keying (PSK). Figure 2.4 shows constellation diagrams for the different modulation schemes [3].

M-ary QAM is a hybrid modulation technique which includes both amplitude and phase modulation. The c^{th} signal is represented by [18]:

$$x_c(t) = \sqrt{\frac{2E_0}{T}}[x_I(t) \cdot \cos(2\pi f_c t) + x_Q(t) \cdot \sin(2\pi f_c t)], \quad iT \leq t \leq (i+1)T \qquad (2.2)$$

where a complex baseband signal, $x_Z(t) = x_I(t) + j \cdot x_Q(t)$, is converted to a passband signal, $x_c(t)$. The "in-phase" and "quadrature" portions of the complex signal are represented by $x_I(t)$ and $x_Q(t)$, respectively [3].

2.1.4 Pilot Tones. OFDM symbols are comprised of data and pilot tones. The pilot tones are known by the system receiver and are used primarily for frequency

synchronization [3]. For IEEE 802.11a, the pilot tones are a pseudo-random sequence of ±1's [16]. Pilot tones can be inserted in any sequence/constellation with respect to the signal structure. Figure 2.5 illustrates the pilot tone constellation for the ESTI DVB standard [19]. However, for the purpose of this research, an arbitrary pilot tone constellation was chosen merely to confirm symbol estimations made by the feature correlation process and not as a complimentary synchronization scheme. The system described in this research does not require knowledge of the pilot tones. Figure 2.6 depicts the pilot tone constellation used to test the system described in this research [3].

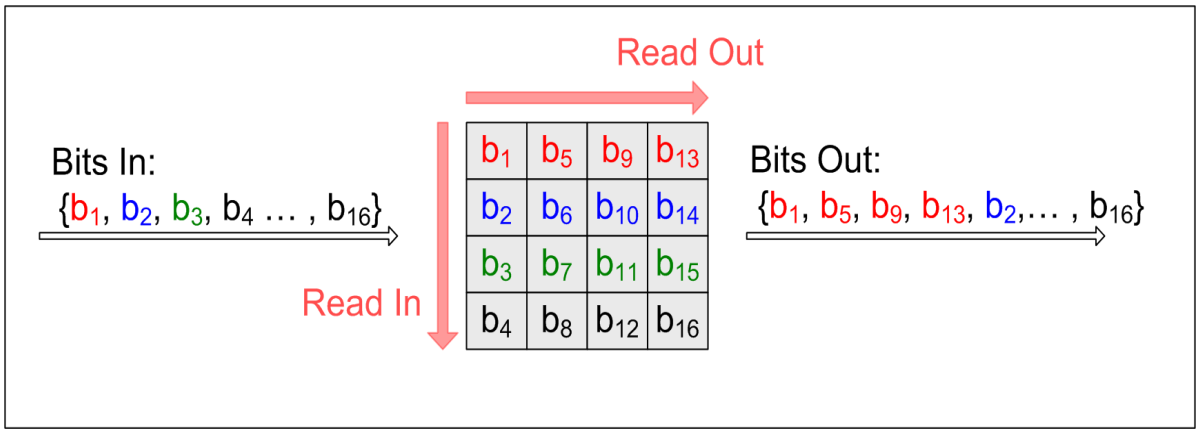

(a) Interleaver

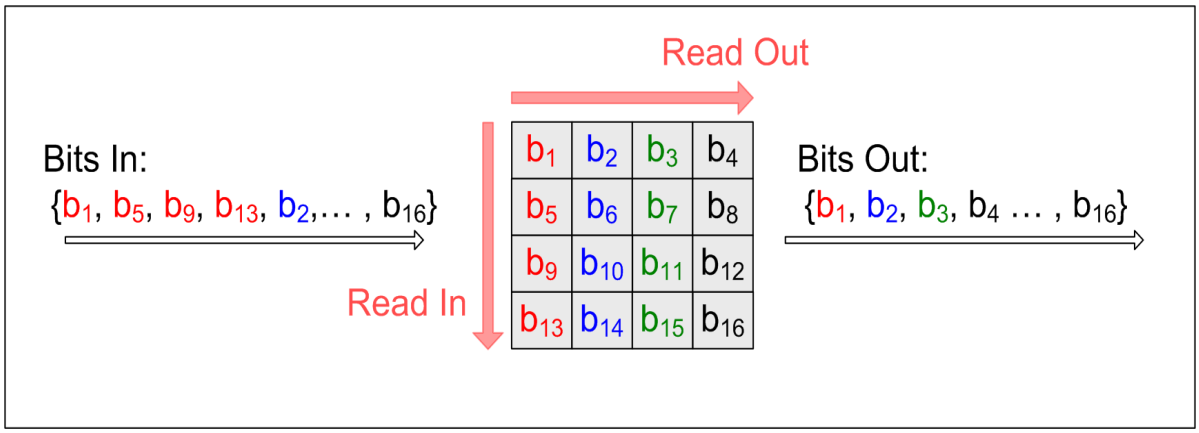

(b) De-Interleaver

Figure 2.3: Interleaving Process. (a) Interleaver. (b) De-Interleaver [3].

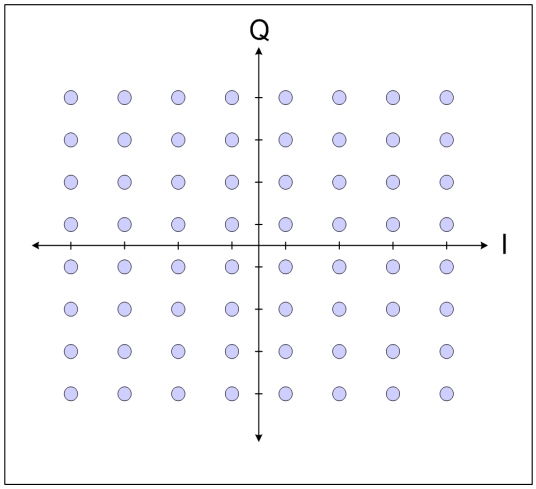

(a) 64-QAM

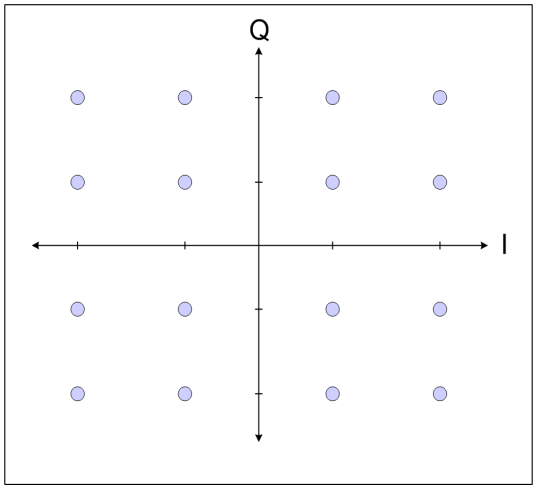

(b) 16-QAM

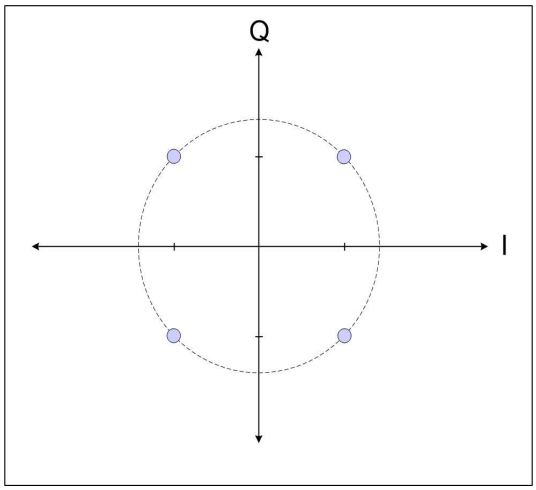

(c) 4-QAM / QPSK

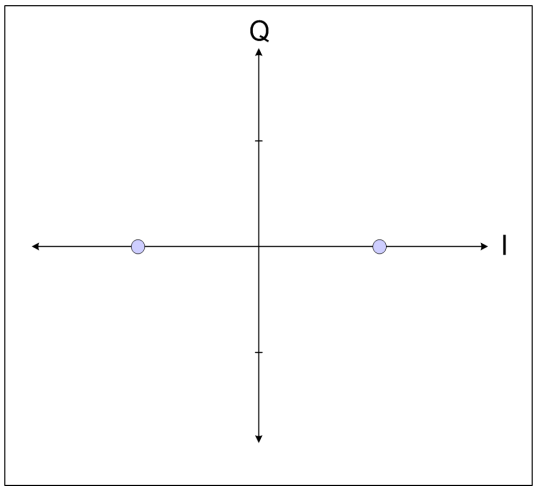

(d) BPSK

Figure 2.4: QAM/PSK Constellations. (a) 64-QAM. (b) 16-QAM. (c) 4-QAM/Quadrature Phase-Shift Keying (QPSK) (d) Binary Phase-Shift Keying (BPSK) [3, 15]

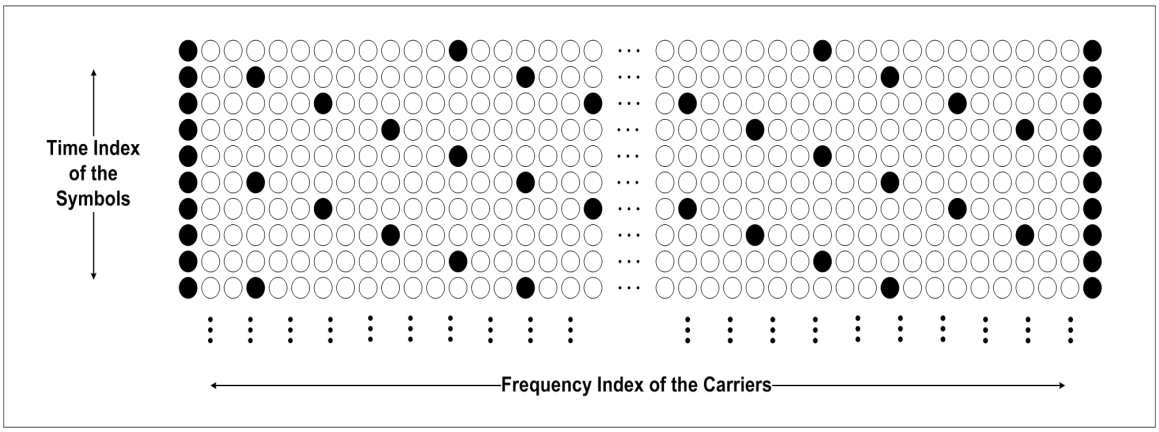

Figure 2.5: DVB Pilot Tone Constellation [19].

2.1.5 OFDM Modulation Using IFFT. OFDM systems in the past were difficult to implement in high speed digital communications due to the complex computations involved with multicarrier modulation. However, advances in digital signal processing in the 1980's and 1990's have made OFDM implementation less computationally intense and, thus, more cost effective. In particular, the use of Fast Fourier Transforms (FFTs)/Inverse Fast Fourier Transforms (IFFTs) eliminated the need for

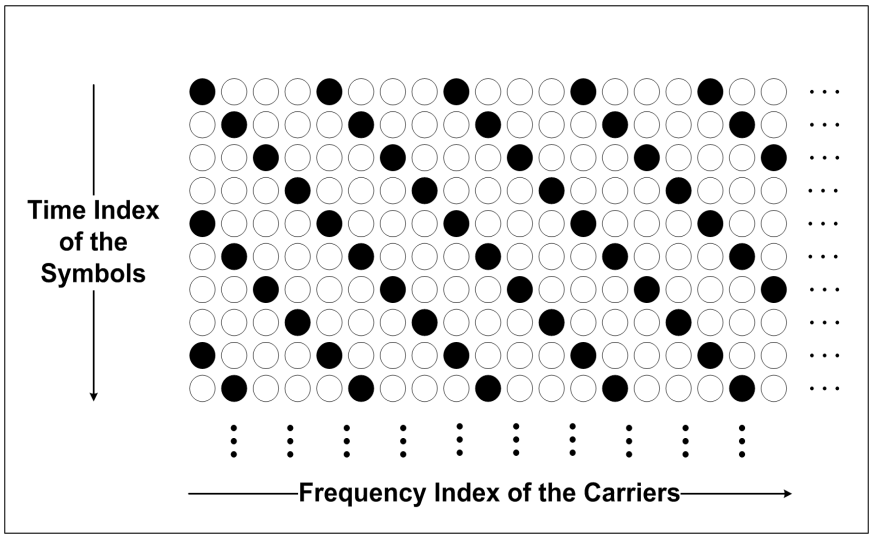

Figure 2.6: Pilot Tone Constellation Used for Research. The length of Frequency Index of the Carriers is 64. The length of the Time Index of the Symbols is 64. The constellation repeats every 64 symbols [3].

arrays of sinusoidal generators and coherent demodulation, all of which are required for parallel communications [3, 18].

As shown in Figure 2.2, IFFTs are used in the transmitter to modulate the data after it has been mapped to the specified constellation. FFTs, likewise, are used in the receiver for demodulation. Since the purpose of this research is not to decipher (i.e., demodulate/decode) the transmitted signal for communication purposes, the remaining focus of this section is on the modulation technique in the OFDM transmitter. The following equations define the IFFT for the c^{th} signal [3]:

$$x_c(n) = \frac{1}{N} \cdot \sum_{k=0}^{N-1} S_n(k) \cdot W_N^{-kn}, \quad n = 0, 1, ..., N-1 \tag{2.3}$$

$$W_N = e^{-\frac{j2\pi}{N}} \tag{2.4}$$

The variable $S_n(k)$ represents the n^{th} data symbol at the k^{th} sample, where n and k range from 0 to $N-1$. N is the total number of samples and the length of the IFFT. The input signal $S_n(k)$ is complex (i.e. $S_n(k) = a_n(k) + j \cdot b_n(k)$) for the purposes of this research [3, 20].

2.1.6 Cyclic Prefix. The OFDM signal uses a cyclic prefix to mitigate the effects of inter-symbol interference (ISI). This is accomplished by copying a specified number of samples of the OFDM symbol and appending them to front of the symbol in order to create a guard period between adjacent symbols. In practice, this guard period needs to exceed the maximum expected delay of the channel in order to avoid ISI. In other words, as long as the maximum excess delay, τ_{max}, is less than the cyclic prefix length, T_g seconds (or ν samples), the delayed multipath signal will remain within the cyclic prefix interval and be removed by the receiver [3, 21].

Figure 2.7 illustrates how the cyclic prefix is appended to the beginning of the symbol inside the signal structure before transmission. This results in transmitting a symbol that is $N + \nu$ samples (or $T + T_g$ seconds) long. Mathematically, the purpose

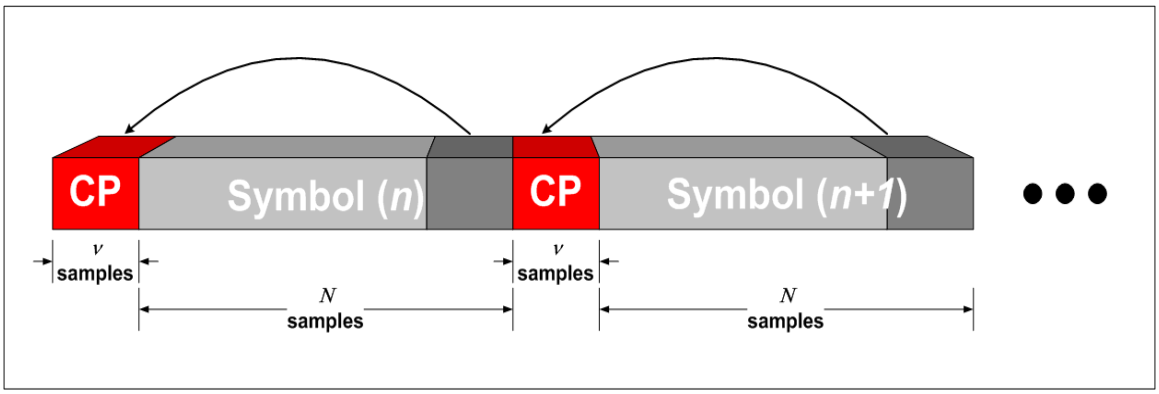

Figure 2.7: Cyclic Prefix Extension. The last ν samples are appended to the beginning of the symbol to create the guard interval between symbols.

of the cyclic prefix is to convert the linear convolution of the transmitted signal with the channel into a circular convolution and, thereby, causing the FFT of the circularly convolved signal and channel to simply be the product of their respective FFTs [3].

2.2 Multipath

Multipath occurs when a RF receiver collects a transmitted signal from more than one path. The total received signal usually consists of a LOS signal and one or more reflected signals, although a LOS signal may not be present in every case. The LOS signal is usually the strongest to be received, unless it passes through an absorbent material. The multipath signals are usually reflected off of a building, tower, atmosphere, mountains, or some solid structure. These reflected signals are attenuated, resulting in power loss and phase distortion. They also arrive after the LOS signal, which results in a delay since they take an indirect path (see Figure 2.8).

Multipath signals can either constructively or destructively combine with the dominant signal by adding signals with different attenuation, time-delays, and phase shifts. The distortion amount depends on a number of different factors like relevant power of any dominant signal, range in the delays experienced by the multipath signals, and the properties of the reflecting surface [5].

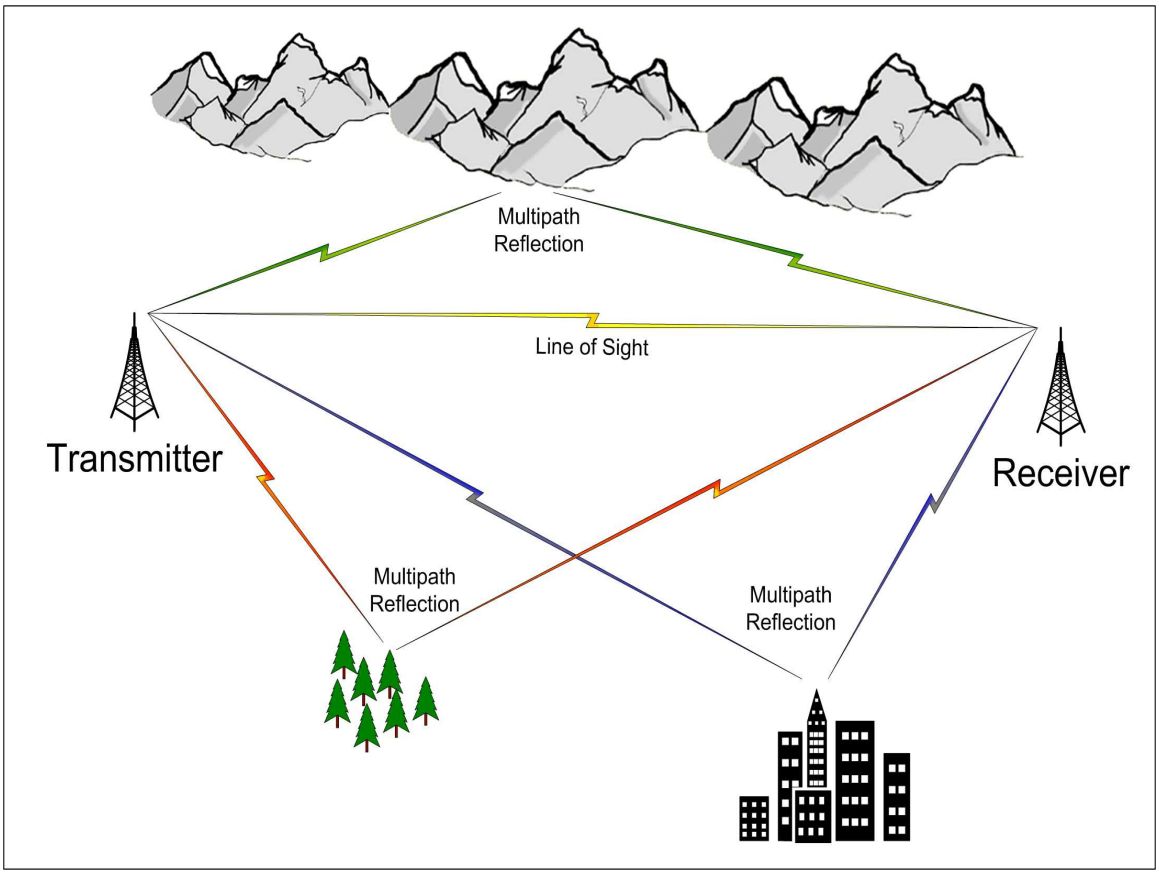

Figure 2.8: Multipath. The receiver received multiple signals of the same transmission due to multipath [3].

2.3 TDOA Positioning

This section derives the TDOA position estimation equations and closely follows the description given in [5]. TDOA positioning is a multilateration process which calculates position estimates based on distances from known sources. The system described here consists of a transmitter, a reference receiver, and a mobile receiver (see Figure 2.9) to estimate the range between one mobile receiver and the transmitter. The transmitter and reference receiver are at known locations. The range provides a sphere (three dimensions), or a circle (two dimensions), of possible locations for the mobile receiver with respect to the transmitter. Assuming enough measurements are available, the intersection of these points provides the final position estimate (see Figure 2.10). These figures represent a case where the clocks in the reference and

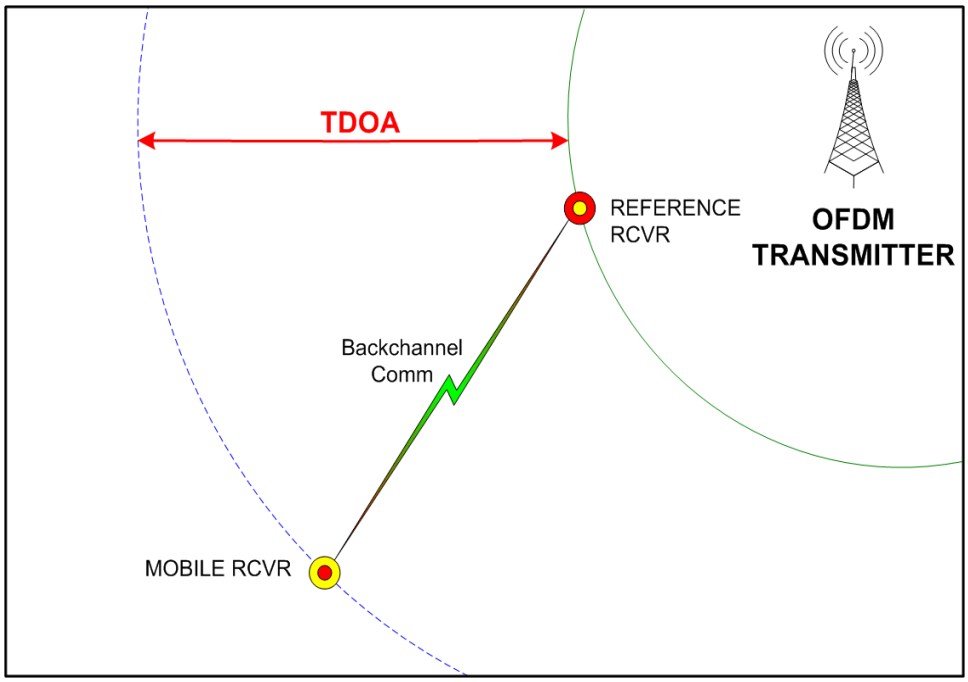

Figure 2.9: System Model. The model consists of one OFDM transmitter and two receivers, the reference and mobile receivers [3].

mobile receivers are synchronized. This concept will now be developed for the case of unsynchronized receivers.

2.3.1 TDOA Calculation. This section illustrates how to mathematically derive the final position estimate for the system described above. First, a local time for each receiver is defined in terms of the true time [5]:

$$\hat{t}_{REF} = t_{REF} + \epsilon_{REF} \tag{2.5}$$

$$\hat{t}_{MOB} = t_{MOB} + \epsilon_{MOB} \tag{2.6}$$

where

$\hat{t}_{REF}$ is the time of arrival according to the reference receiver's clock
$\hat{t}_{MOB}$ is the time of arrival according to the mobile receiver's clock
t_{REF} and t_{MOB} are the true times of arrival at each receiver
ϵ_{REF} and ϵ_{MOB} are the clock errors in each receiver

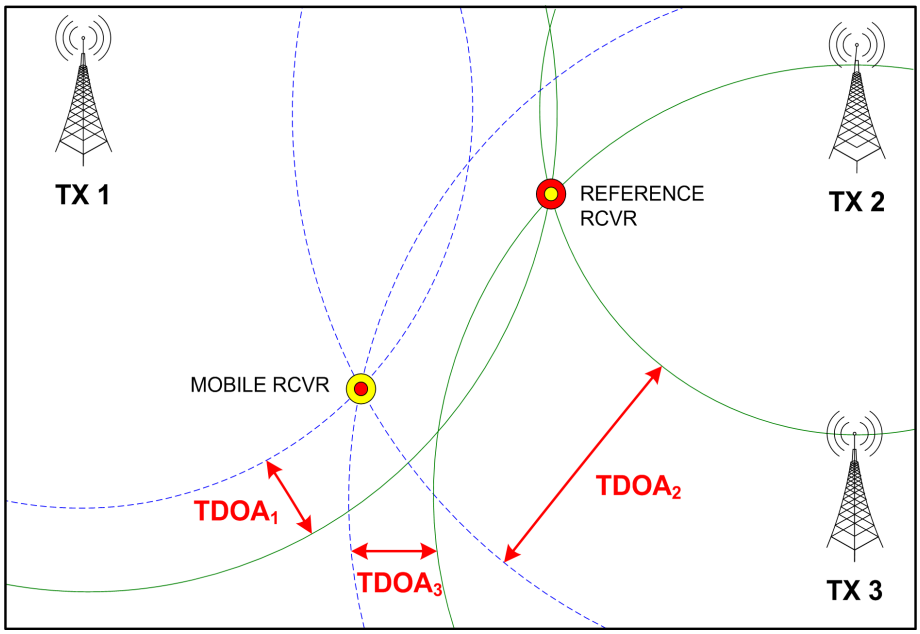

Figure 2.10: TDOA Technique. Position is calculated by differencing the arrival time of a single transmission signal to two separate receivers [3].

Taking these errors into account, the TDOA measurement then becomes:

$$\begin{aligned} TDOA &= \hat{t}_{MOB} - \hat{t}_{REF} \\ &= (t_{MOB} + \epsilon_{MOB}) - (t_{REF} + \epsilon_{REF}) \\ &= (t_{MOB} - t_{REF}) + (\epsilon_{MOB} - \epsilon_{REF}) \\ &= \frac{RANGE_{MOB} - RANGE_{REF}}{c} + \delta t \end{aligned} \tag{2.7}$$

where

$RANGE_{MOB}$ and $RANGE_{REF}$ are the actual ranges between the transmitter and the receivers

δt is the difference between the clock errors of the receivers

c is the speed of light

It is evident from the above equations that the clock errors from the receivers create an error in the TDOA measurement of δt. If it is assumed that the receivers have synchronized clocks, the errors would be the same and $\delta t = 0$. In that case,

the clock error difference between the two receivers, or clock bias, is negated. The clock bias must also be estimated by the TDOA algorithm. Since this is another unknown, four TDOAs (or range estimates) are now required in order to resolve the three-dimensional position estimate along with the clock bias [5].

The clock errors for each receiver are not set. They can vary over time and, thus, change the clock bias between the receivers. As a result, Equation (2.7) becomes:

$$\begin{aligned} TDOA &= \frac{RANGE_{MOB} - RANGE_{REF}}{c} + \delta t \\ cTDOA &= RANGE_{MOB} - RANGE_{REF} + c\delta t \\ cTDOA + RANGE_{REF} &= RANGE_{MOB} + c\delta t \end{aligned} \tag{2.8}$$

where

$cTDOA + RANGE_{REF}$ is similar to a pseudorange measurement
$RANGE_{MOB}$ is the true range
$c\delta t$ is the clock bias converted to meters (unknown)

The parameters derived in Equation (2.8) can be used to solve for a position estimate. The following equations derive the mobile receiver position estimate using a similar development for GPS positioning found in [6]. The system structure here has multiple transmitters sending signals to the reference and mobile receiver. First, the range from each transmitter to the mobile receiver is expressed in terms of their positions [5]:

$$r^{(k)} = \sqrt{[x^{(k)} - x]^2 + [y^{(k)} - y]^2 + [z^{(k)} - z]^2} \tag{2.9}$$

where

$r^{(k)}$ is the true range from transmitter k to the mobile receiver
$[x^{(k)}, y^{(k)}, z^{(k)}]$ is the position of transmitter k (known)
$[x, y, z]$ is the position of the mobile receiver (unknown)

Using Equation (2.8), the range estimate becomes

$$\rho^{(k)} = r^{(k)} + c\delta t \tag{2.10}$$

where $\rho^{(k)}$ is the range estimate from transmitter k to the mobile receiver.

Four unknowns exist in Equation (2.9) and Equation (2.10): the three-dimensional position coordinates and the clock bias. One way to solve for these unknowns is to linearize about an initial guess and iteratively solve for the solution until the magnitude of the error vector is below a predefined threshold. This method is known as the *Newton-Raphson Method* and is summarized below [5, 6].

The initial guesses of the mobile receiver position and the clock bias are defined as $[x_0, y_0, z_0]$ and $c\delta t_0$, respectively. The range from transmitter k at position $[x^{(k)}, y^{(k)}, z^{(k)}]$ to this initial position, with clock bias included, is:

$$\rho_0^{(k)} = \sqrt{[x^{(k)} - x_0]^2 + [y^{(k)} - y_0]^2 + [z^{(k)} - z_0]^2} + c\delta t_0 \tag{2.11}$$

The range estimate error for transmitter k is then

$$\delta\rho^k = \rho^{(k)} - \rho_0^{(k)} \tag{2.12}$$

A vector or range estimate errors for all transmitters is then constructed as follows:

$$\delta\boldsymbol{\rho} = \begin{bmatrix} \delta\rho^{(1)} \\ \delta\rho^{(2)} \\ \vdots \\ \delta\rho^{(K)} \end{bmatrix} \tag{2.13}$$

where K is the total number of transmitters [5].

The corrections to the initial estimates are now calculated using the least-squares method, where the coordinate $[x, y, z]$ is represented by $\mathbf{x}$.

$$\begin{bmatrix} \delta\hat{\mathbf{x}} \\ \delta(c\hat{\delta}t) \end{bmatrix} = (\mathbf{G}^T\mathbf{G})^{-1}\mathbf{G}^T\delta\boldsymbol{\rho} \tag{2.14}$$

where

$$\mathbf{G} = \begin{bmatrix} (-\mathbf{e}^{(1)})^T & 1 \\ (-\mathbf{e}^{(2)})^T & 1 \\ \vdots & \vdots \\ (-\mathbf{e}^{(K)})^T & 1 \end{bmatrix} \tag{2.15}$$

$$(-\mathbf{e}^{(k)})^T = -\frac{1}{\sqrt{[x^{(k)} - x_0]^2 + [y^{(k)} - y_0]^2 + [z^{(k)} - z_0]^2}} \cdot [x^{(k)} - x_0, y^{(k)} - y_0, z^{(k)} - z_0] \tag{2.16}$$

The position and clock bias estimates are then calculated for the next iteration using the initial estimates and the results from Equation (2.14):

$$\hat{\mathbf{x}} = \mathbf{x}_0 + \delta\hat{\mathbf{x}} \tag{2.17}$$

$$c\hat{\delta}t = c\delta t_0 + \delta(c\hat{\delta}_t) \tag{2.18}$$

As stated before, the iteration process continues until the error magnitude from Equation (2.14) is less than a predetermined, acceptable threshold. The final position and clock bias estimates then become the system estimates [5].

2.4 Summary

This chapter discussed the OFDM system architecture, multipath effects, and TDOA measurements. These topics are key to understanding the research performed, the development of which is outlined in Chapter III.

III. Simulation Development

This chapter details the algorithm developed to evaluate the potential for using an OFDM signal as a source for navigation. The calculations for determining symbol boundaries and the correlation process using symbol features are discussed in Section 3.1. Section 3.2 presents the algorithm designed to oversample the transmitted signal. The multipath channel model developed for this research is described in Section 3.3. Lastly, Section 3.4 explains the TDOA measurements using the OFDM system.

3.1 OFDM Model

The model used in this research was created by Velotta and, therefore, the information presented in this section closely follows that which is presented in [3]. The OFDM system, shown in Figure 2.9, is comprised of a transmitter, reference receiver, and a mobile receiver. The basic premise of this system is that the transmitter and reference receiver have known positions while the mobile receiver is at an unknown location. The transmitter sends the signal to the receivers, each of which receive the signal over a unique channel. Each channel is unique and adds multipath effects and AWGN to the signals.

There are two separate correlation calculations performed in this algorithm. The symbol boundary correlator takes the received signal and attempts to find the point where the next symbol starts. This value, $\hat{\delta}$, defines the number of samples it takes to get to the beginning of that symbol. The correlation calculation takes place independently in both the reference and the mobile receiver. On the other hand, the feature correlation attempts to determine the symbol difference between the reference and the mobile receiver. The reference receiver sends its data to the mobile receiver to perform the correlation. The stored value, Δ_{Symbol}, is the number of symbols by which one received signal is ahead or behind another. The feature correlation calculation occurs only once, unlike the symbol boundary correlation which takes place independently at each receiver. This process is discussed in more detail in

Section 3.3.3. These three values are used to determine the TDOA measurement, which is discussed in Section 3.4.

3.1.1 OFDM Signal Generator. The OFDM signal created here is based on the IEEE 802.11a standard for WLANs. The data length is 64 samples while the cyclic prefix consists of a copy of the last 16 samples of data appended to the front of the data. The resulting OFDM symbol is 80 samples long with a symbol period of 4 μs and a sample period of 50 ns [16].

The algorithm which creates the OFDM signal is a modified version of the system presented in Figure 2.2 since it begins with constellation mapping instead of channel coding. The reason channel coding and interleaving are not included is because this research is focused on exploiting signal characteristics in order to navigate, as opposed to transmitting and receiving data correctly or reduce bit errors. Generating random bits, encoding the bits, and interleaving the bits would yield random bits entering the constellation mapping process. Also, the information used for the feature correlation process, described in Section 3.3.3, is calculated before the de-interleaving and decoding processes are implemented. Thus, starting at the constellation mapping process has no ill effects on the system and saves processing time by removing the encoding and interleaving processes.

The transmitted signal consists of 512 OFDM symbols, each of which is created by randomly choosing from a 64-QAM constellation. Next, pilot tones are inserted into the signal in the pattern shown in Figure 2.6. The pilot tones, though, are used only to validate the feature correlation process [3]. After that, the symbols are modulated using a 64-point IFFT. Finally, the cyclic prefix is added to create the OFDM symbol.

3.2 Oversampling Algorithm

The generated OFDM signal is oversampled before transmission. To accomplish this task, the signal has to be upsampled first. Upsampling by a factor of L simply

adds $L-1$ zeros after each sample of the signal. Next, the upsampled signal is convolved with a sinc function in the time domain. This is akin to multiplying by an ideal filter in the frequency domain. The sinc function used in this research has only five sidelobes on each side of the peak and was created using the `Matlab`® *sinc* function.

$$sinc(t) = \begin{cases} 1, & t = 0 \\ \frac{sin(\pi t)}{\pi t}, & t \neq 0 \end{cases} \tag{3.1}$$

This implies that the filter is not exactly ideal since a sinc is infinite in length. The sinc function also has to have a sampling rate of $\frac{1}{L}$. Sampling at this rate ensures that the original samples are preserved while replacing the zeros with interpolated values once the convolution is complete. Figure 3.1 and Figure 3.2 illustrate this point for oversampling by a factor of 3.

These figures illustrate how the sinc function and the upsampled signal line up. When the peak of the sinc function, $y = 1$, lines up with one of the original samples of the signal, that sample is preserved. The other samples of the signal line up with the zeros of the sinc and the other values of the sinc line up with the zeros of the signal. Therefore, that sample is mulitplied by 1 (the peak of the sinc) and is preserved. When the index shifts by one, a value is calculated to replace the zero in the upsampled signal. In essence, this process keeps the original samples intact and interpolates to find values for the zeros between the original samples. The convolution of the upsampled signal and the sinc function is performed using:

$$y(n) = \sum_{k=1}^{X+H-1} x(k) \cdot h(n-k) \tag{3.2}$$

where x and h refer to the upsampled signal and the sinc function, respectively. Also, the values X and H are the lengths of the upsampled signal and the sinc function, respectively.

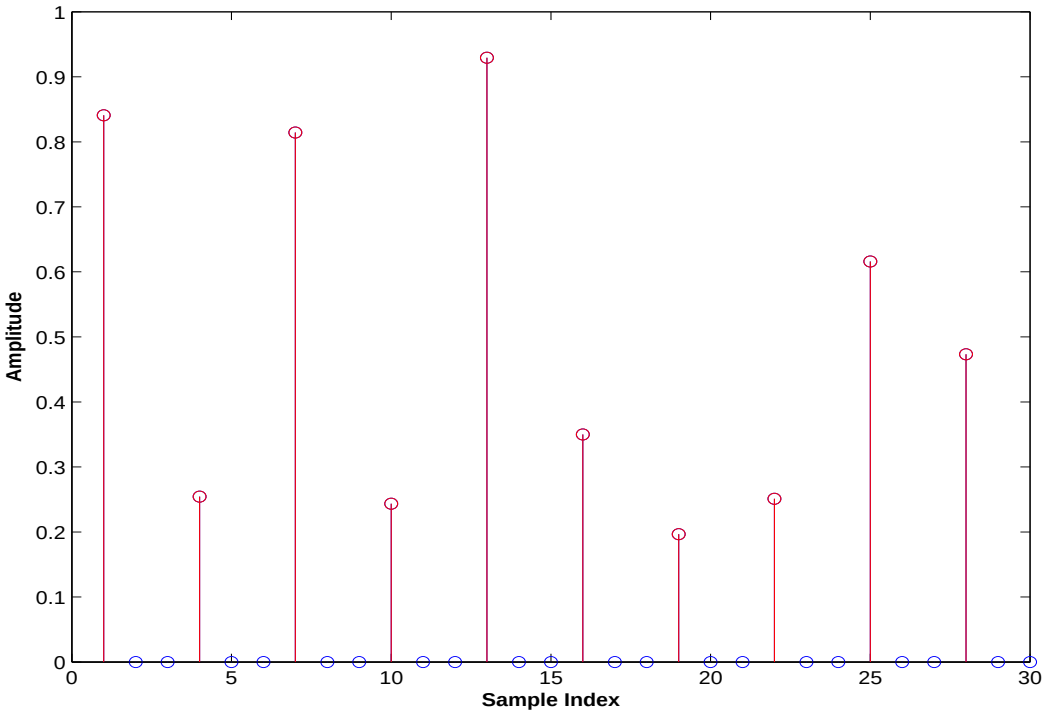

(a) Upsampled Signal of Random Numbers

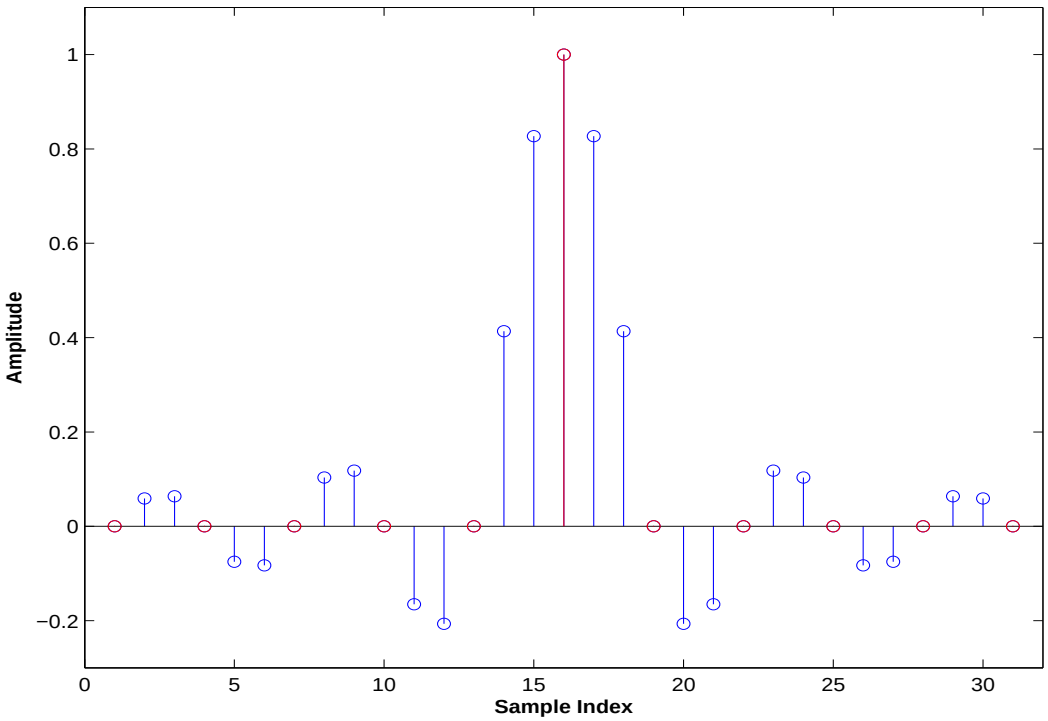

(b) Sinc Function

Figure 3.1: 3× Signal Oversampling. a) The signal of randomly generated numbers is upsampled by $L = 3$ where the original samples are highlighted in red. b) The sinc function has a step size of $\Delta = \frac{1}{L} = \frac{1}{3}$ with the points where $y = 0$ and the peak of the sinc are highlighted in red.

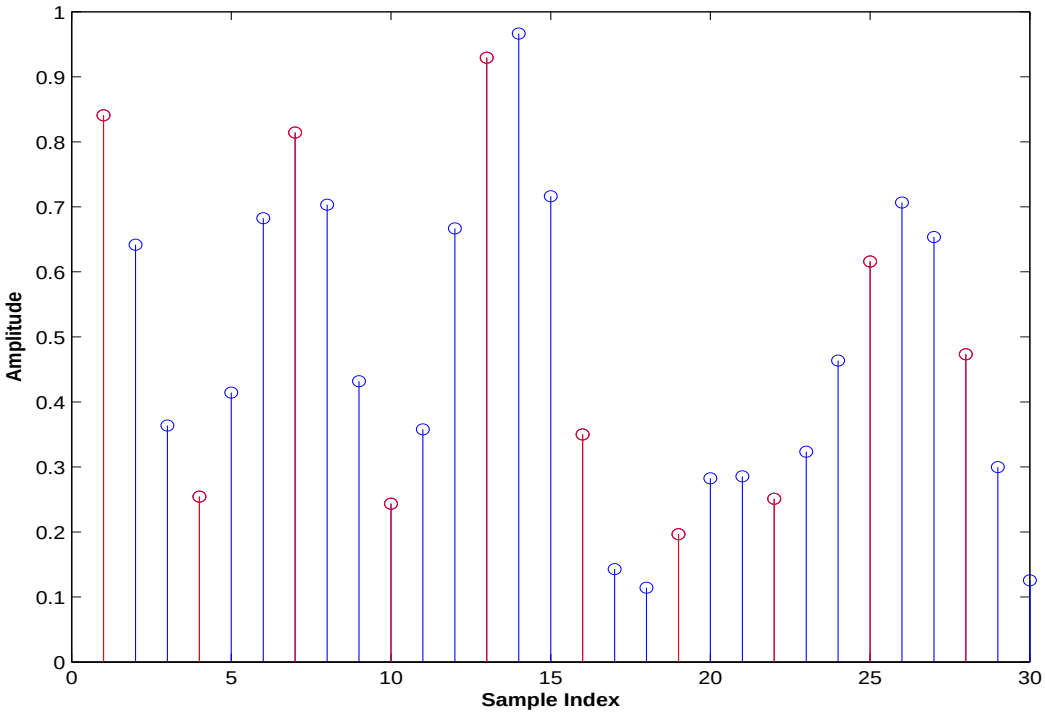

Figure 3.2: Plot of a 3× oversampled signal where the original samples are highlighted in red.

All equations derived in the following sections are shown for the case of no oversampling. If oversampling is involved, parameters such as cyclic prefix length, data length, symbol length, and delay must all be multiplied by L to compensate.

3.3 Multipath Model

The propagation effects of multipath are implemented by using a two ray model. Figure 3.3 illustrates the delay profile of the ray model used in this research. It consists of two elements, a LOS signal and a multipath signal which arrives with some delay and a smaller amplitude than the LOS signal. The LOS signal takes a direct path and therefore arrives first. The multipath signal reflects off some surface which attenuates the signal and results in a loss of power while taking longer to arrive (non-direct path). The reflected signal amplitude, designated as σ_z, is shown in relation to the normalized amplitude of the LOS signal, which is 1.

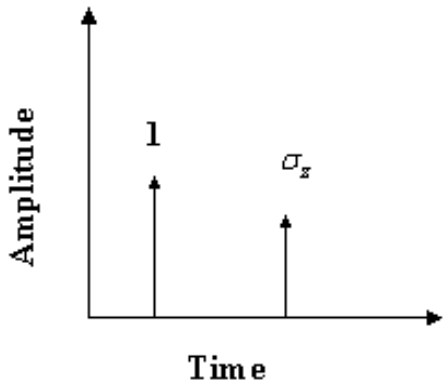

Figure 3.3: Delay Profile. The multipath delay profile includes a LOS signal with an amplitude of 1 and an attenuated, delayed reflection with an amplitude of σ_z.

The multipath signal strength is controlled during simulations by varying the input σ_z, which represents the standard deviation of each quadrature component in the reflected signal. The higher the value, the greater the standard deviation and the more disruptive the multipath signal is to the LOS signal, and vice versa. The multipath signal is expressed as:

$$z = (x + jy)\sigma_z \tag{3.3}$$

where

$|z| \sim$RAYLEIGH(σ_z)
$\angle z \sim$UNIFORM$[0, 2\pi]$
$x, y \sim$NORMAL$(0, 1)$

The variable σ_z is taken directly from the model in Figure 3.3 and the values x and y are independently generated using the *randn* function in `Matlab`® . The magnitude of the multipath signal, $|z|$, is Rayleigh distributed [22].

The multipath signal is combined with the LOS signal by convolving the LOS signal with the vector below:

$$h[n] = [1 \ \mathbf{d} \ \mathrm{z}] \tag{3.4}$$

where the value 1 is the normalized LOS signal amplitude from Figure 3.3, **d** is a vector of zeros with a length of $delay - 1$, and z is generated by Equation (3.3). As a result of this convolution operation, the transmitted signal is multiplied by z which attenuates it to form the multipath signal by changing the amplitude and phase. The multipath signal is then added to the LOS signal starting at *delay* samples to produce the combined signal.

3.3.1 OFDM Receiver. Once the signal arrives at the receiver via a multipath channel, noise is added to the signal using the `Matlab®` *AWGN* function. This function measures the power of the incoming signal and adds the appropriate level of noise in order to achieve the specified SNR. Next, the symbol boundary correlator attempts to find the boundary of the first symbol in the received signal. It does so by using Equation (3.5), which correlates the cyclic prefix with the samples at the end of the symbol from which it was copied [3]. Recall that N is the number of data samples and ν is the number of samples in the cyclic prefix.

$$R_{rx}(m) = \sum_{k=m}^{m+\nu-1} y_{rx}(k) \cdot y_{rx}^{*}(k+N) \tag{3.5}$$

It is also possible to rewrite Equation (3.5) using a vector dot product as follows [3].

$$R_{rx}(m) = \left[\; y_{rx}(m), \;\; y_{rx}(m+1), \; \ldots \; , \; y_{rx}(m+\nu-1) \; \right] \bullet \begin{bmatrix} y_{rx}(m+N) \\ y_{rx}(m+N+1) \\ \vdots \\ y_{rx}(m+N+\nu-1) \end{bmatrix}^{*} \tag{3.6}$$

In Equations 3.5 and 3.6, m is the sample index and the subscript rx identifies the receiver. This correlation calculation basically takes the first sixteen samples and correlates the sequence with samples 65 through 80. Then it adds one to the index and correlates samples 2 through 17 with samples 66 through 81. The process continues until the second sequence reaches the end of the signal. In an ideal environment (no

noise or multipath), correlation peaks will occur where each symbol begins because the cyclic prefix will correlate highly with the data it was copied from at the end of the symbol. In a plot of $R_{rx}(m)$ each peak will be separated by $N+\nu$ samples. When noise and multipath are added, however, the peaks may not always be at the correct locations.

Equations (3.7) and (3.8) below are the mathematical expressions used to determine individual maximums per symbol and then averaging them over the total number of symbols.

$$\hat{\delta}_{rx} \cong \arg \max_{1 \leq m \leq (N+\nu)} \Re \{\mu_{R_{rx}}(m)\} \tag{3.7}$$

where $\Re\{\bullet\}$ is the real portion of $\{\bullet\}$ and

$$\mu_{R_{rx}}(m) = \frac{1}{A-1} \sum_{k=1}^{A-1} \sum_{i=m+1}^{m+\nu} y_{rx}((N+\nu)k+i) \cdot y_{rx}^{*}((N+\nu)k+i+N) \tag{3.8}$$

In the above equations, A is a predetermined length of the received signal in symbols. For this thesis $A = 512$ symbols. The averaging in Equation (3.8) is a necessary step in order to get a more accurate estimate of the sample shift from the symbol boundary correlator described in Equation (3.5) [3]. The idea behind averaging is that the first symbol boundary is within the first $N + \nu = 80$ samples of the received signal. If found correctly, the next symbol boundary should occur 80 samples later, and so on. The averaging equation takes the entire correlation value vector, divides it into sections 80 samples in length, and then adds the sections together to get one section of 80 samples. The value which occurred in a majority of the symbols is enhanced while the false peaks can be rooted out, since the algorithm uses all available symbols. Figure 3.4 shows an example of the averaged correlation vector where the index of the first symbol was set to 20 samples [3]. The first graph shows the correlation results for 10 symbols and marks the indexes of the peaks. It is clear that the peaks are not always 80 samples apart and the first peak is at 19 samples. The second graph

depicts the averaged correlation vector. The averaged results put the first peak at 20 samples which is the correct index.

The maximum value of the averaged correlation vector, $\hat{\delta}_{rx}$, is defined as the number of samples which need to be removed to arrive at the first symbol boundary. These samples are removed from the beginning of the received signal vector to align the signal with the symbol boundary while $N + \nu - \hat{\delta}_{rx}$ samples are removed from the end of the vector in order to have an integer number of symbols. Now that the signal is aligned to the symbol boundary, the feature correlation process can be implemented to determine the difference in symbols between the mobile and reference receivers [3].

3.3.2 Symbol Features. Velotta tested the performance of using statistical features about each symbol to correlate two signal responses [3]. The statistical features tested were mean, variance, skewness, kurtosis, standard deviation, PAPR, and RMS value. These eight statistics were calculated for each symbol in both the time and frequency domains, which allowed for 16 different cases. Velotta's research concluded that statistics from the time domain response performed better than its frequency domain counterpart in correctly determining the correlation between the two received signals. The statistics are ranked below from best performance to worst [3]:

1. Mean (1^{st} Moment)
2. Average Symbol Phase
3. Root-Mean-Squared (RMS)
4. Variance (2^{nd} Moment) and Standard Deviation
5. Peak-to-Average Power Ratio (PAPR)
6. Skewness (3^{rd} Moment)
7. Kurtosis (4^{th} Moment)

This research uses the top three performing statistics for the feature correlation process. These are the time domain calculations for mean, phase, and RMS. In

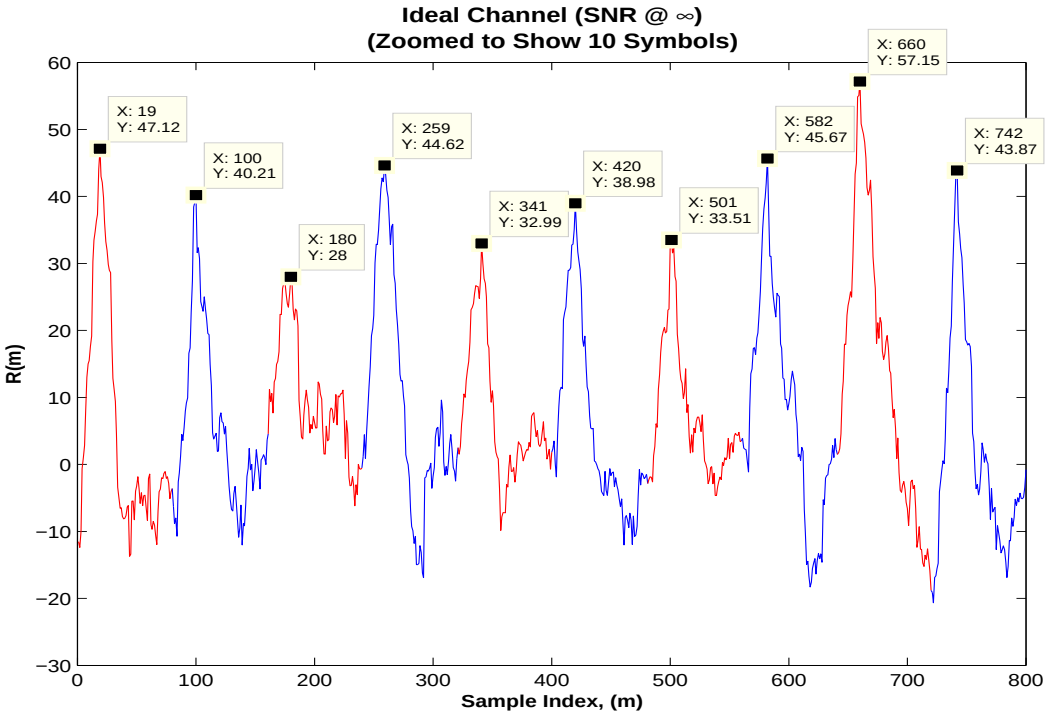

(a) Symbol Boundary Correlator Results

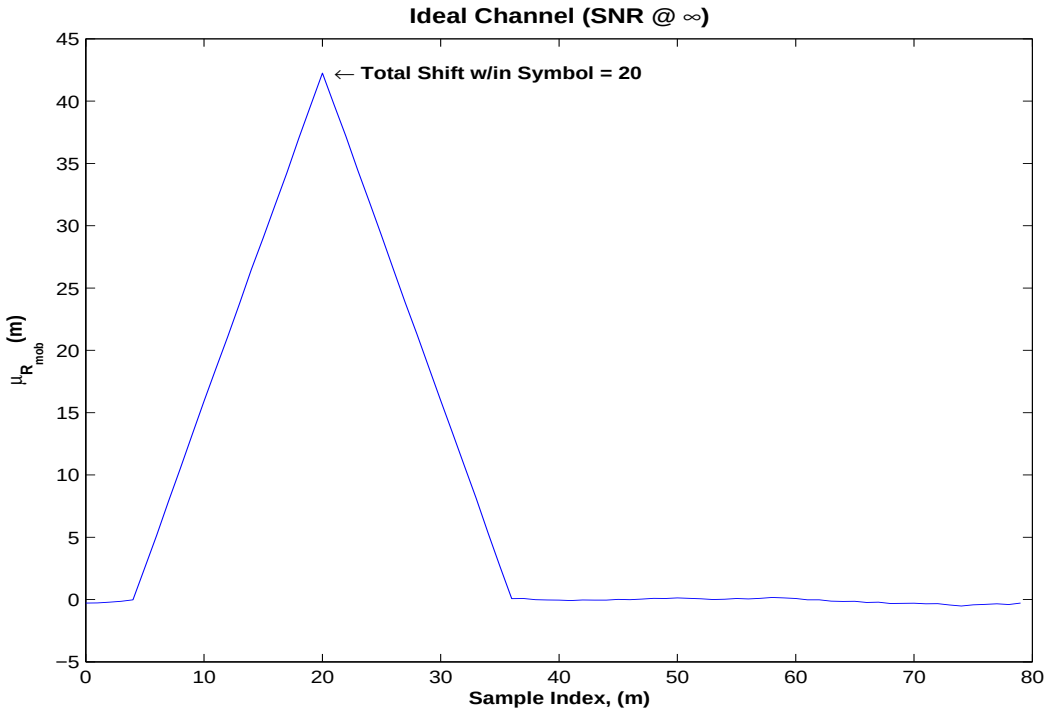

(b) Averaged Symbol Boundary Correlator Results

Figure 3.4: a) Graph of symbol boundary correlation results with the index of each peak. The alternating colors represent 10 different symbols of the received signal. b) Graph of the averaged symbol boundary correlation vector [3].

addition, another time domain statistic was added and is referred to as the mini-mean. Below are the equations used to calculate these statistics:

1. *Mean:* (1^{st} Moment)

$$\mu_{rx}(k) = \frac{1}{M}\sum_{i=1}^{M} y_{rx}(Mk + i + \hat{\delta}_{rx}) \tag{3.9}$$

2. *Average Symbol Phase:*

$$\Phi_{rx}(k) = \arctan\left[\frac{\sum_{i=1}^{M} Im\left(y_{rx}(Mk + i + \hat{\delta}_{rx}\right)}{\sum_{i=1}^{M} Re\left(y_{rx}(Mk + i + \hat{\delta}_{rx}\right)}\right] \tag{3.10}$$

3. *Root-Mean-Squared:*

$$RMS_{rx}(k) = \sqrt{\frac{1}{M}\sum_{i=1}^{M}\left(y_{rx}(Mk + i + \hat{\delta}_{rx}) - \mu_{rx}(k)\right)^2} \tag{3.11}$$

4. *Mini-mean:*

$$\overline{\mu}_{rx}(k) = \frac{1}{2\nu}\left(\sum_{i=1}^{\nu} y_{rx}(Mk + i + \hat{\delta}_{rx}) + \sum_{i=N+1}^{M} y_{rx}(Mk + i + \hat{\delta}_{rx})\right) \tag{3.12}$$

where $M = N + \nu$ [3].

The mini-mean equation takes the mean of the vector containing only the 16 cyclic prefix samples and the 16 data samples from which it was copied. Therefore, the length of the vector becomes 32 samples, not the 80 samples characteristic of the OFDM symbol. It was chosen because of its theoretical advantage in SNR over the mean. To demonstrate this advantage, a comparison between the two is demonstrated

below. The mean is theoretically computed as follows [23]:

$$\begin{aligned}\mu_{ref}(k) &= \frac{1}{M}\sum_{i=1}^{M} x(Mk+i) + \frac{1}{M}\sum_{i=1}^{M} n_{ref}(Mk+i) \\ &= X(k) + N_{ref}(k) \\ \mu_{mob}(k) &= \frac{1}{M}\sum_{i=1}^{M} x(Mk+i) + \frac{1}{M}\sum_{i=1}^{M} n_{mob}(Mk+i) \\ &= X(k) + N_{mob}(k)\end{aligned} \tag{3.13}$$

where k is the symbol index which spans all of the symbols in the received signal. By applying the central limit theorem, $X(k)$, $N_{ref}(k)$, and $N_{mob}(k)$ become approximately Gaussian with zero mean and have variances as follows [23]:

$$\begin{aligned}\sigma_X^2 &= \frac{M+2\nu}{M^2}\sigma_x^2 \\ &= \frac{1+2\nu/M}{M}\sigma_x^2\end{aligned} \tag{3.14}$$

$$\sigma_{N_{ref}}^2 = \frac{1}{M}\sigma_{ref}^2 \tag{3.15}$$

$$\sigma_{N_{mob}}^2 = \frac{1}{M}\sigma_{mob}^2 \tag{3.16}$$

where the term 2ν in Equation (3.14) accounts for the correlation of the last ν samples of a symbol with the cyclic prefix. The mini-mean is very similar to the mean, except that only the first and last ν samples are correlated with each other. Therefore, the variances become [23]:

$$\begin{aligned}\sigma_X^2 &= \frac{2\nu+2\nu}{(2\nu)^2}\sigma_x^2 \\ &= \frac{2}{2\nu}\sigma_x^2\end{aligned} \tag{3.17}$$

$$\sigma_{N_{ref}}^2 = \frac{1}{2\nu}\sigma_{ref}^2 \tag{3.18}$$

$$\sigma_{N_{mob}}^2 = \frac{1}{2\nu}\sigma_{mob}^2 \tag{3.19}$$

When comparing the mini-mean to the mean, the "feature SNR" σ_X^2/σ_N^2 improves by a factor of $2/(1+2\nu/M)$, which is about 1.4 to 2 for typical OFDM systems. This improvement is the reason that the mini-mean was chosen [23].

3.3.3 Symbol Feature Correlator. Once both receivers calculate the statistical data, the reference receiver transmits the data to the mobile receiver in order to perform the correlation calculations. Recall that the symbol boundary correlator used all received symbols to determine the symbol boundary. This is because Velotta sought to prove the effectiveness of the feature correlator, not the symbol boundary correlator. Therefore, all available data was used to try to correctly identify the symbol boundary, because an error in the symbol boundary estimation will have a direct effect on the feature correlation. Velotta's feature correlator, however, used several different "window sizes" with which to perform the correlation process. The window sizes limited the amount of data used in the correlation process by selecting data for a specified number of symbols from the reference receiver's data and only using that data. The selected data is for successive symbols and is taken from the middle of the vector of statistical data. This research limits the window size to $K = 10$ and $K = 100$ symbols worth of data in order to reduce excessive processing power required by the receiver. The following algorithm is used to compute the feature correlations for a window size of K:

$$\hat{R}_F(m) = \sum_{k=1}^{K} \left[f_{ref}(k) - \mu_{f_{ref}}(1) \right] \cdot \left[f_{mob}(k+m) - \mu_{f_{mob}}(1+m) \right]^* \tag{3.20}$$

where

$$\mu_{f_{rx}}(n) = \frac{1}{K} \sum_{i=n}^{(K)+n-1} f_{rx}(i) \tag{3.21}$$

The selection window is set to select data from symbol 256 to symbol $256 + K - 1$ from the reference receiver. This data is then correlated with a section of data from the mobile receiver using Equation (3.20). Since the maximum shift of each signal is set to $D = 100$ symbols in either direction, the maximum symbol difference between

the two receivers is $\pm D$. With a buffer of two symbols added to each end, the mobile receiver data section stretches from symbol $256 - D - 2$ to symbol $256 + K - 1 + D + 2$ for a total of $204 + K$ symbols. The expression for the symbol difference estimate between the two receivers is expressed below:

$$\Delta_{Symbol} = \arg \max_{-D \leq d \leq D} \Re \left\{ \hat{R}_F(d) \right\} \tag{3.22}$$

where d is the index of the correlation calculations. The index, though, must be adjusted to correspond with the symbol numbers. This is accomplished by simply taking $d - D - 1$ to find the appropriate number of the difference in symbols between the two receivers. If the number is negative, then the mobile receiver received the signal before the reference. This information implies that the mobile receiver was closer to the transmitter than the reference receiver. The opposite is true if the number is positive [3].

The peaks in the RMS feature correlation results were not as prevalent as those of the other statistical features. Therefore, it was necessary to filter the results using a second-order differential filter to better interpret the correlation peaks. This filter is designed to highlight amplitude changes between sequential samples. It was implemented by convolving the unfiltered correlation data with [-1, 2, -1] [3].

3.4 TDOA Calculations

With the values obtained from the two correlation algorithms, the TDOA measurement between the reference and mobile receivers can be calculated using:

$$\delta_{Sample} = \hat{\delta}_{mob} - \hat{\delta}_{ref} \tag{3.23}$$

$$TDOA_{OFDM} = (\delta_{Sample} + M\Delta_{Symbol}) \cdot T_{samp} \tag{3.24}$$

where $T_{samp} = 50$ ns for the case of no oversampling, δ_{Sample} is the difference between the symbol boundary correlation indexes at the two receivers, and Δ_{Symbol} is the

peak of the feature correlation. Equation (3.24) uses the peak estimations from the correlation calculations in order to find the difference in arrival times between the two receivers. This value can be multiplied by the speed-of-light to obtain a range estimate of the difference in ranges of the two receivers with respect to the transmitter. Since the reference receiver is at a known location and, therefore, its distance from the transmitter is known, a range estimate from the mobile receiver to the transmitter is now available. This is done by adding the true distance from the reference receiver to the transmitter to the range difference between the two receivers.

3.5 Summary

This chapter details the OFDM system simulator and its functions. The system input parameters which control the simulation were described. Also, the difference between the two correlation functions being performed was highlighted. This information is key to understanding the results of the simulations, which are detailed in Chapter IV.

IV. Simulation Results and Analysis

This chapter presents the results of the OFDM system simulations conducted during the course of this research and gives an analysis of the effects of multipath and oversampling. Also, the feature correlator performance is discussed along with the TDOA calculation method. Results are displayed for different transmitter and receiver setups. Finally, a summary of the results are given. Only the results necessary to convey a specific point are shown in this section. However, Appendix A contains the entire set of data collected during this research.

4.1 Simulation Specifications

There are several variables which needed to be set before the simulations could be run. These variables are listed in Table 4.1 and discussed in greater detail below.

Table 4.1: OFDM Simulation Input Parameters.

Parameter	**Variable**	**Value**
Data Length	$data\ \ length$	$64 * L$ samples
Cyclic Prefix Length	$CP\ \ length$	$16 * L$ samples
Symbol Length	$symbol\ \ length$	$(16 + 64) * L$ samples
Oversampling Factor	L	1×, 3×, and 9×
Multipath Factor	σ_z	0 to 0.9 in steps of 0.1
Multipath Delay	$delay$	$1 * L$, $10 * L$, $20 * L$, and $30 * L$ samples
Window Size	K	10, 100 symbols
SNR	SNR	-20, -10, 0, and 10 dB

4.1.1 Signal Parameters. For this research, the number of data samples per symbol is set to 64 and the cyclic prefix length is set to 16. The total OFDM symbol length is, therefore, is 80 samples. These values are made consistent with Velotta's [3] to enable expansion of his research. The symbol period is 4 μs according to the IEEE 802.11 standards [16] and the sample period becomes 50 ns ($4\mu s/80$). The signal length is set to 512 symbols in order to reduce the computational load which would occur if 2048 symbols were used as in [3], since the oversampling and multipath calculations performed here significantly increase the processing time and

complexity. These numbers remain constant throughout all simulations, except in the case of oversampling, which will be discussed shortly. The SNR at the receivers varies from -20 dB to 10 dB in steps of 10 dB. In an effort to limit the number of simulations, cases involving multiple receivers have the same SNR. The channel characteristics, however, are unique to each receiver. Therefore, the input variables of the multipath channel are different for each receiver in the same simulation.

4.1.2 Oversampling Parameters. For the oversampling process, the upsample factor, L, was set to 1, 3, and 9. Oversampling the signal effectively increases the number of total samples, data samples per symbol, and the cyclic prefix length by a factor of L. The length of the signal, however, remains at 512 symbols. The window size, K, was set to 10 and 100 symbols in order to keep computations performed by the receiver at a reasonable level since the window size limits the amount of data from the reference receiver which is used in the feature correlation process. Another point to consider is that the window size will affect the TDOA accuracy when the mobile receiver is moving. The larger the window size, the longer it takes the receiver to collect those symbols and transmit to the reference receiver. For a fast moving vehicle or aircraft, the position estimate may no longer be relevant because the vehicle would be a significant distance away by the time it was calculated [3].

4.1.3 Multipath Parameters. The variables needed to produce a specific multipath channel are σ_z and the delay of the reflected signal. The variable σ_z denotes the variation of power in the reflected signal. This variable ranges from 0 to 0.9 in steps of 0.1, where a value 0 implies there is no multipath reflection and a value of 0.9 implies a reflection almost as strong as the LOS signal. If the reflected signal has the same power as the LOS signal, it is assumed that the LOS signal has lost power during transmission from passing through an absorbent material. The delay of the reflected signal was chosen arbitrarily and its units are the number of samples it is delayed with respect to the time the LOS signal was received. The values chosen were $1 * L$, $10 * L$, $20 * L$, and $30 * L$ samples. These values were chosen in order to identify

the effects of reflected signals with short and long delays on both of the correlation processes. These short and long delays were chosen based on the cyclic prefix length and are not representative of a specific environment. Note that the first two values are shorter than the cyclic prefix length, and the last two values are longer.

For this research, the reference receiver is assumed to be in an optimized location, which is defined here as an open area with few obstacles (reflecting surfaces) and a LOS to the transmitter. The location has low multipath and, therefore, $\sigma_z = 0.2$ for the reference receiver unless the mobile receiver has a smaller σ_z value. In this case only, the reference receiver is assigned the same value as the mobile receiver. This is done because of the assumption that the reference receiver is in an optimized location, and it is assumed that if the reference receiver experiences a value less than 0.2, then the reference receiver will also experience this low multipath environment. The delay value for the reference receiver is picked at random from the set of values listed above. On the other hand, the mobile receiver cycles through all combinations of σ_z and *delay* during the simulations.

4.2 Types of Errors

There are three types of errors considered here which are directly related to the OFDM algorithm and one which is not. The fourth error occurs in the physical receiver and is important to address with the simulation based errors, because of its contributions to the magnitude of the errors affecting the accuracy of the TDOA calculations. These four errors and their individual effects on the OFDM algorithm and/or TDOA calculation accuracy are discussed below.

4.2.1 Measurement Noise. The first type of error is referred to as "measurement noise." This error occurs when the symbol boundary correlator is tracking the correct peak but chooses the wrong value within the vicinity of the correct peak due to noise. A threshold was set for determining this error in the symbol boundary correlation calculations. For this research, it is assumed that an error up to, and

including, $\pm L$ samples is considered a correct identification of the correlation peak. The reason behind this is that most of the energy in the sinc function (described in Section 3.2 is located within the region between the zero crossings on either side of the peak and is strong enough to cause an error. Therefore, these errors are attributed to measurement noise, and the larger errors, due to tracking the wrong peak, are attributed to non-LOS errors (as described in the next section). Note that multipath reflections with a delay of 1 sample fall within this range. This case is still identified as measurement noise, however, because the main peak is presumably still the dominant factor.

4.2.2 Non-LOS Error. The next type of error is due to the multipath reflection and is referred to as a non-LOS error. This error results from the symbol boundary correlator selecting the multipath signal instead of the LOS signal. The process for determining the peak, as described in Section 3.3.1, finds peaks in the received signal for 80 samples of data at a time. Each 80 sample section is added together and then averaged to find the main peak. As a result, this method restricts the magnitude of the largest error to 80 samples for the case of no oversampling. This process synchronizes the receiver to the edge of the symbol. Once the synchronization occurs correctly, TDOA measurements can be taken without non-LOS errors using this synchronized signal.

4.2.3 Ambiguity Resolution Failure. The third type of OFDM algorithm error is referred to as an ambiguity resolution failure. This occurs as a result of the feature correlator selecting the wrong index, meaning that it has selected the wrong symbol. An error of this type is at least one symbol and is only limited by the window size and D. As a result, this proves to have the largest error magnitude. An error of just one symbol translates into a distance error of 1.2 km. It is assumed that an error of this size or larger will be relatively easy to identify and discard when TDOA measurements are taken.

4.2.4 Receiver Sampling Algorithm Error. In addition to the three errors listed above, there is another error to consider which is not directly related to the OFDM algorithm, but rather the receiver itself. This error is a result of the way the receiver samples the incoming signal. The receiver doesn't always sample the signal at the exact time it should in order to get the original transmitted samples. It varies with some tolerance when sampling the signal. The maximum sample timing error without oversampling is $\pm\frac{1}{2}$ of a sample off with respect to the actual data sample. An error of $\frac{1}{2}$ sample (without oversampling) translates into a distance error of 7.5 meters. An error of this magnitude is a major concern when trying to match the sub-meter accuracy of GPS for military purposes. Oversampling reduces this error since it creates intermediate samples between the original samples. Oversampling the signal by $3\times$ reduces the error by a factor of $\frac{1}{3}$ to 2.5 meters. Likewise, oversampling the signal by $9\times$ reduces the error by a factor of $\frac{1}{9}$ to 0.83 meters. It is identified as an error source but not researched as part of this thesis.

4.3 Baseline Setup: One Receiver

The baseline setup consists of the transmitter and a single receiver and was designed in order to characterize the effects of the multipath channel on the symbol boundary correlation method. A simulation was run which encompassed varying combinations of SNR, σ_z, the delay of the reflected signal ($delay$), window size (K), and the oversampling factor (L). Each case was run 1000 times to determine the error characteristics of the correlation process. A case is a single combination of the above mentioned variables.

The probability of error serves as an indicator of the performance of the symbol boundary correlation process. The results are shown for both the mobile and the reference receiver, but more attention is given to the results for the mobile receiver, since it covers all possible cases regarding multipath. The reference receiver covers only low multipath conditions, and the results are provided in an effort to paint a

complete picture since these results factor into the feature correlation results discussed later (see Section 4.4).

4.3.1 Transmitter - Mobile Receiver. This section provides results for the data taken at the mobile receiver. The analysis is broken up into two parts. The first part is a look at how the SNR, multipath parameters, and the oversampling factor individually affect the measurement error. The second part is a broad look at the errors themselves and how they relate to the distance error that would come from a TDOA measurement. After that, some of the key observations will be given.

4.3.1.1 Effects of Parameters. Figure 4.1 shows the probability of error, $P_{e_{symbol}}$, of the symbol boundary correlator plotted versus the multipath factor, σ_z, for the case with no oversampling ($L = 1$) and SNR = -20 dB (top) and SNR = -10 dB (bottom). The top graph shows that all cases have greater than an 80% probability of error for SNR = -20 dB. When the SNR is increased to -10 dB, the errors are dramatically reduced. Therefore, the SNR can have a significant effect on the probability of error in the symbol boundary correlation process. Simply increasing the SNR, however, reaches a point of diminishing returns. A SNR significantly higher than -10 dB does not greatly improve the probability of error. Figure 4.2 shows the graphs of probability of error for SNRs of 10 and 40 dB. By comparing these to the graph for SNR = -10 dB, it is evident that they are similar and simply increasing the SNR does not necessarily improve results. It implies that there is a limitation to the effect SNR has on the performance of the symbol boundary correlator and other factors need to be considered.

A minimum of SNR = -10 dB is determined to be the threshold for normal operation of the symbol boundary correlator. Lower SNRs yield a worse performance and higher SNRs yield roughly the same performance. The results for SNR = 10 dB, though, will be primarily discussed from here on because, as will be shown later, the feature correlator requires a minimum of SNR = 10 dB for normal operation. Remember that the specified SNR of the received signal is the same in both correlation

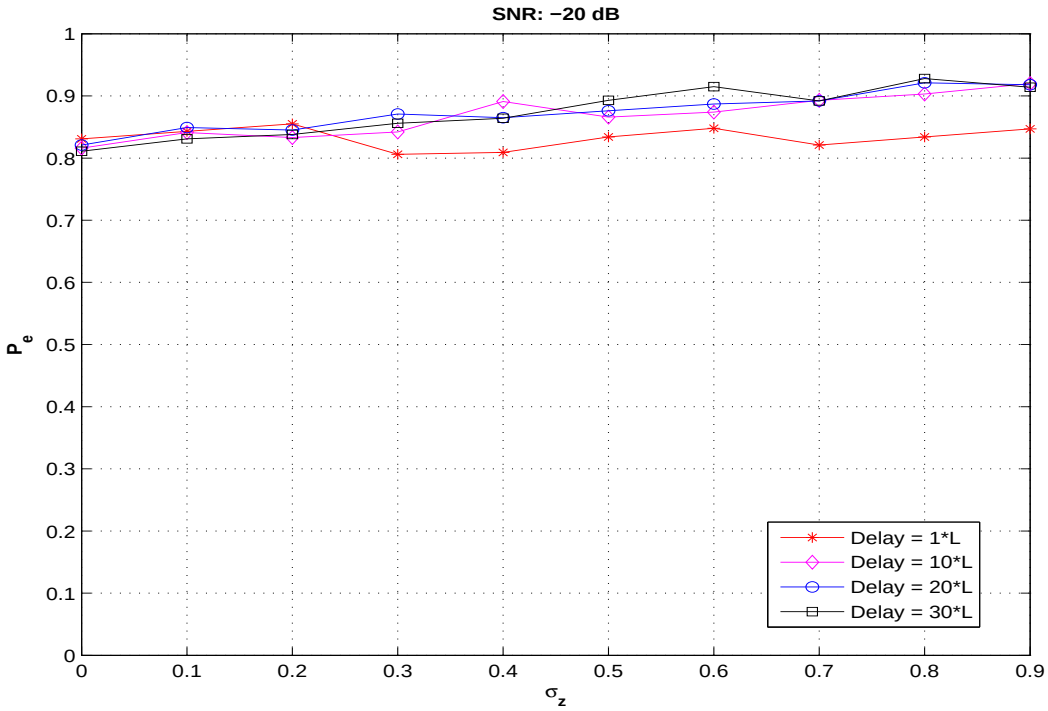

(a) $P_{e_{symbol}}$ Graph for SNR = -20 dB

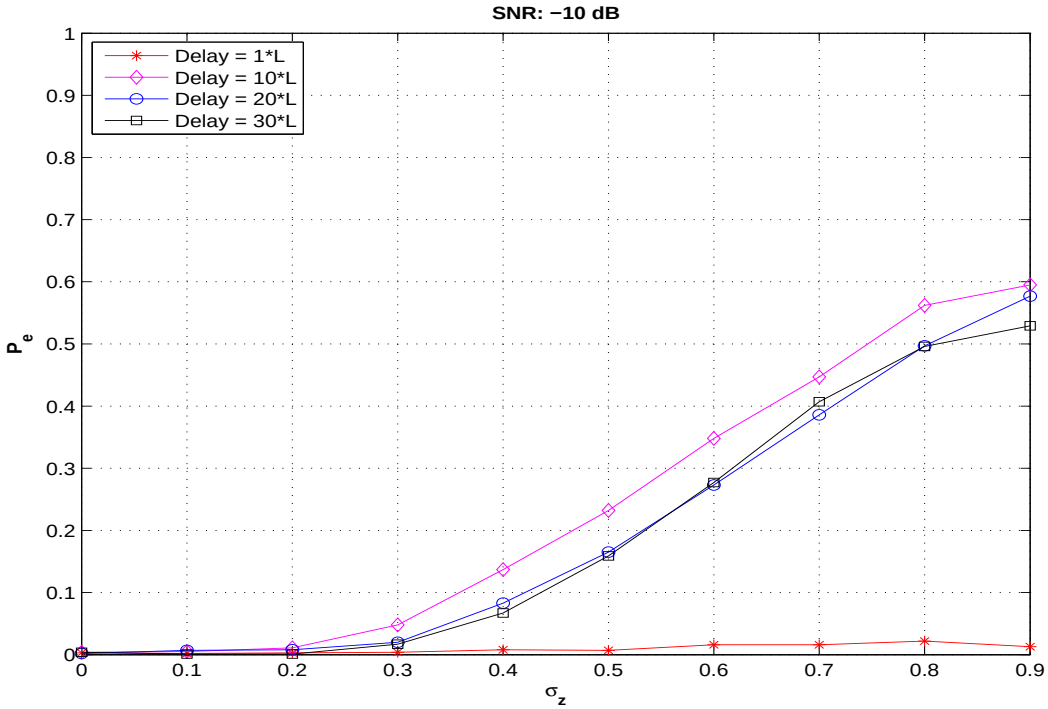

(b) $P_{e_{symbol}}$ Graph for SNR = -10

Figure 4.1: Graphs of $P_{e_{symbol}}$ vs. σ_z with no oversampling for: a) SNR = -20 dB b) SNR = -10 dB

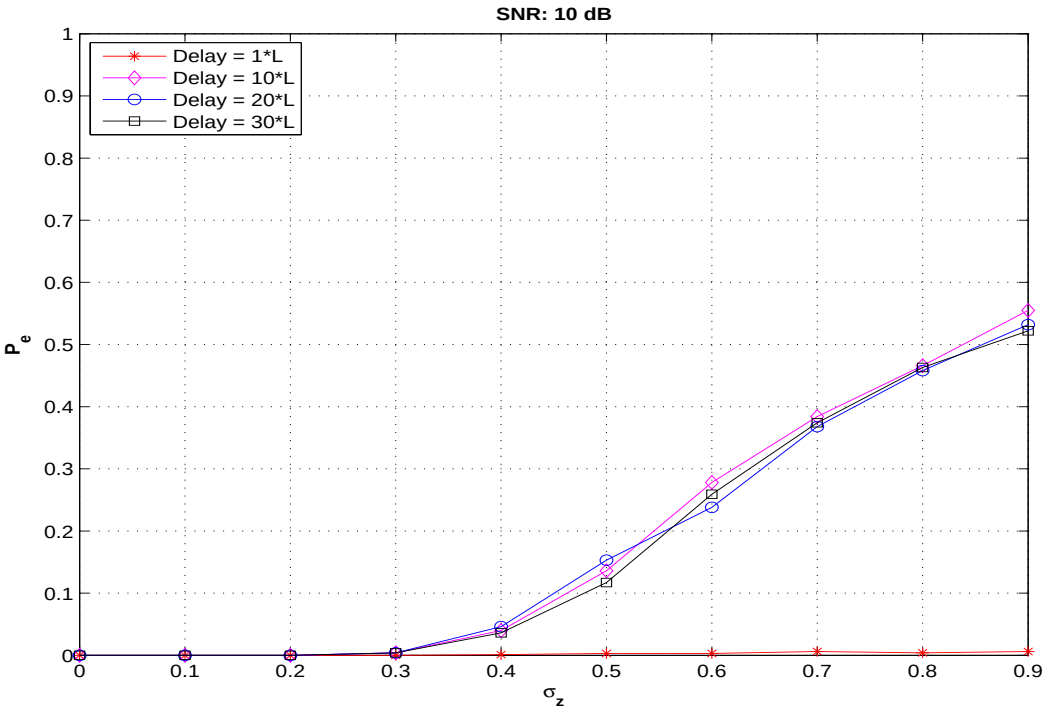

(a) $P_{e_{symbol}}$ Graph for SNR = 10 dB

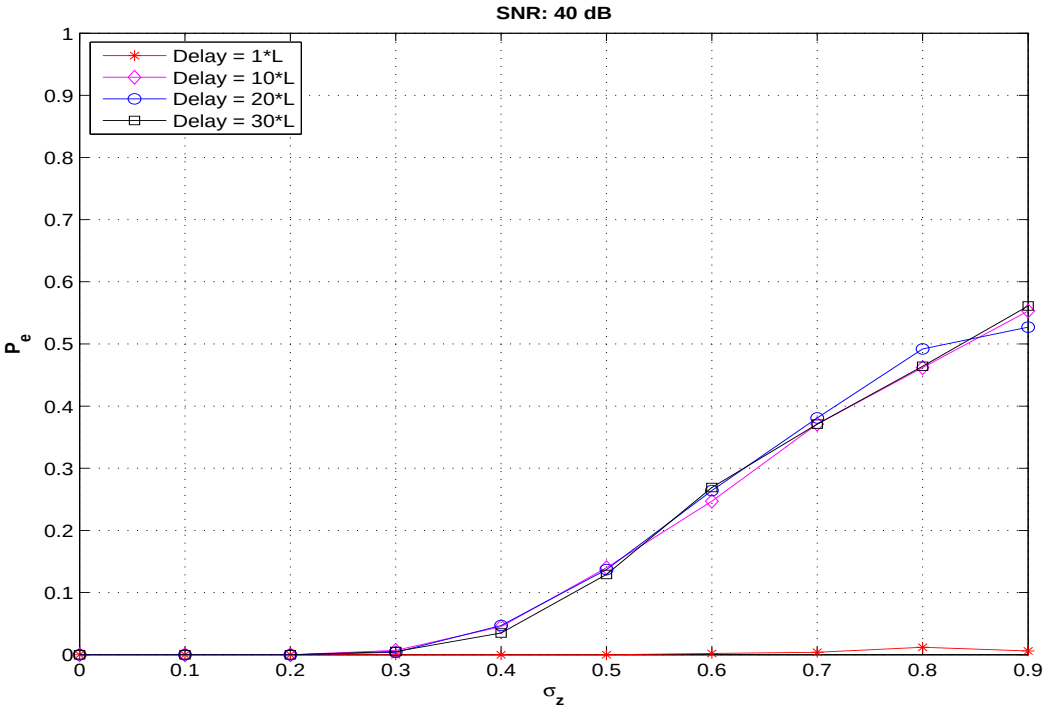

(b) $P_{e_{symbol}}$ Graph for SNR = 40

Figure 4.2: Graphs of $P_{e_{symbol}}$ vs. σ_z with no oversampling for: a) SNR = 10 dB b) SNR = 40 dB

processes. This means that for every case simulated, the SNR was constant at both the symbol boundary correlator and the feature correlator. By looking at the results for both correlation processes at the same SNR, it allows for better analysis and insight into the contributions of errors from each process.

When looking at the case for SNR = -10 dB or greater, it is clear that multipath becomes the dominant factor affecting performance. Figure 4.1b shows that the plots of the multipath delays, except for when $delay = 1$ sample, closely follow each other. This implies that the delay value doesn't affect the probability of error as much as σ_z does. From analyzing the data, it is also evident that most of the errors for $delay = 1$ sample fall within the measurement noise error category. This delay value causes very few errors outside of the threshold, but there are some. Figure 4.3, however, shows the same trials for SNR of 10 dB with the threshold removed. It clearly shows that the plots for *all* delay values follow the same trend.

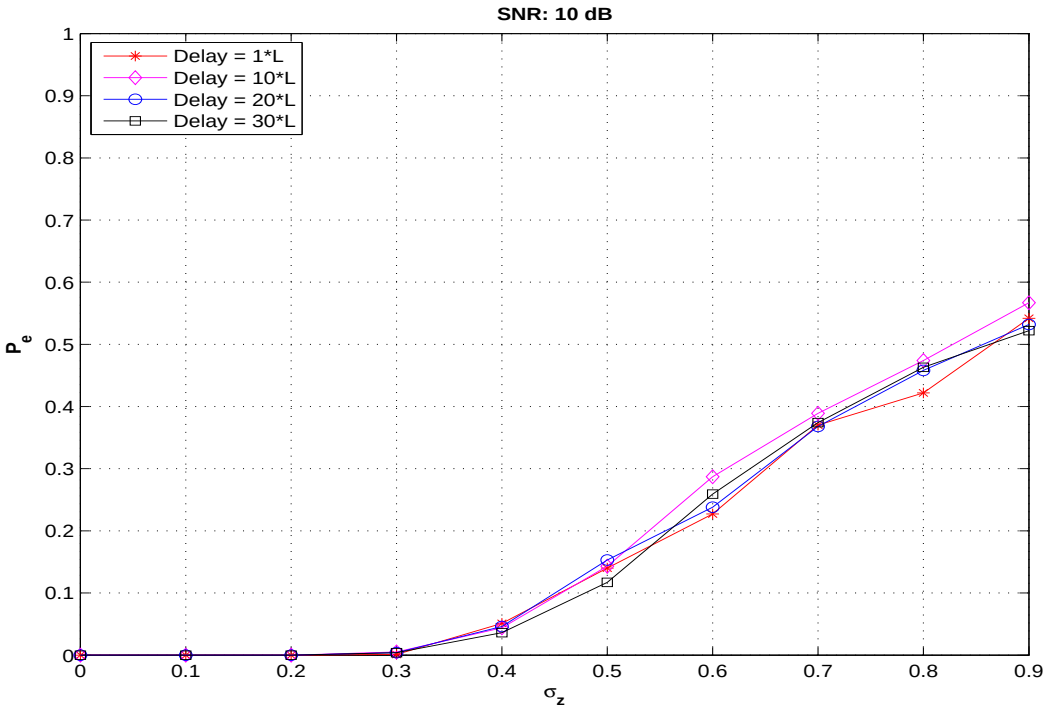

Figure 4.3: Graph of $P_{e_{symbol}}$ vs. σ_z without the error threshold for SNR = 10 dB. The correlation peak must be exact to avoid registering an error.

Figure 4.4 shows the graph of probability of error for 3× and 9× oversampling for SNR = -20 dB to illustrate the small performance gain from oversampling. At high SNRs, this effect is less noticeable. A quick comparison of these two graphs to Figure 4.1a shows that the performance improves slightly as the oversampling factor L is increased. By virtue of creating more samples, it increases the correlation SNR and, in the process, slightly improves the probability of error.

The oversampling method provides a small gain in performance at the expense of an increased computational load from creating and processing more samples. At $SNR = 10$ dB, however, there is no noticeable improvement in the probability of error. It translates into an increased effective SNR which does not improve the probability of error. The more important benefit, as far as navigation is concerned, is that the smaller sample period has the potential to yield more accurate position estimates.

4.3.1.2 Error Analysis. It is important to not only look at the probability of error in the cases described above, but to understand why those errors occurred and how they affect the TDOA measurements as well. For the case of no oversampling and $SNR = 10$ dB, the histogram in Figure 4.5 displays the distribution of the errors averaged over all delay values for an interval of one symbol, from -40 samples to 40 samples, for σ_z values of 0.4 and 0.9.

For σ_z values of 0 (no multipath), 0.1, and 0.2, no errors occur (these cases are not shown). For values of 0.3 up to 0.9, the errors generally occur in the same locations. It is apparent that the locations of the errors tend to be the same as the delay values used. This implies that the multipath signal is strong enough to fool the correlator into thinking it is the correct signal. The noise and attenuation of the signal also play a part in drawing the correlator off course. There is one exception, though, and it occurs between -10 and 0. Errors occur all along this region, not just at -10 and -1 samples. This may be due to how close the multipath signal is to the LOS signal. It is still drawing the correlator off of the correct value, but not enough to choose the multipath signal.

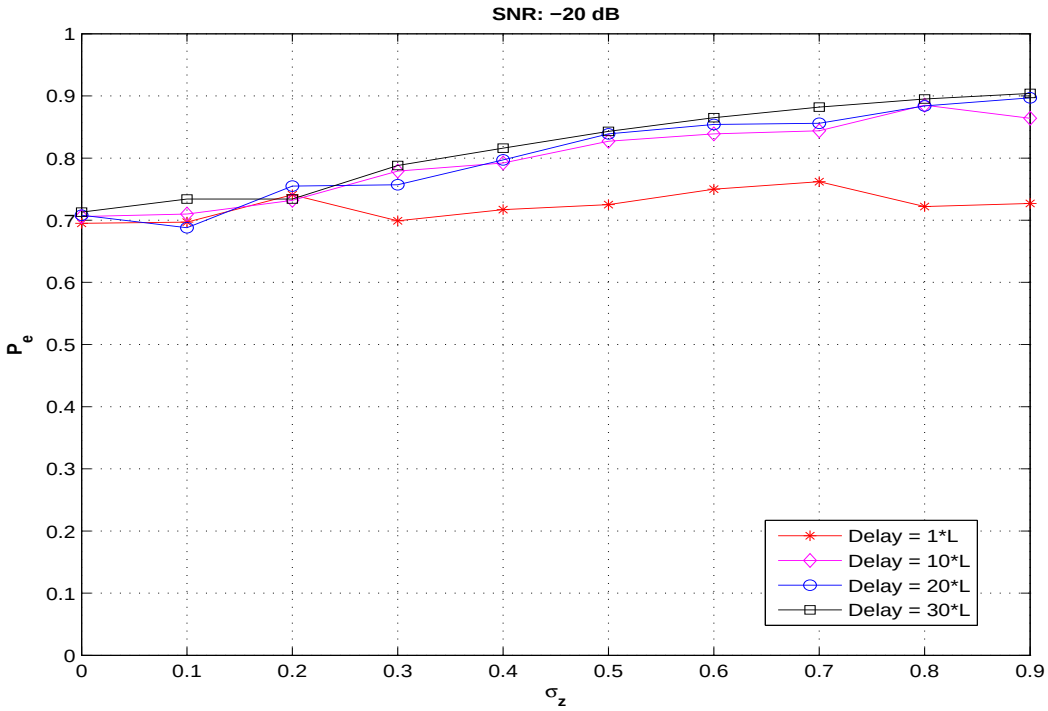

(a) $P_{e_{symbol}}$ Graph for 3× oversampling

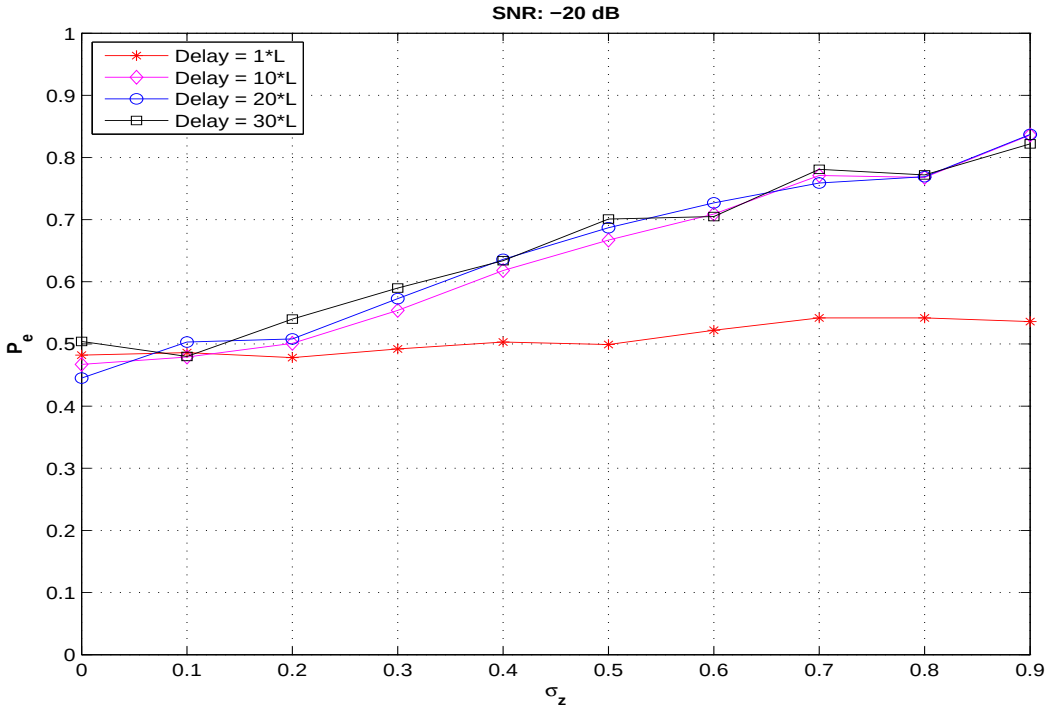

(b) $P_{e_{symbol}}$ Graph for 9× oversampling

Figure 4.4: Graphs of $P_{e_{symbol}}$ vs. σ_z for an oversampled signal with SNR = -20 dB: a) $L = 3$ b) $L = 9$

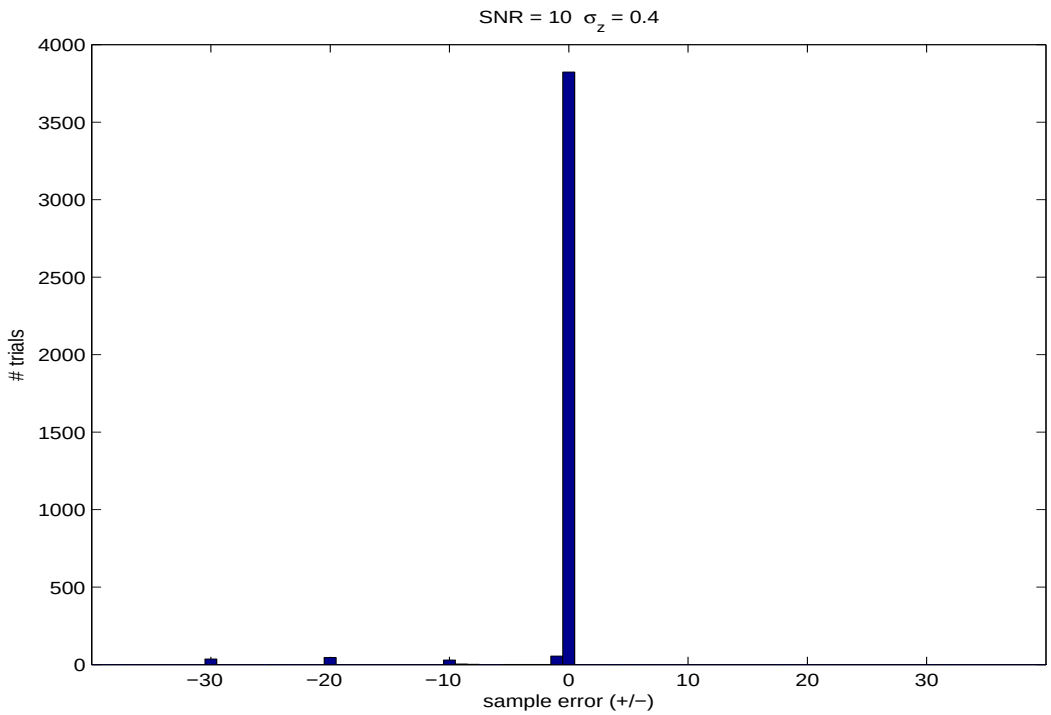

(a) $\sigma_z = 0.4$

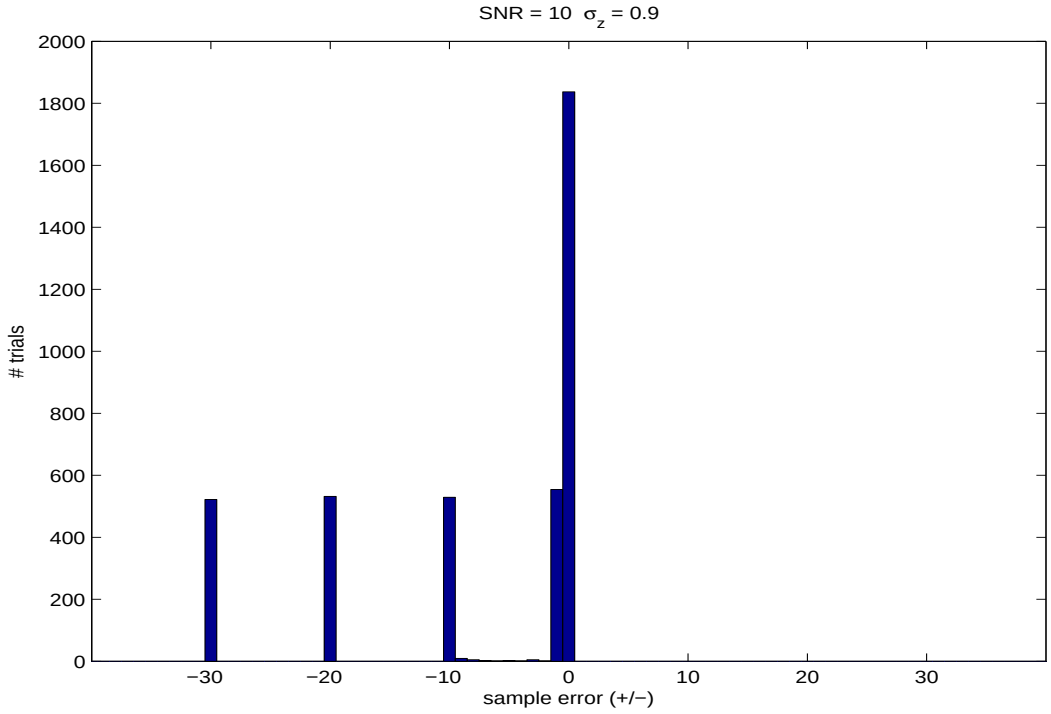

(b) $\sigma_z = 0.9$

Figure 4.5: Histograms of sample errors with no oversampling and $SNR = 10$ dB. a) $\sigma_z = 0.4$ b) $\sigma_z = 0.9$

Another factor to look at is how these sample errors translate into distance errors. Since the non-LOS errors will be mitigated once the receivers are synchronized, only the measurement noise errors are of concern here. Figures 4.6 through 4.8 show the standard deviation of the measurement noise errors with respect to σ_z for the three oversampling values. The signal with a one sample delay has a standard deviation range of 0 to 7.5 meters as σ_z increases while the 10 sample delay has a standard deviation range of 0 to 2.5 meters. It should be noted that the one sample delay also produces more measurement noise errors than the other delay values. It is also important to note that the multipath signals with high delays have a standard deviation of 0 meters. This is because the signals with a delay greater than one sample don't produce very many errors within this measurement noise region. Most of the errors are located at the sample value equal to the delay value which makes these errors non-LOS errors. As a result, the multipath signal with a delay of one sample has the largest error because most of the errors fall within the measurement noise category.

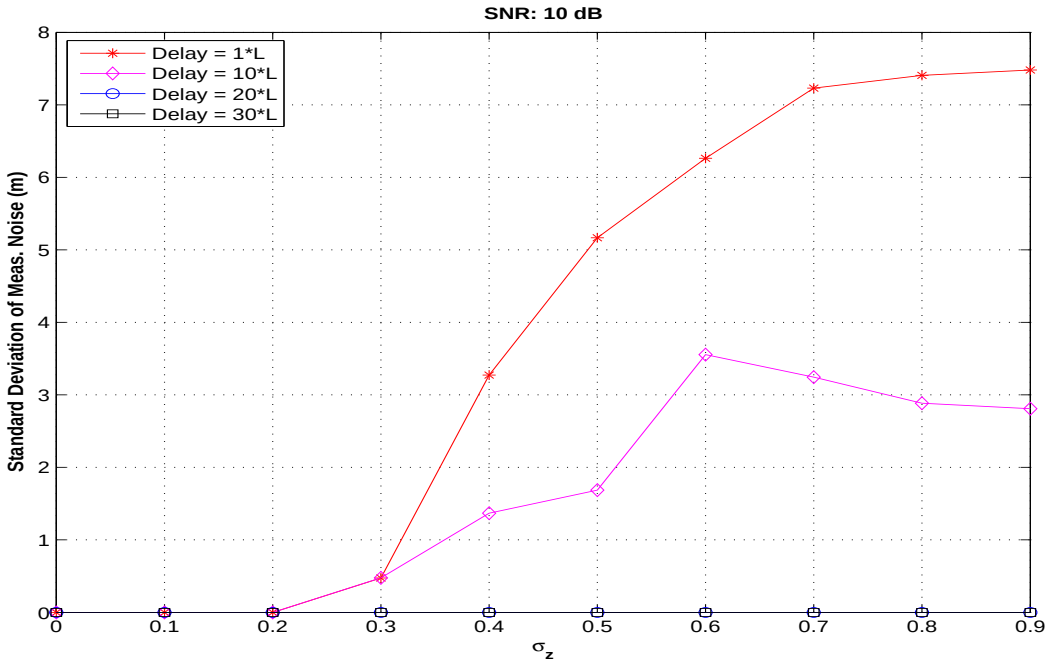

Figure 4.6: Standard deviation of measurement noise errors (in meters) for the no oversampling case and $SNR = 10$ dB.

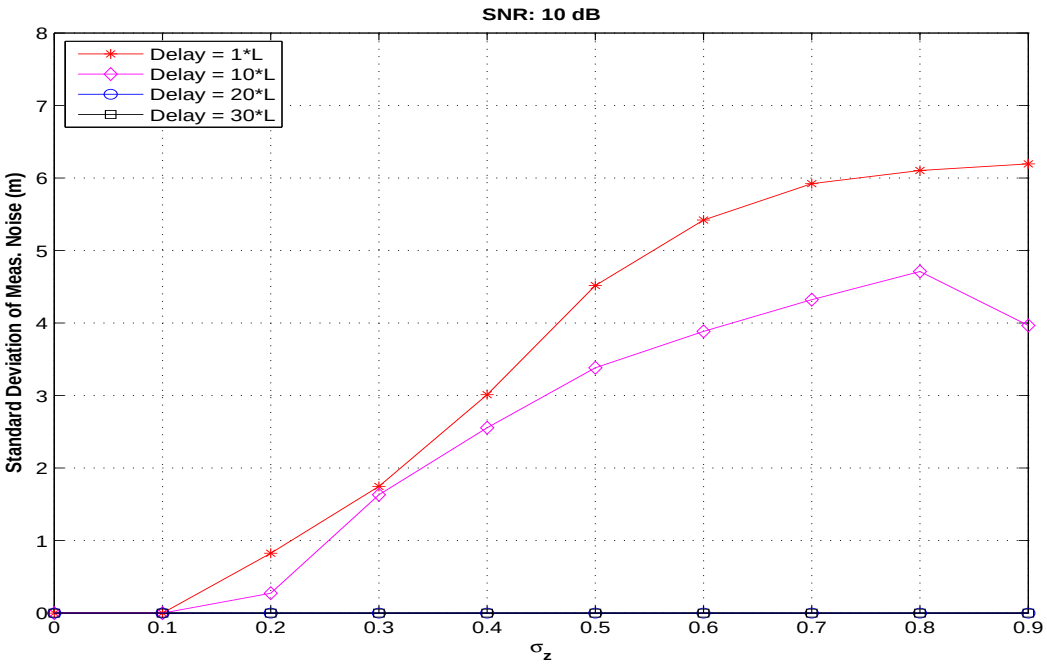

Figure 4.7: Standard deviation of measurement noise errors (in meters) for 3× oversampling case and $SNR = 10$ dB.

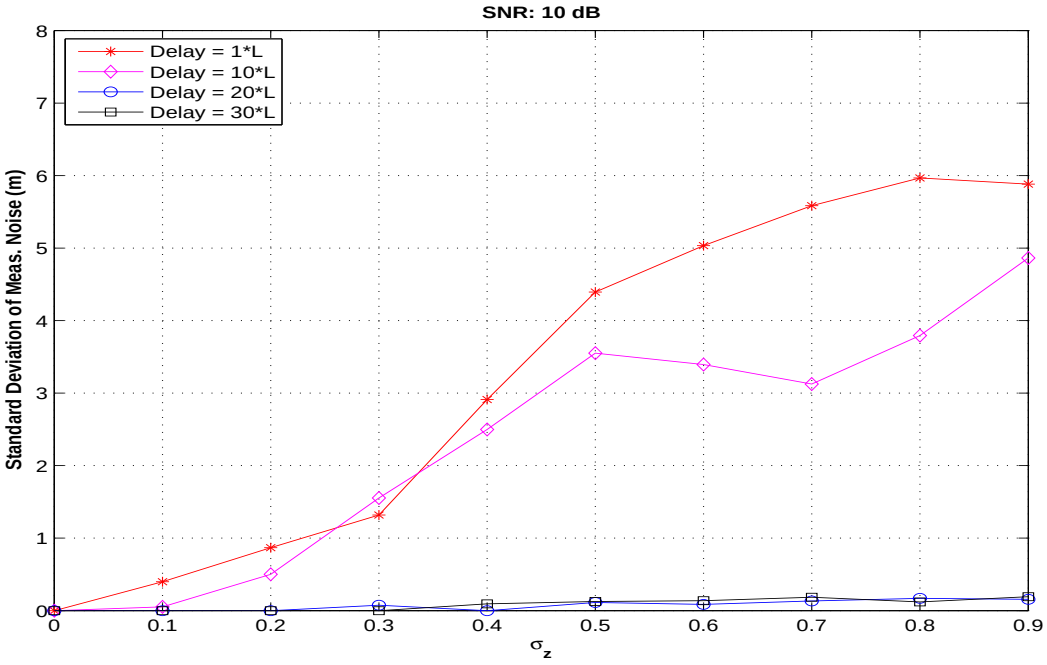

Figure 4.8: Standard deviation of measurement noise errors (in meters) for 9× oversampling case and $SNR = 10$ dB.

Oversampling the signal produces varied results. For the one sample delayed signal, the standard deviation decreases from a maximum of 7.5 meters to a maximum of 5.9 meters as the oversampling factor is increased. For the 10 sample delayed signal, the standard deviation actually increases from a maximum of 2.5 meters to a maximum of 3 meters when the signal is 3× oversampled. When the signal is 9× oversampled, the standard deviation reduces to a maximum of 1.9 meters. Further investigation is needed to determine the reason for this behavior.

Figures 4.9 through 4.11 show the mean of the measurement noise errors for the three cases of oversampling. At high multipath values, the one sample delayed signal has a mean error down to -9 meters. Oversampling by a factor of 3 improves the mean to -8.5 meters for the ones sample delayed signal, but the 10 sample delayed signal had a worse error magnitude. It went from -0.5 meters with no oversampling to -2 meters with 3× oversampling. The results for 9× oversampling are similar to the results for 3× oversampling for the mean. Note that the values referred to here are maximum values. Positive and negative values only specify which direction the error

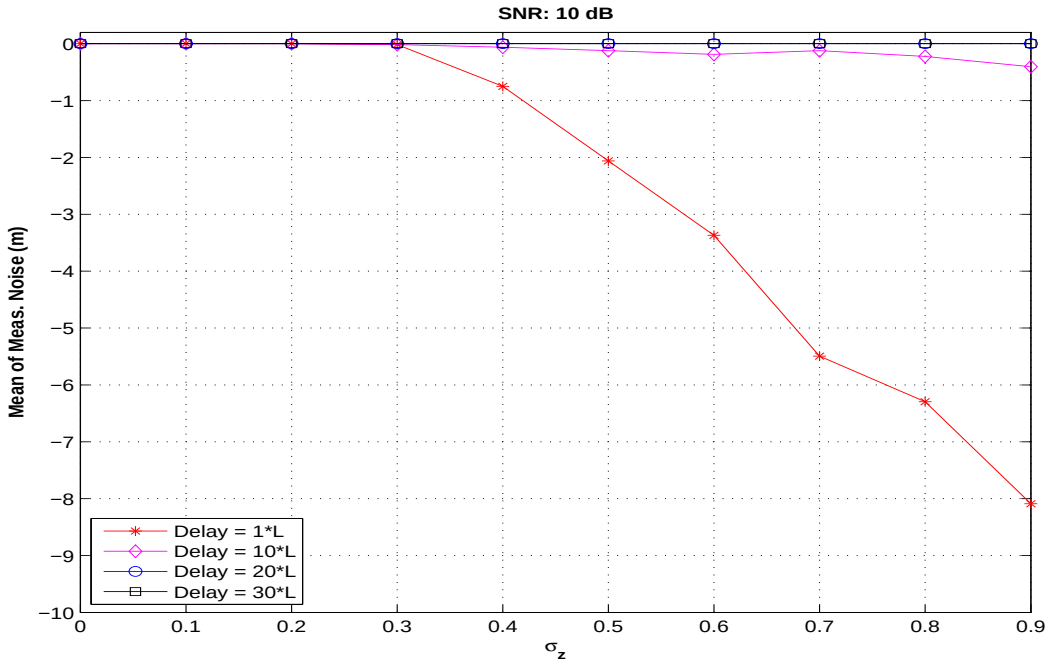

Figure 4.9: Mean of measurement noise errors (in meters) for no oversampling case and $SNR = 10$ dB.

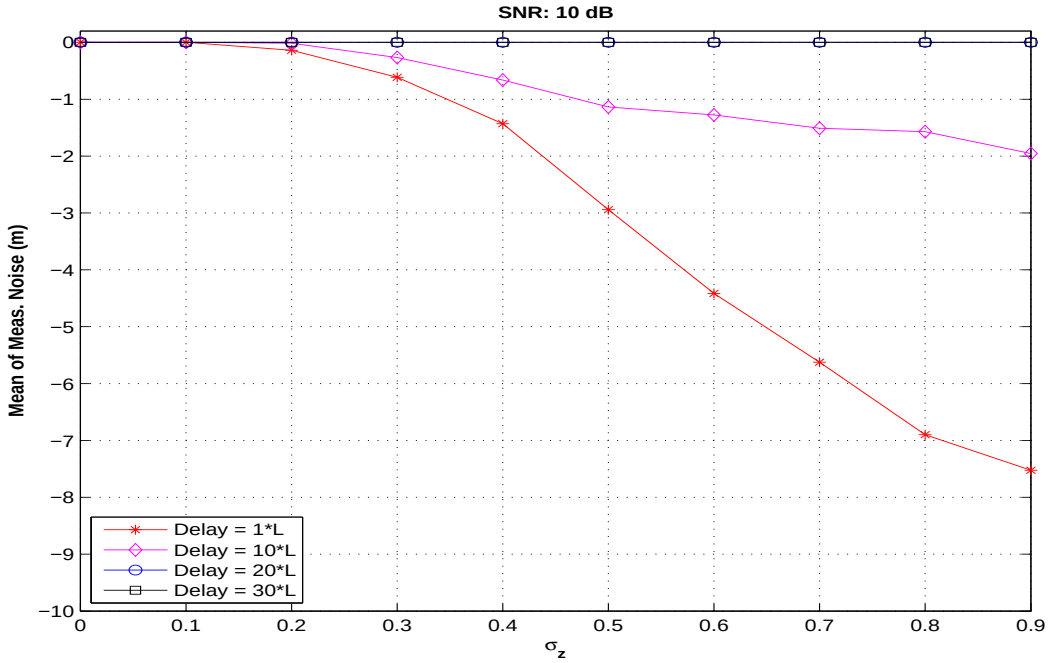

Figure 4.10: Mean of measurement noise errors (in meters) for 3× oversampling case and$SNR = 10$ dB.

is in. For example, an error of 10 meters means that the estimate is 10 meters ahead of the actual position and -10 meters means that the estimate is 10 meters behind the actual position. Both are 10 meter errors.

4.3.1.3 Key Observations. In summary, the baseline case allowed the multipath channel to be characterized and shows what the dominant factors are affecting the probability of error for the symbol boundary correlation. The effects of SNR were put aside since it was shown that setting the SNR to -10 dB and above will yield similar results. Therefore, setting $SNR = -10$ dB is sufficient to allow for "normal" operation of the symbol boundary correlator while a lower SNR will severely degrade the performance. Then, it was shown that σ_z is the major factor influencing the probability of error given a sufficiently high SNR. As this factor increases, so too does the probability of error. This happens regardless of the delay of the reflected signal, even when the error threshold is applied. Also, the oversampling factor affects

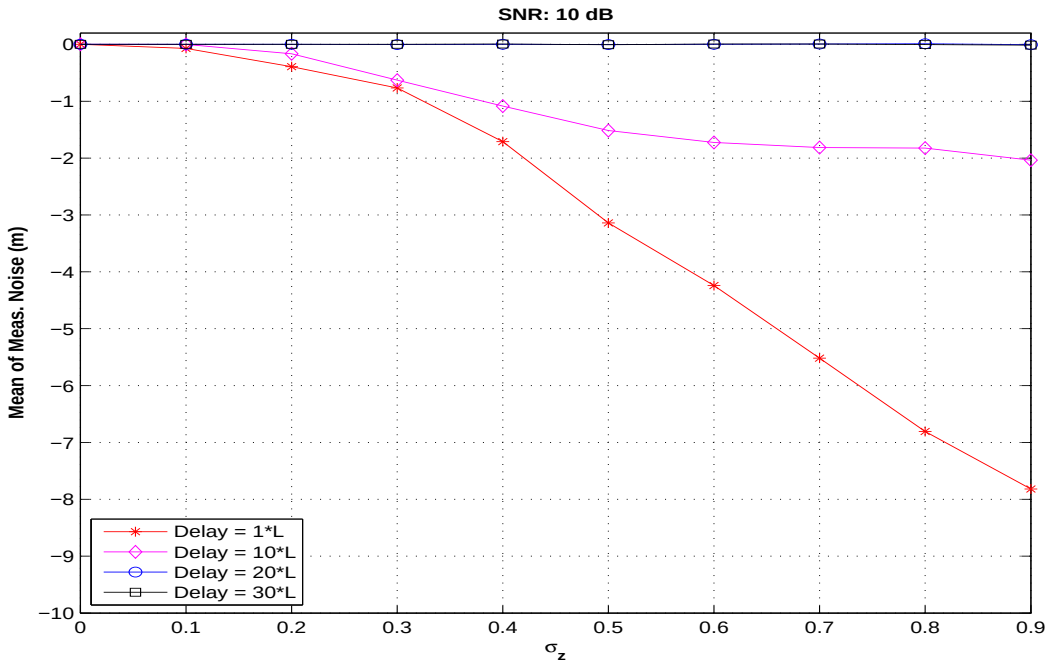

Figure 4.11: Mean of measurement noise errors (in meters) for 9× oversampling case and $SNR = 10$ dB.

the probability of error due to the fact that it increases the correlation SNR at low SNRs.

The errors were analyzed next. The errors in the symbol boundary correlation process were shown to be caused by the delay of the multipath signal. Because of this, the delay affected the errors which fell into the measurement noise category. These errors directly translate into errors in the TDOA measurements. The data showed that high delay multipath signals did not produce very many measurement noise errors while the low delay multipath signals did.

4.3.2 Transmitter - Reference Receiver. This section provides results for the data taken at the reference receiver. The reference receiver only experiences σ_z values 0 and 0.1 at the same time the mobile receiver experiences these values. It experiences a σ_z value of 0.2 during the remainder of the trials. This produces an optimized area for signal reception which yields a small amount of errors. For the cases of 1×, 3×, and 9× oversampling at $SNR = 10$ dB, there were only 1, 0, and 12 total errors,

respectively. These errors were out of a total of 44,000 trials for each of the three oversampling cases. Therefore, it is easy to see that a low σ_z value produces a very small number of errors.

4.4 Test Setup: Two Receivers

For the test case, two receivers were used which allows for the feature correlator performance to be analyzed while collecting the necessary data to perform the TDOA measurements. As stated in Section 4.1.3 above, the reference receiver is at an optimized location in order to receive the signal from the transmitter with minimal multipath interference, while the mobile receiver was run for the cases described in Section 4.3.1. Window sizes of 10 and 100 were used to determine the effect on the probability of error. An error occurs when the estimated peak in the feature correlation calculation is not the true peak. The feature correlator algorithm calculated the estimated symbol differences for the mean, phase, RMS, and mini-mean features. All plots shown are with respect to the parameters of the mobile receiver. The raw data is analyzed below and the results are given without regard to the errors which may have occurred in the symbol boundary correlator. After that, an analysis is given which delves into how the errors in the symbol boundary correlator affect the feature correlator. Finally, some key observations will be given.

4.4.1 Raw Data Analysis. Figure 4.12 shows the plots of $P_{e_{feature}}$ versus σ_z for all four features with $SNR = 10$ dB, no oversampling, and $K = 10$ symbols. It shows that the mean performs slightly better than the mini-mean and significantly better than the phase and RMS features. Each curve combines the errors for the delays without distinguishing between them. As a result, it can be seen that the curves for all four features increase as σ_z increases. The results shown here for $\sigma_z = 0$ are consistent with obtained by Velotta. The percentages, however, are not exact due to a few minor code changes.

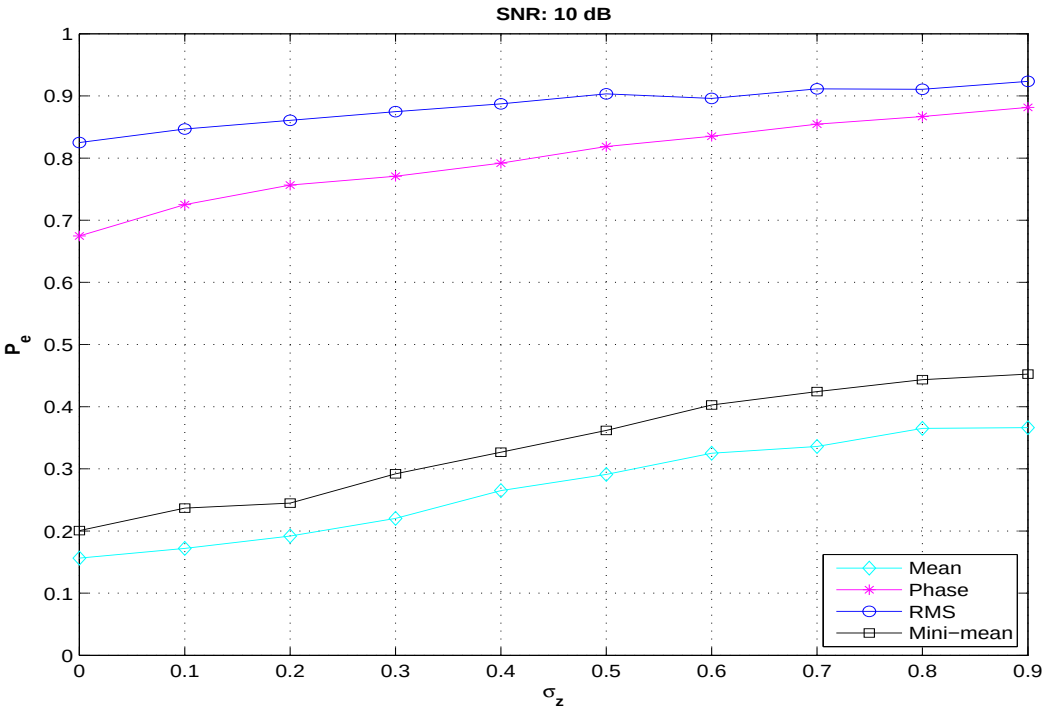

Figure 4.12: $P_{e_{feature}}$ vs. σ_z for feature correlation calculations with $SNR = 10$ dB, no oversampling, and $K = 10$ symbols.

Figure 4.13 shows the probability of an error in the feature correlator for $SNR = 10$ dB, no oversampling, and $K = 10$ symbols. The data for the four delay values were separated and plotted independently. Thus, each graph shows the $P_{e_{feature}}$ for all features for a given delay value. It is evident that the curves in the four separate plots follow the same overall trend, but the probability of error increases slightly as the delay increases.

Figure 4.14 shows the performance of the feature correlator for $3\times$ and $9\times$ oversampling. The $P_{e_{feature}}$ decreases as the oversampling factor increase. The oversampling factor, as in the Baseline Setup, merely causes a slight increase in the correlation SNR and the features perform better at a slightly lower SNR. Once again, the trade-off here is increased computations for the potential increase in TDOA measurement accuracy.

The next parameter to analyze is the window size. Figure 4.15 shows the feature correlation results for the case of no oversampling, but with $K = 100$ symbols instead

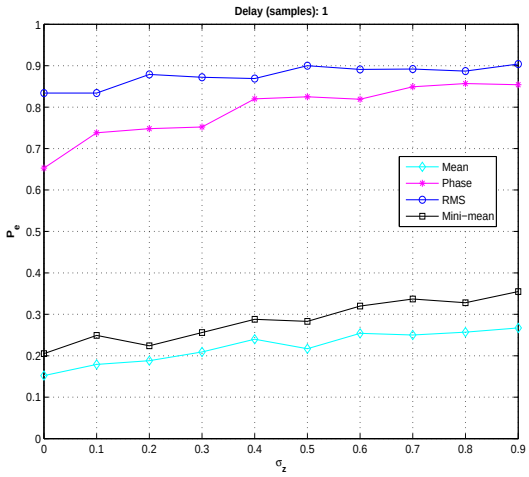

(a) $delay = 1$ sample

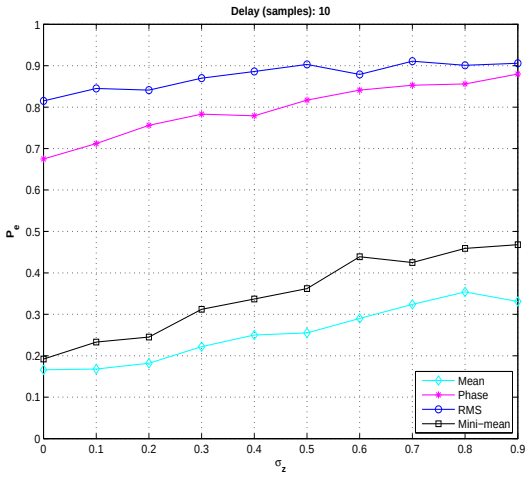

(b) $delay = 10$ samples

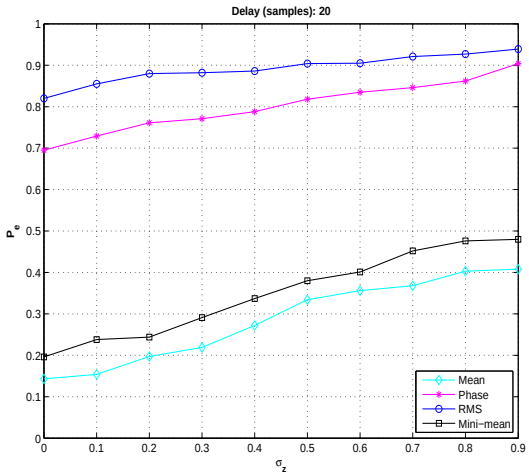

(c) $delay = 20$ samples

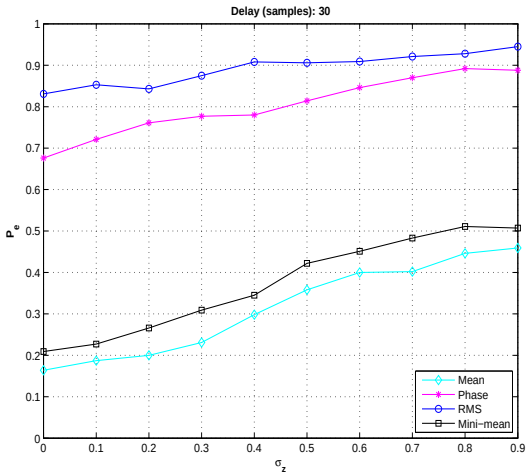

(d) $delay = 30$ samples

Figure 4.13: $P_{e_{feature}}$ of all features for $SNR = 10$ dB and no oversampling. The graphs are distinguished by the delay value in order to visualize its effect on performance (a) $delay = 1$ sample (b) $delay = 10$ samples (c) $delay = 20$ samples (d) $delay = 30$ samples

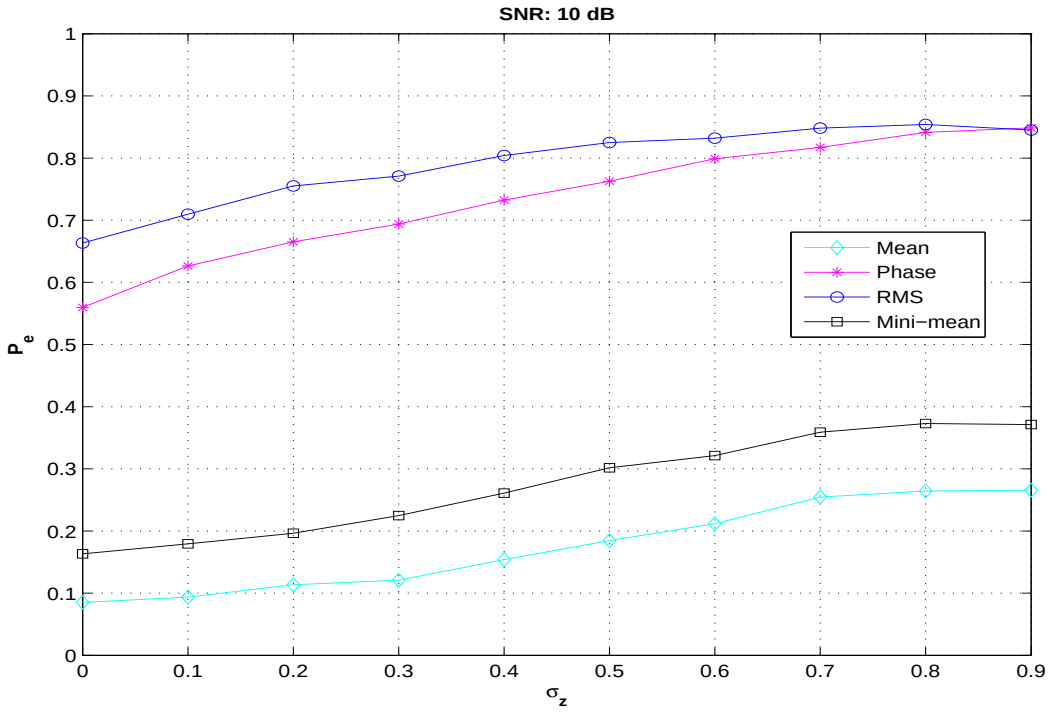

(a) $P_{e_{feature}}$ Graph for 3× oversampling

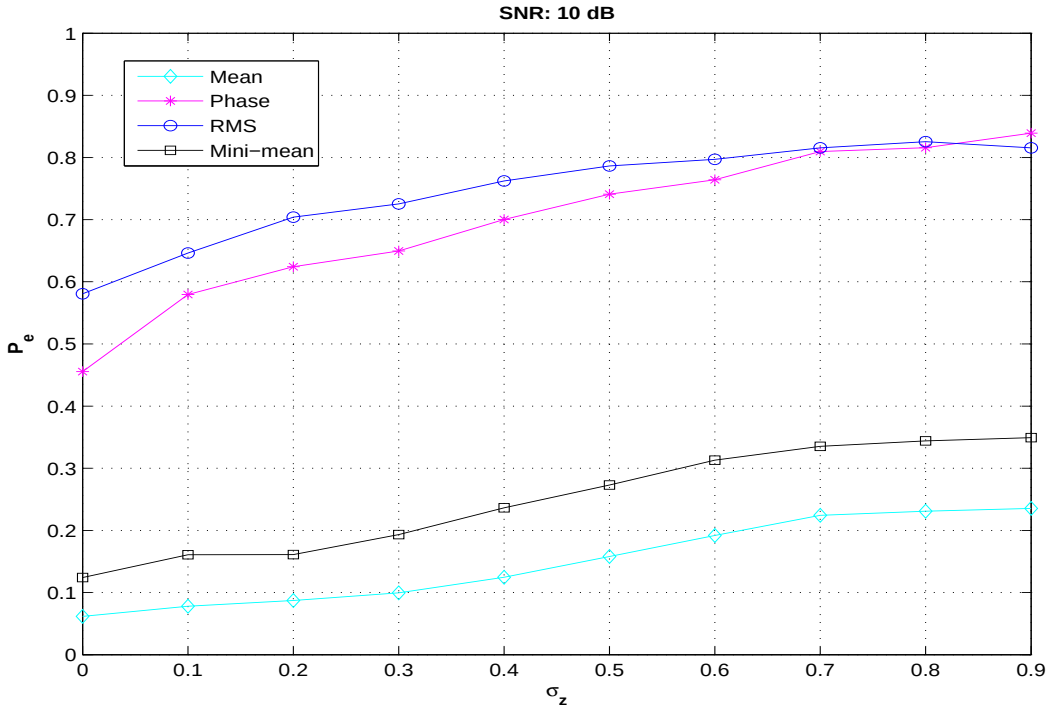

(b) $P_{e_{feature}}$ Graph for 9× oversampling

Figure 4.14: Graphs of $P_{e_{feature}}$ vs. σ_z for an oversampled signal with $SNR = 10$ dB with $K = 10$ symbols. a) $L = 3$ b) $L = 9$

of 10. Comparing the graphs for the SNR of 10 dB and 0 dB, it is evident that the mean and mini-mean features change very little with the change in SNR while the phase and RMS have a decrease significantly in the probability of error with the increase in SNR. For $SNR = 10$ dB, all four features perform very well compared to the performance when the window size is 10 symbols (see Figure 4.12). The RMS feature actually performs as well as the mean and the mini-mean for this scenario, where it had lagged in performance for other scenarios. All three show a maximum $P_{e_{feature}}$ of about 10% when σ_z is high. The phase, however, remains the worst performer. The window size improves performance in the feature correlator by significantly raising the correlation SNR.

4.4.2 Error Analysis. This section takes a look at the errors in the symbol boundary correlator and how they relate to the errors in the feature correlator. For the simulations where the SNR is 10 dB and there is no oversampling, there were a total of 176,000 individual trials run. Out of these, 83.6% of the trials had the symbol boundary correlator for both the reference and the mobile receiver correctly identifying the symbol boundary. Figure 4.16 shows the probability of error for the feature correlator when the symbol boundary correlators in both the mobile and references receivers were successful. For comparison, it also shows the probability of error for the feature correlator for all trials (bottom graph).

The similarity of these two graphs suggests that the feature correlator may be the limiting factor in generating accurate TDOA measurements, and there is definitely room for improvement in this process. Both of the symbol boundary correlators were correct a majority of the time, yet there are still many errors in the feature correlation process. Even for the mean, which performed the best in this scenario, there are errors roughly 15% of the time even though there is no multipath. Figure 4.17 shows the probability of error for 3× and 9× oversampling. Oversampling did slightly improve the results from the feature correlator. The symbol correlators were both correct for 83.5% and 83% of the time for 3× and 9× oversampling, respectively. These are very

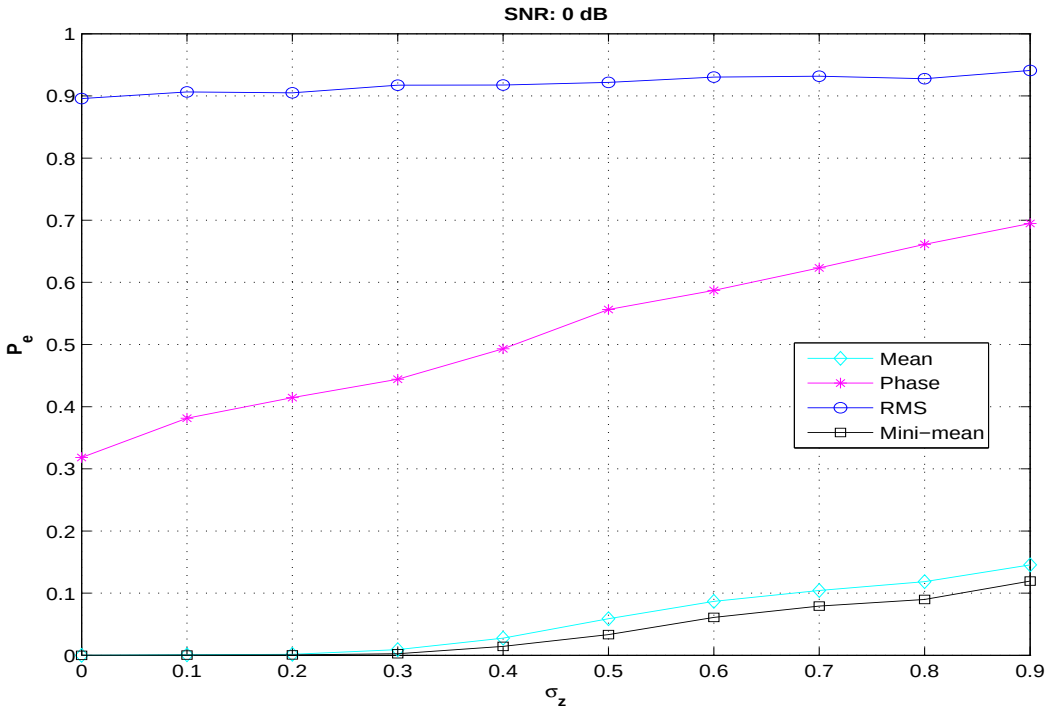

(a) $P_{e_{feature}}$ Graph for SNR = 0 dB

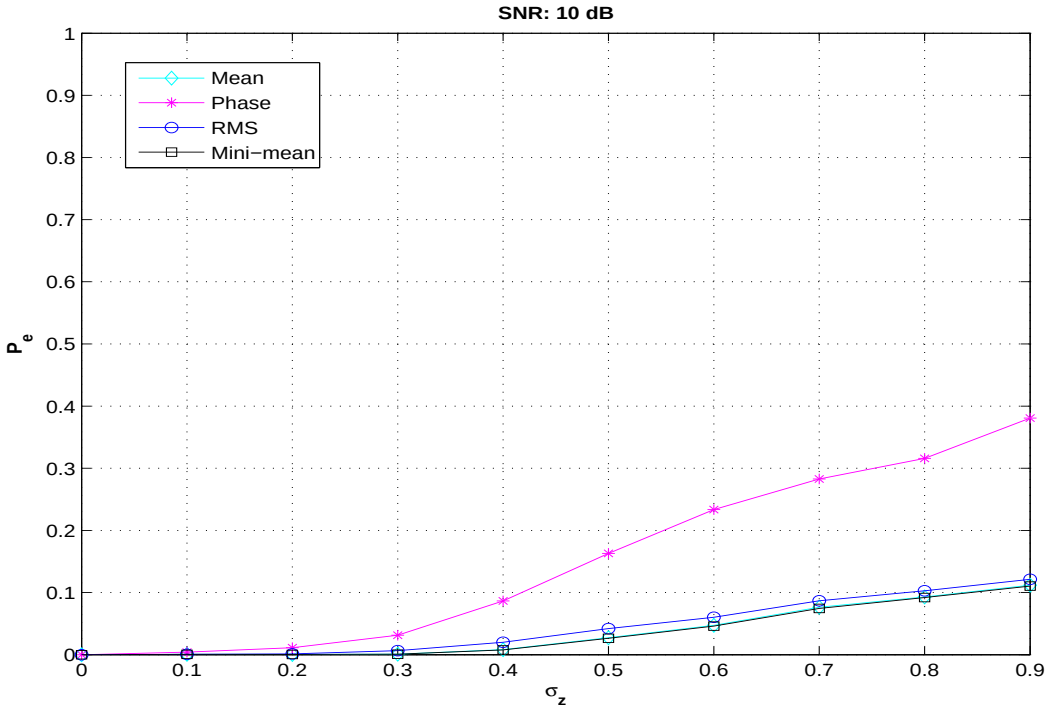

(b) $P_{e_{feature}}$ Graph for SNR = 10

Figure 4.15: Graphs of $P_{e_{feature}}$ vs. σ_z with no oversampling and $K = 100$ symbols for the feature correlation results. a) SNR = 0 dB b) SNR = 10 dB

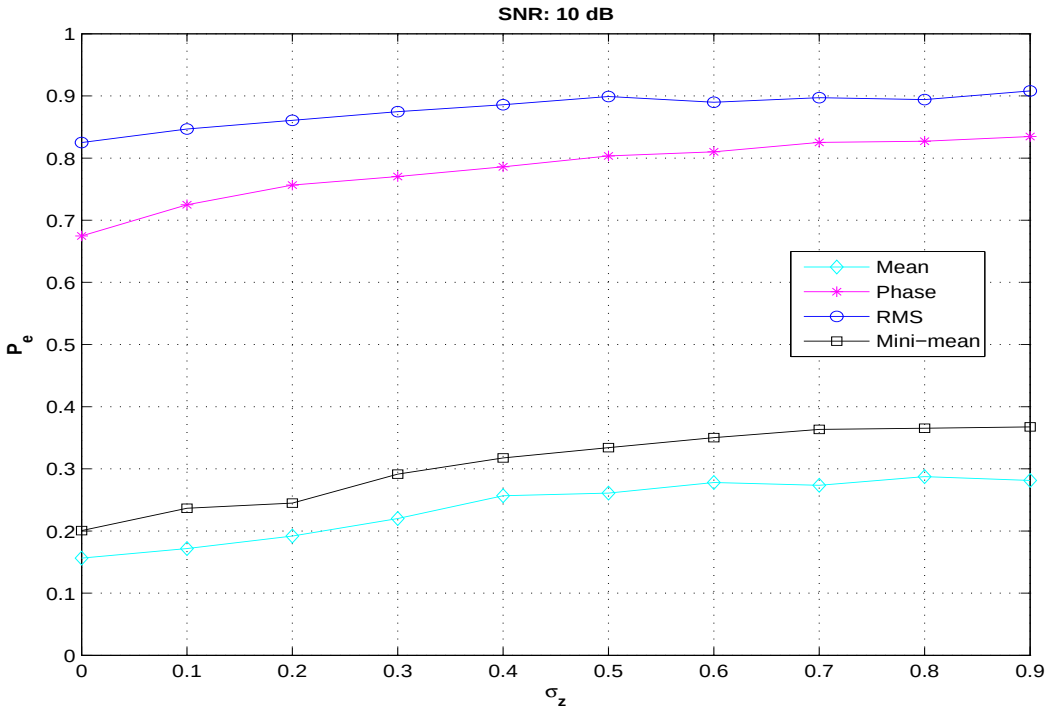

(a) $P_{e_{feature}}$ when both symbol correlators are correct

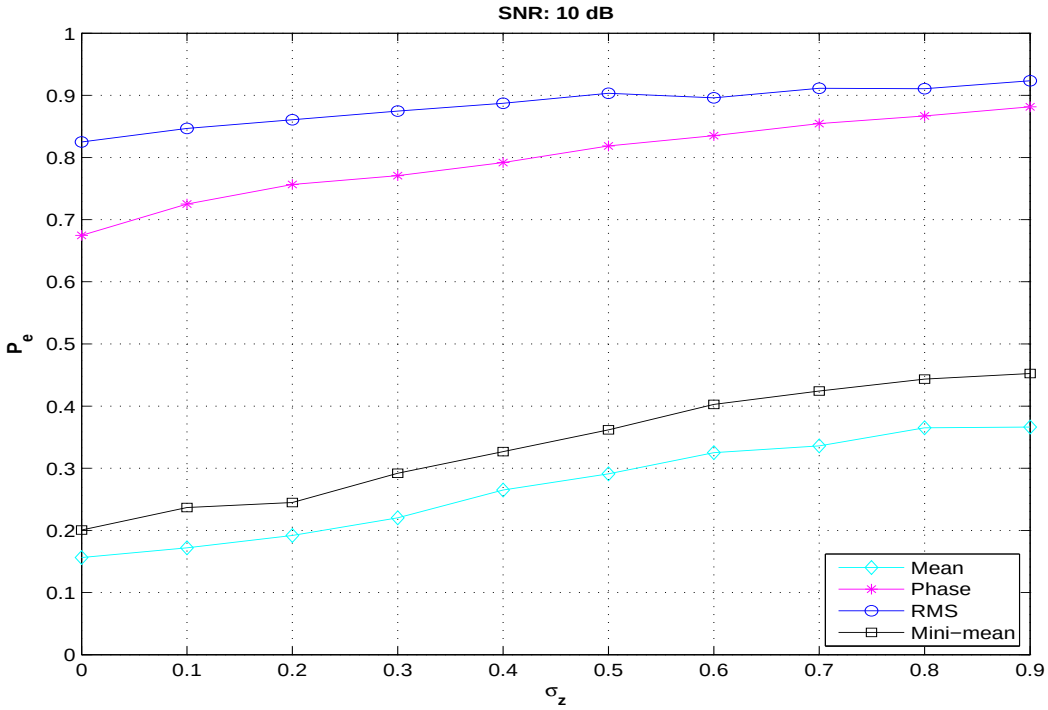

(b) $P_{e_{feature}}$ for all trials

Figure 4.16: Graphs of $P_{e_{feature}}$ for the feature correlator vs. σ_z with no oversampling, $K = 10$ symbols, and $SNR = 10$ dB. a) Symbol boundary correlation in mobile and reference receivers are successful b) All trials.

close to the value of the case of no oversampling. Yet the probability of error in the feature correlator dropped slightly compared to the case with no oversampling shown in Figure 4.16a. Further investigation is required to determine the cause.

When the window size is increased to 100 symbols, there is a more pronounced effect on the feature correlator. Figure 4.18 shows the results for the feature correlator when both of the symbol boundary correlators are correct. It shows the scenario for $SNR = 10$ dB, no oversampling, and $K = 100$ symbols. In this case, the symbol boundary correlators are correct a the same time for 86.3% of the trials.

Increasing the window size improved the accuracy of the feature correlator. When accounting for the errors in the symbol boundary correlator, the probability of error for the mean, mini-mean, and RMS features approach 0, even in high multipath conditions. Figure 4.19 shows the probability of error for the feature correlator for 3× and 9× oversampling. By oversampling, the probability of error in the feature correlator decreases further. The symbol boundary correlators were correct at the same time for 85.9% and 86.2% of the time for 3× and 9× oversampling, respectively.

4.4.3 Key Observations. As with the symbol boundary correlator, the probability of error for the feature correlator depends heavily on the SNR. It takes $SNR =$ 10 dB, however, for normal operation to occur for the feature correlator. Remember, this value was -10 dB for the symbol boundary correlator. When the SNR is set to 10 dB or above, the main factors affecting the probability of error are the multipath factor and the window size. The probability of error increases as σ_z increases. Increasing the window size significantly lowers the probability of error, while increasing the oversampling factor only causes a slight decrease in the probability of error. The results also showed that an increased delay slightly increased the probability of error. A more in-depth look at the data revealed that when both symbol boundary correlators are correct and the window size is increased to 100 symbols, the probability of error for the feature correlator is reduced to nearly 0 for all multipath values for all features except the phase.

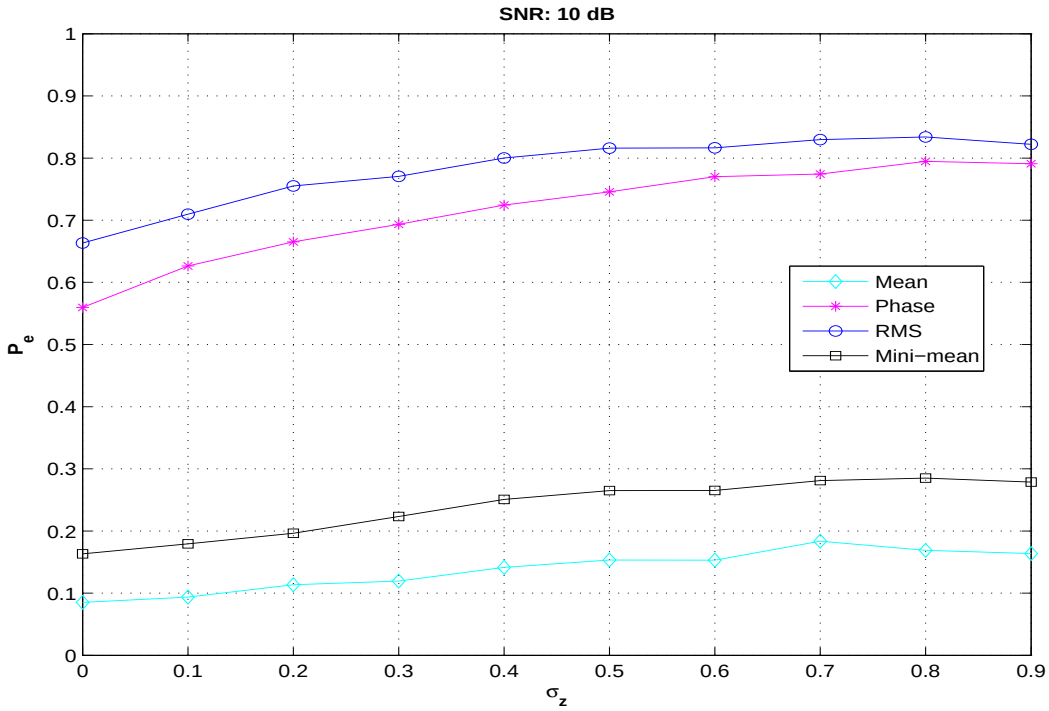

(a) 3× oversampling

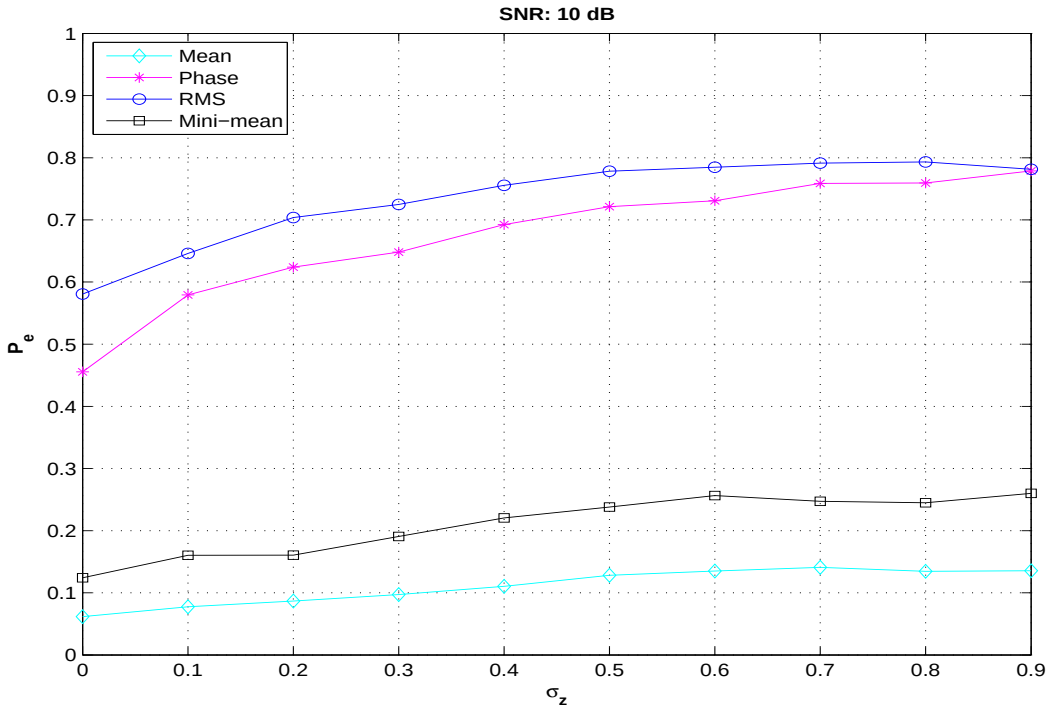

(b) 9× oversampling

Figure 4.17: Graphs of $P_{e_{feature}}$ for the feature correlator vs. σ_z when symbol boundary correlators are correct, with 3× and 9× oversampling, $K = 10$ symbols, and $SNR = 10$ dB. a) 3× oversampling b) 9× oversampling.

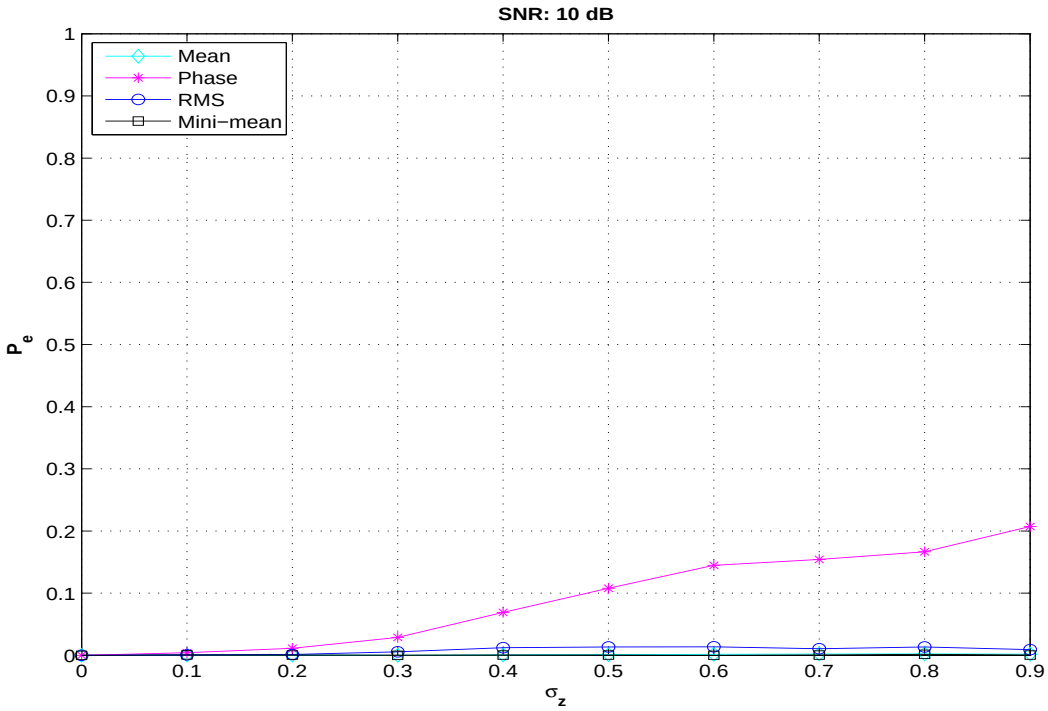

(a) $P_{e_{feature}}$ when both symbol correlators are correct

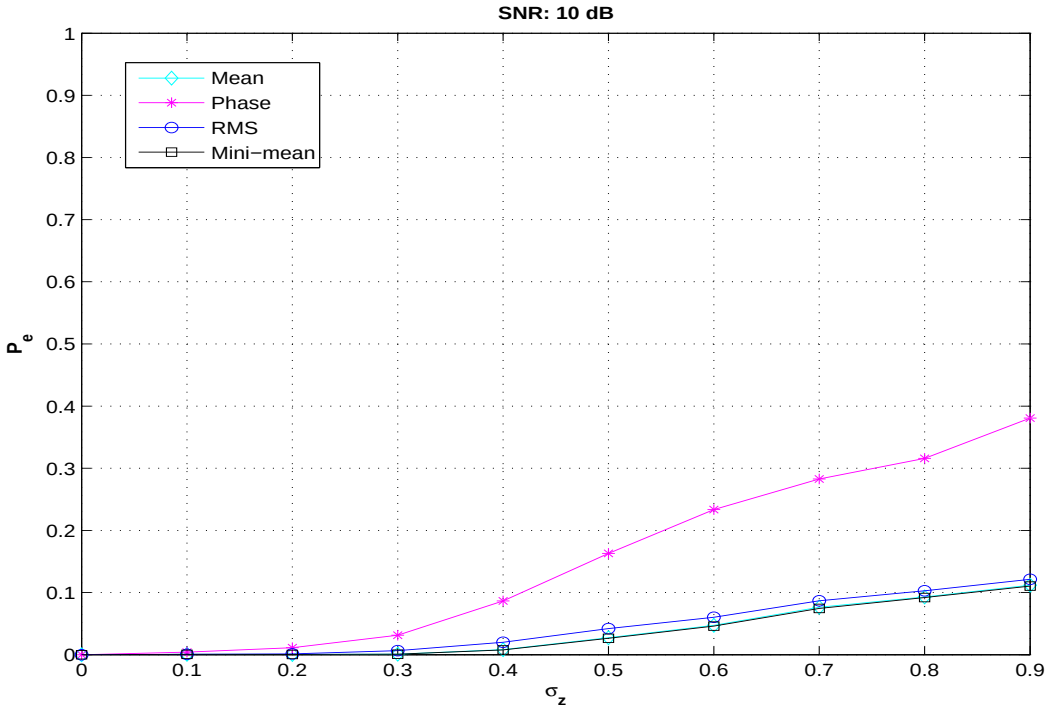

(b) $P_{e_{feature}}$ for all trials

Figure 4.18: Graphs of $P_{e_{feature}}$ for the feature correlator vs. σ_z with no oversampling, $K = 100$ symbols, and $SNR = 10$ dB. a) Symbol boundary correlation in mobile and reference receivers are successful b) All trials.

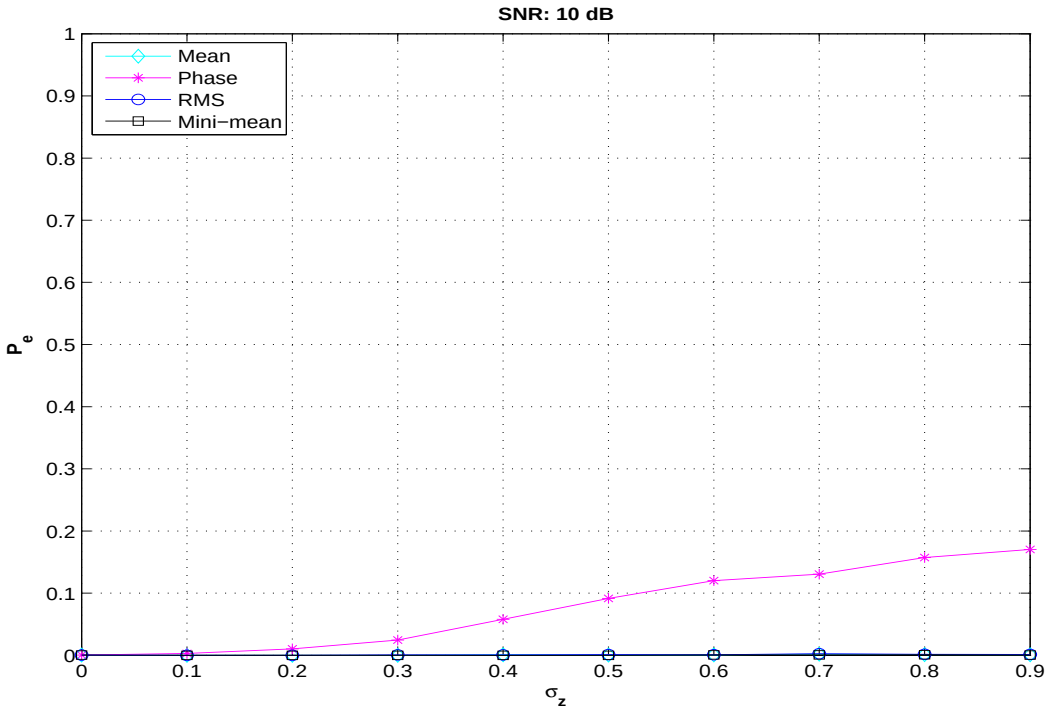

(a) 3× oversampling

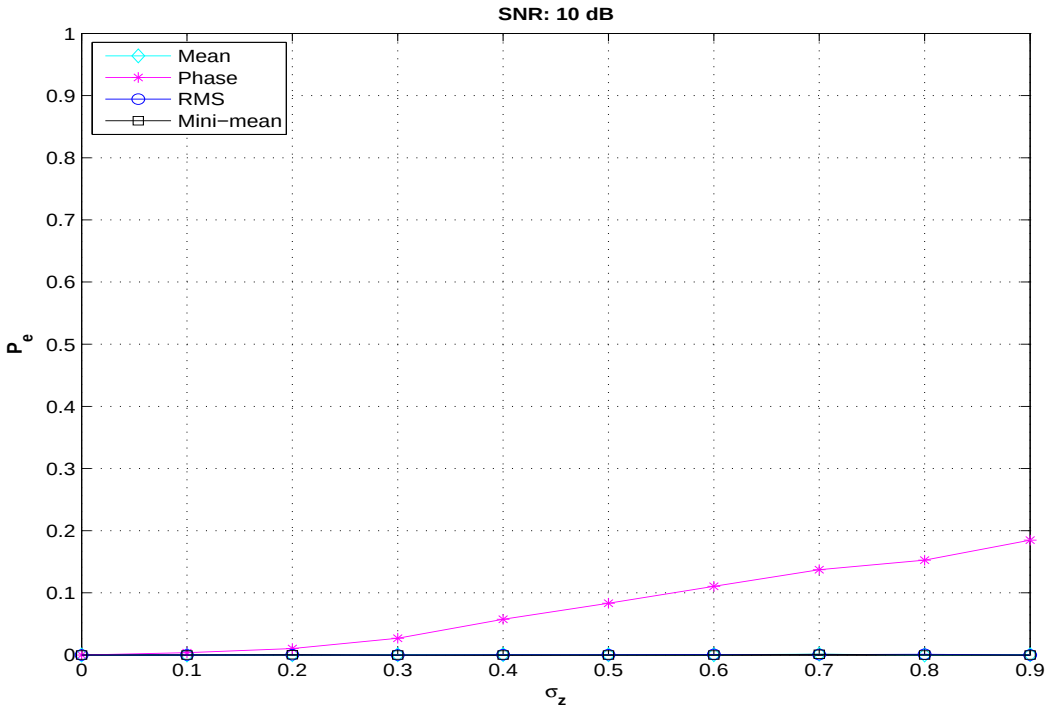

(b) 9× oversampling

Figure 4.19: Graphs of $P_{e_{feature}}$ for the feature correlator vs. σ_z when the symbol boundary correlators are correct, with 3× and 9× oversampling, $K = 100$ symbols, and $SNR = 10$ dB. a) 3× oversampling b) 9× oversampling.

4.5 Mean vs. Mini-mean

Recall from Section 3.3.2 that the mini-mean feature was added because it theoretically offered improved performance versus the mean, which performed the best in Velotta's [3] research. Figure 4.20 shows the probability of error as a function of the SNR at the receiver for the mean and mini-mean features. The simulation was run 1000 times for each data point and implemented a multipath-free AWGN channel. The top and bottom graphs represent $K = 10$ and 100 symbols, respectively.

Figure 4.20a shows that for $K = 10$ symbols, the mean actually has a lower P_e for SNRs above 7 dB but is outperformed by the mini-mean for SNRs below 7 dB. Figure 4.21 displays the graphs for $K = 10$ and SNRs of 0 and 10 dB when the multipath effects are added. It shows that the mini-mean is the top performer for $SNR = 0$ dB and the mean becomes the top performer when the SNR is increased to 10 dB. A reason for this behavior may be that the mean performs better at higher SNRs because the calculation uses more samples (80) than the calculation for the mini-mean (32). Therefore, the effective SNR is increased due to the correlation of more data and the higher SNR has less distortion of samples. At the lower SNRs, there is more distortion but the mini-mean feature correlates redundant data and it is easier to recognize.

Figure 4.20b shows that for $K = 100$ symbols, the mini-mean consistently performed better for almost all SNR values. This also holds true in the presence of multipath as Figure 4.22 shows that the mini-mean clearly outperforms the mean for this window size at SNRs of -10 and 0 dB. The mini-mean also performs better for $SNR = 10$ dB, but it small improvement over the mean and is more evident when zooming in on the curves.

4.6 Summary

This chapter started off by detailing the simulation specifications in which the input parameters were discussed, along with their respective values. Next, four types

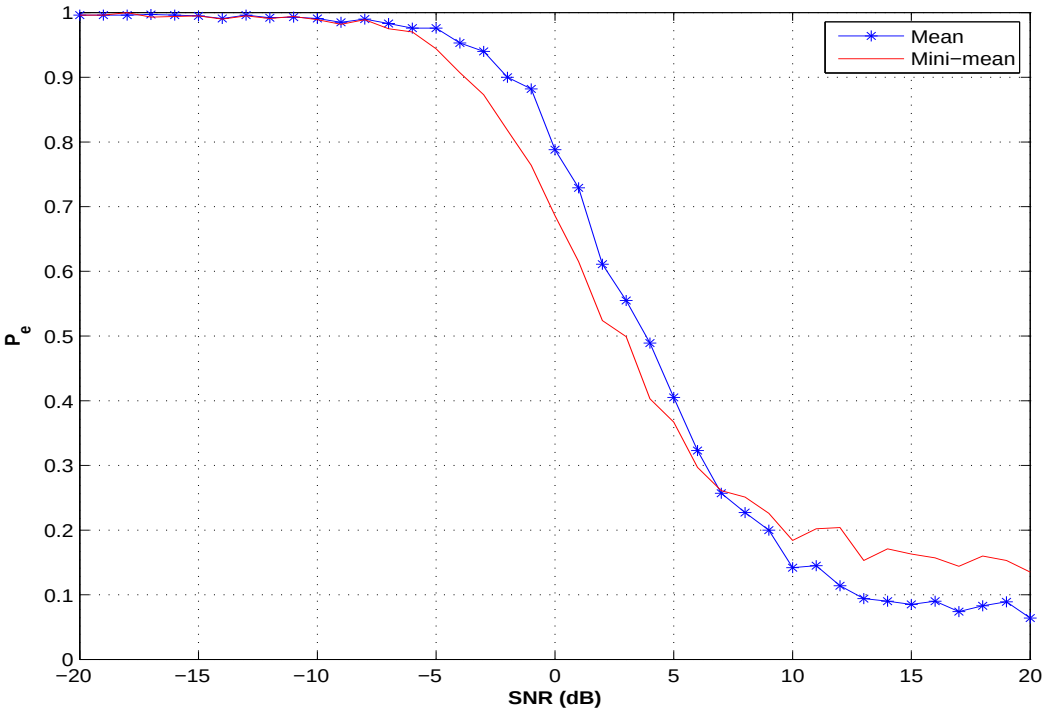

(a) Window Size of 10 Symbols.

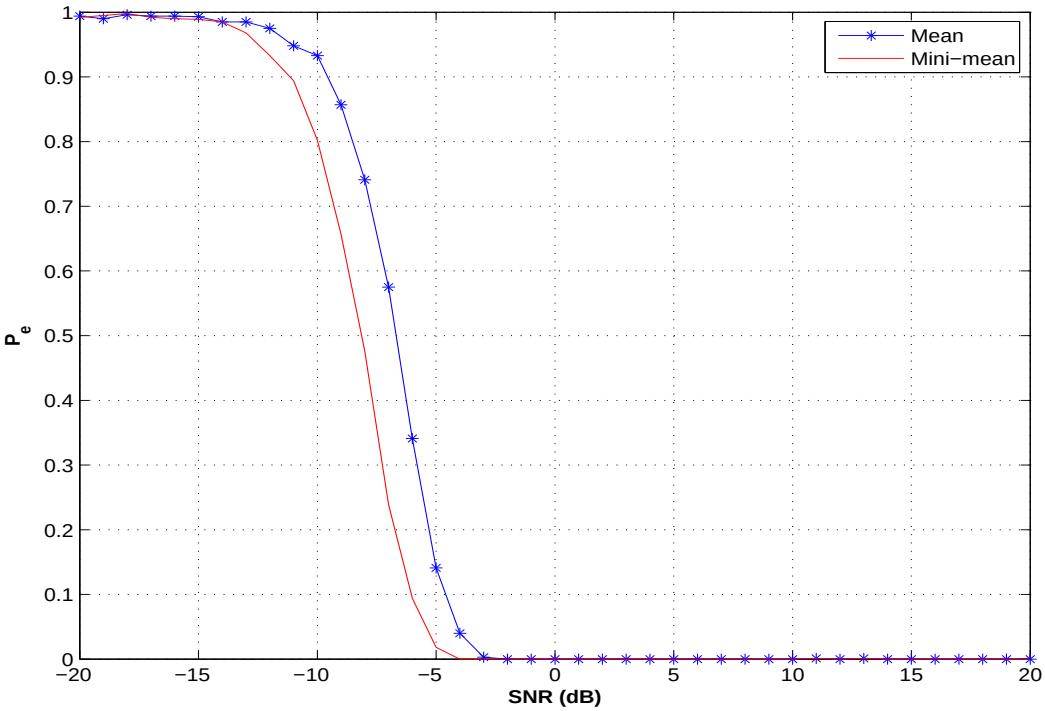

(b) Window Size of 100 Symbols

Figure 4.20: Graphs of $P_{e_{feature}}$ vs. SNR comparing Mean vs. Mini-mean with no oversampling, no multipath, and window sizes of a) 10 symbols and b) 100 symbols.

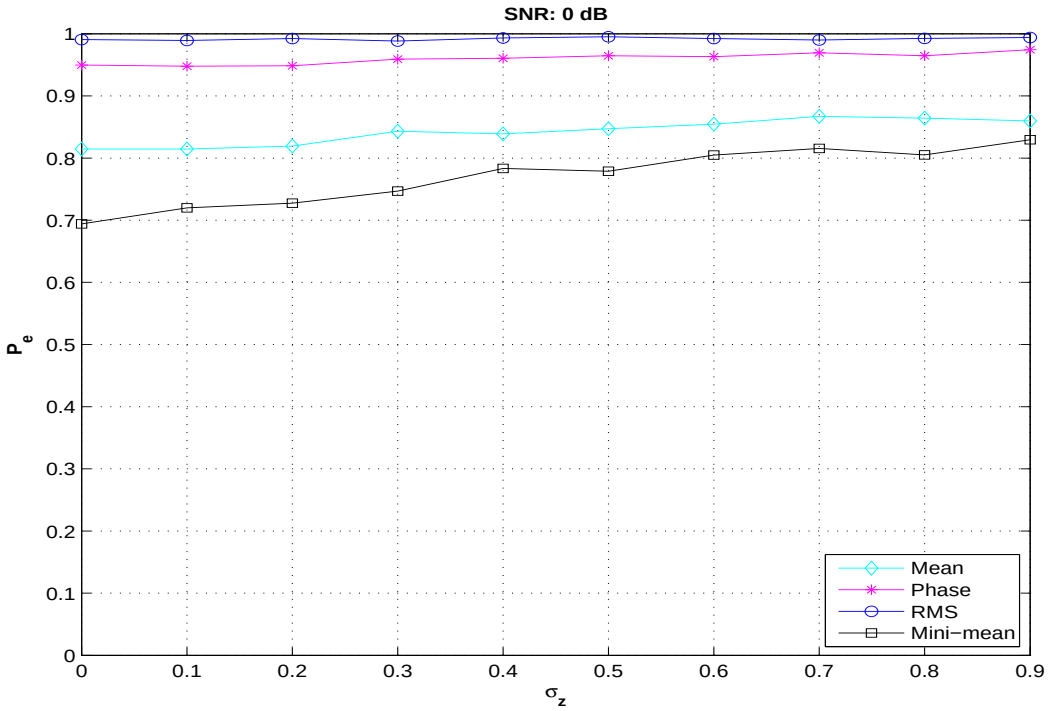

(a) $P_{e_{feature}}$ Graph for SNR = 0 dB

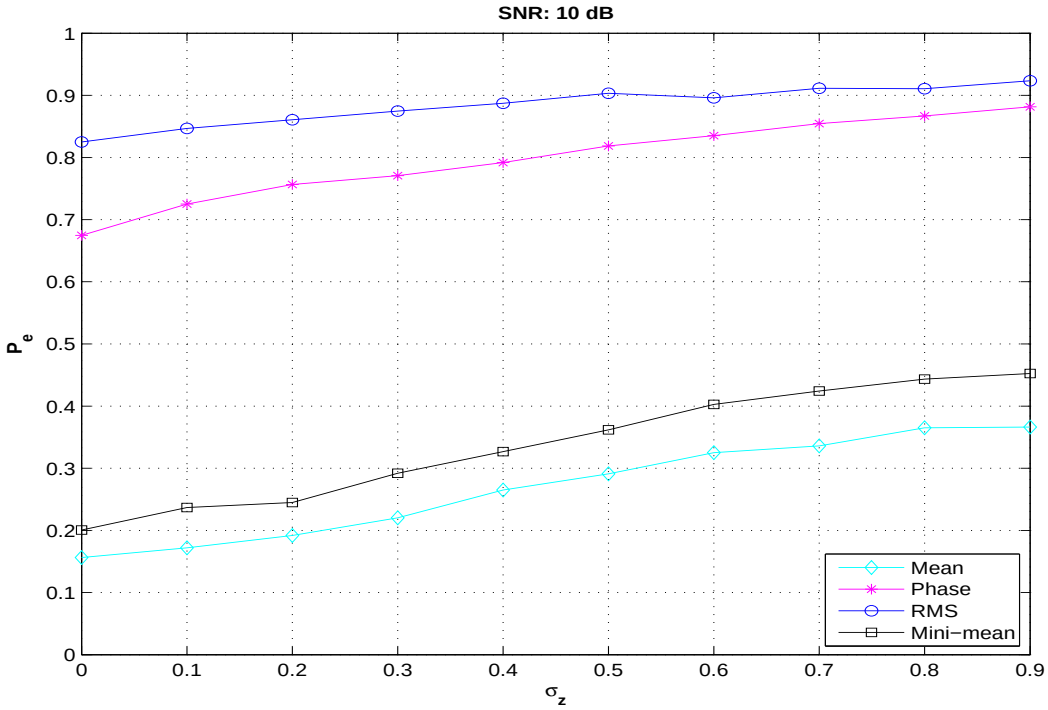

(b) $P_{e_{feature}}$ Graph for SNR = 10

Figure 4.21: Graphs of $P_{e_{feature}}$ vs. σ_z with no oversampling and $K = 10$ symbols for the feature correlation results. a) SNR = 0 dB b) SNR = 10 dB

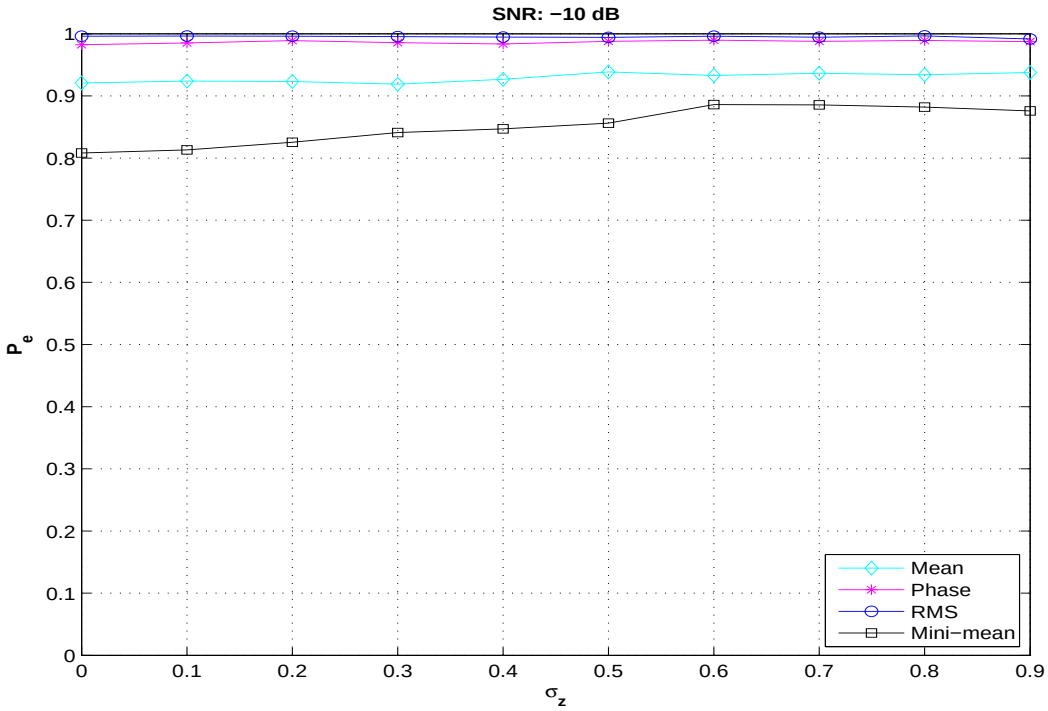

(a) $P_{e_{feature}}$ Graph for SNR = -10 dB

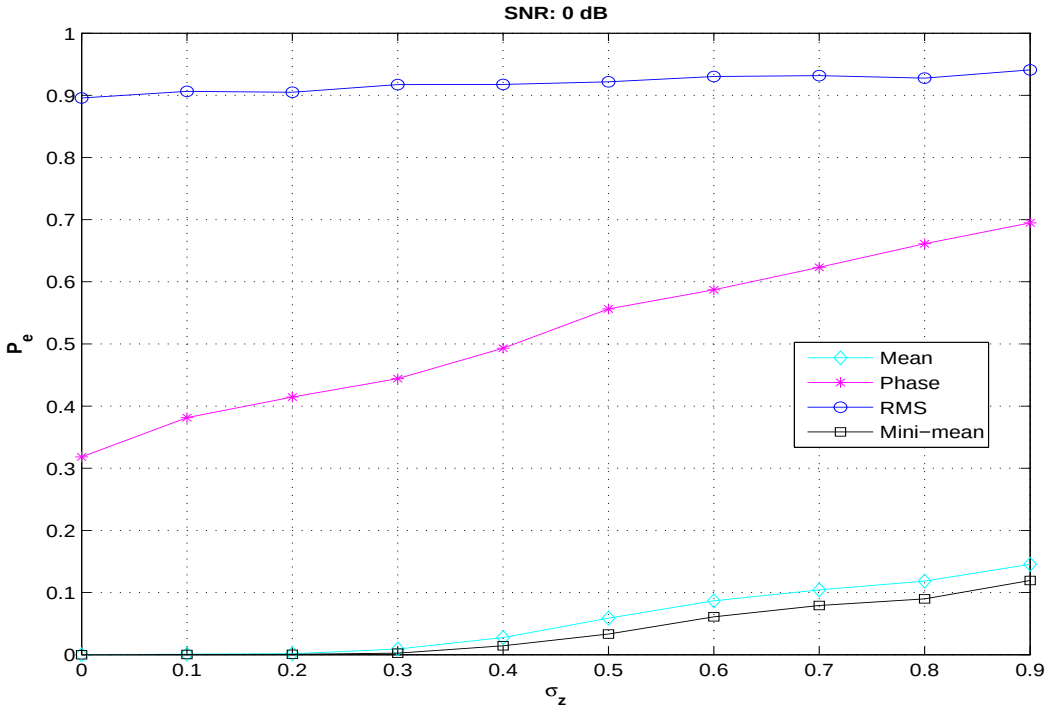

(b) $P_{e_{feature}}$ Graph for SNR = 0

Figure 4.22: Graphs of $P_{e_{feature}}$ vs. σ_z with no oversampling and $K = 100$ symbols for the feature correlation results. a) SNR = -10 dB b) SNR = 0 dB

of errors were defined and each error's origin and magnitude were presented. Then, results of OFDM simulations conducted for this research were displayed and showed which features performed better when correlating two received signals. The features are ranked (best to worst) below according to performance:

1. Mean and Mini-mean
2. Phase
3. Root Mean Squared

The mean and mini-mean are tied because each one performed better than the other in different cases. However, both consistently outperformed the average symbol phase and RMS features. An analysis of results was given in which the impact of various input parameters on the correlation processes is characterized. Finally, an analysis comparing mean and mini-mean results was presented.

V. Conclusions and Recommendations

This chapter summarizes the research results of feature-based correlation performance in the presence of multipath and its ability to accurately produce position estimates based on time-difference-of-arrival (TDOA) measurements. After that, future areas of research are identified.

5.1 Conclusion

5.1.1 Symbol Boundary Correlator. Each of the input parameters discussed in Section 4.1 affects symbol boundary correlator performance. The impact of each parameter is analyzed briefly below:

1. The multipath factor σ_z had a significant impact on symbol boundary correlator performance. As this value increased, the probability of error increased for all cases simulated. An optimal value could not be determined for σ_z for this parameter because it is not a system-based parameter, but rather a natural phenomena. Multipath effects can be lessened by positioning the receiver in an open area with no obstructions by implementing mitigation techniques into the receiver algorithm.
2. The delay of the multipath signal had no noticeable effect on the symbol boundary correlator performance. It was shown that if the error threshold is not applied, the curves for the different delay values are very similar. Like σ_z, this parameter could not be optimized.
3. The received signal SNR had a varying effect on the symbol boundary correlator performance. An SNR below -10 dB severely degraded the probability of error for the symbol boundary correlator. An SNR above -10 dB, though did not greatly improve performance. It seems the point of diminishing returns for this process is about -10 dB. Note that these results are only valid for $K = 10$ symbols.

4. Oversampling the signal improved performance, but only slightly. As the oversampling factor L was increased, the probability of error decreased for the symbol boundary correlator. Oversampling improves performance by increasing the correlation SNR because more samples are created and correlated.
5. The feature correlator is not used in this process and, therefore, the window size has no effect on the probability of error for the symbol boundary correlator.

The symbol boundary correlation process evaluated here performed effectively in low multipath environments. The high multipath environment proved to be challenging for the correlator. For $\sigma_z = 0.9$, the probability of error was at its maximum of about 60%. A minimum SNR of -10 dB was determined to provide peak performance for the symbol boundary correlator. Oversampling the signal proved to lower the probability of error slightly. Reducing the probability of error is important in this process because this is where two of the three errors occur. The measurement noise and non-LOS errors are detected during this correlation process. It was shown that delays of 1 and 10 samples produce more measurement noise errors while delays of 20 and 30 samples generate more non-LOS errors.

5.1.2 Feature Correlator. Each of the input parameters specified in Section 4.1 affects the feature correlator performance. The impact of each parameter is discussed briefly below:

1. The multipath factor σ_z had a direct and significant impact on the feature correlator performance. The results clearly show that as this value increases, so too does the probability of an error occurring in the correlation peak. An optimal value could not be established for σ_z as it is not a system-based parameter, but rather a natural phenomena.
2. The delay of the multipath signal had slightly negative effect on the feature correlation performance. When the feature correlator results were separated by

delay value, it was shown that the probability of error for the feature correlator slightly increased as the delay value increased.

3. The received signal SNR had a strong impact on the feature correlator performance. It was shown that performance increased as the SNR increased. The peak performance was obtained at $SNR = 10$ dB, and higher SNRs showed no noticeable improvement in the probability of error. Note that these results are only valid for $K = 10$ symbols.
4. Increasing the window size yielded a significant improvement in feature correlator performance. It increases the amount of data being correlated which, in turn, increases the correlation SNR. An order of magnitude increase, from 10 to 100 symbols, greatly improved the probability of error of all features at SNRs below 10 dB.
5. The oversampling factor L had minimal impact on the feature correlator performance. Due to the fact that oversampling increases the amount of samples, the correlation SNR was increased which led to a slightly lower probability of error.

The feature correlation process evaluated in this research is effective in exploiting OFDM signal characteristics for the purpose of creating TDOA-based positioning measurements. The mean and mini-mean features performed the best for all simulations and appears to be the ideal features to use in further research. Multipath was determined to be the main impediment to obtaining precise results using this process. While increasing the window size greatly improved performance, there is a limit to how large it can be while still providing a real-time position to a receiver in motion (discussed in Section 4.1).

An SNR of 10 dB should be used to gain the best performance with $K = 10$ symbols. Also, while increasing the oversampling factor does slightly improve performance, its main contribution is decreasing the sampling period at a cost of an increased computational load. A tradeoff of position accuracy improvement compared

to increased processing should be performed. $K = 100$ symbols would increase the computational load and backchannel bandwidth but allow for a lower SNR with a significant increase in feature correlator performance. The feature correlator performs almost perfectly for the mean, mini-mean, and RMS with $K = 100$ symbols and $SNR = 10$ dB.

5.2 Future Work

This research primarily focused on simulations of an algorithm based on a specific method of determining TDOA measurements. Opportunities exist to examine other methods and to collect and analyze real data. Several areas of research are listed below.

1. The symbol boundary correlation process used in this research is just one approach. Other synchronization algorithms could be investigated to improve results, especially in high multipath cases. A more sophisticated approach could lead to a reduction in errors and, ultimately, more accurate position estimates.
2. The feature correlation algorithm presented here could be improved. Techniques to enhance feature correlation performance of individual features could be studied which may allow another feature to outperform the mean and mini-mean. New features could be evaluated to determine their viability. Also, multipath mitigation techniques could be studied in an effort to reduce its effect on system performance.
3. There are limitless opportunities in developing alternative algorithms for simulation-based research. This research used a statistical approach to correlate the received signals which has an added benefit of reduced data and bandwidth for transmission between the two receivers. The direct correlation of the OFDM received signals could be studied also. The reduced bandwidth benefit may be lost but there would be an increase in correlation SNR due to the increase in data being correlated.

4. The multipath channel described in this model was designed to be representative of an open, outdoor area with few obstructions. Channel models can be developed with multiple multipath reflections for outdoor as well as for indoor positioning. An exponential delay profile, for example, represents an indoor area with a LOS and many delays which get attenuated more and lose power as the delay increases. Also, multipath mitigation techniques need to be identified and tested.

5. The TDOA algorithm presented in Section 3.4 could be implemented using the data gathered during the course of this research. The accuracy of these measurements will determine if the OFDM signal is a viable navigation source. Measurements can then be drawn from other research for comparison.

6. There is a need for collecting and analyzing OFDM signals to go along with the analysis of simulated data presented here and in [3]. OFDM signal sources need to be identified and the signals collected for exploitation. Satellite radio terrestrial repeaters and HD Radio are a couple of sources for outdoor purposes. Additionally, there is potential to collect signals from wireless routers in an indoor environment. These signals can be exploited and compared to determine the best source for navigation using an OFDM signal.

VI. Complete Simulated Results

Appendix A contains the complete set of results for the symbol boundary correlator and the feature correlator from the OFDM simulations completed for this research. Only the results necessary to completely convey the appropriate conclusions were inserted into Chapter IV. All results are included here in order to allow access to all data sets for comparison.

The figures below display $P_{e_{symbol}}$ for the Baseline Setup discussed in Section 4.3. Figures F.1 through F.4 show the graphs for the case of no oversampling ($L = 1$), Figures F.5 through F.8 show the graphs for the case of $L = 3$, and Figures F.9 through F.12 show the graphs for the case of $L = 9$. Figure F.13 illustrates the results for $SNR =$ 40 dB with no oversampling and Figure F.14 shows the results for $SNR =$ -10 dB with no oversampling and the error threshold removed.

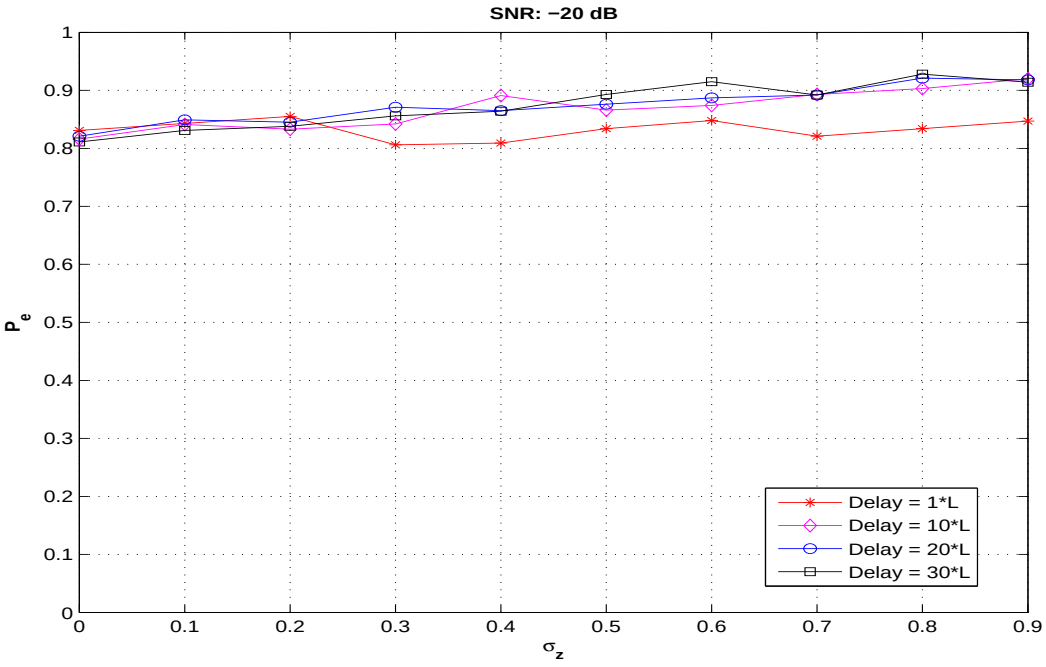

Figure F.1: Graph of $P_{e_{symbol}}$ vs. σ_z with no oversampling and $SNR =$ -20 dB for the symbol boundary correlation results.

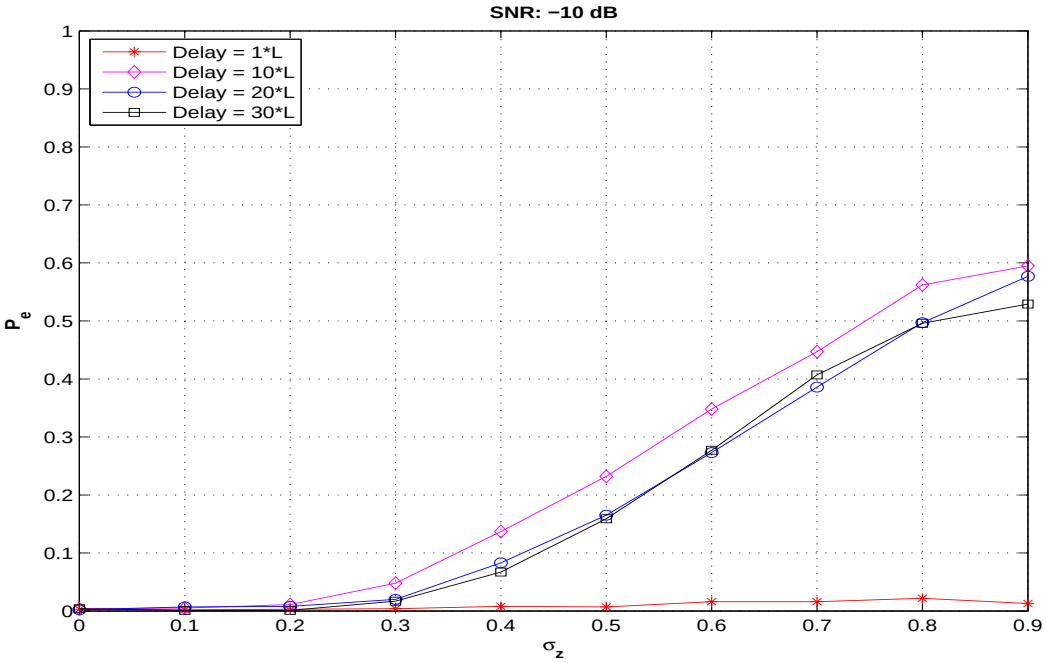

Figure F.2: Graph of $P_{e_{symbol}}$ vs. σ_z with no oversampling and SNR = -10 dB for the symbol boundary correlation results.

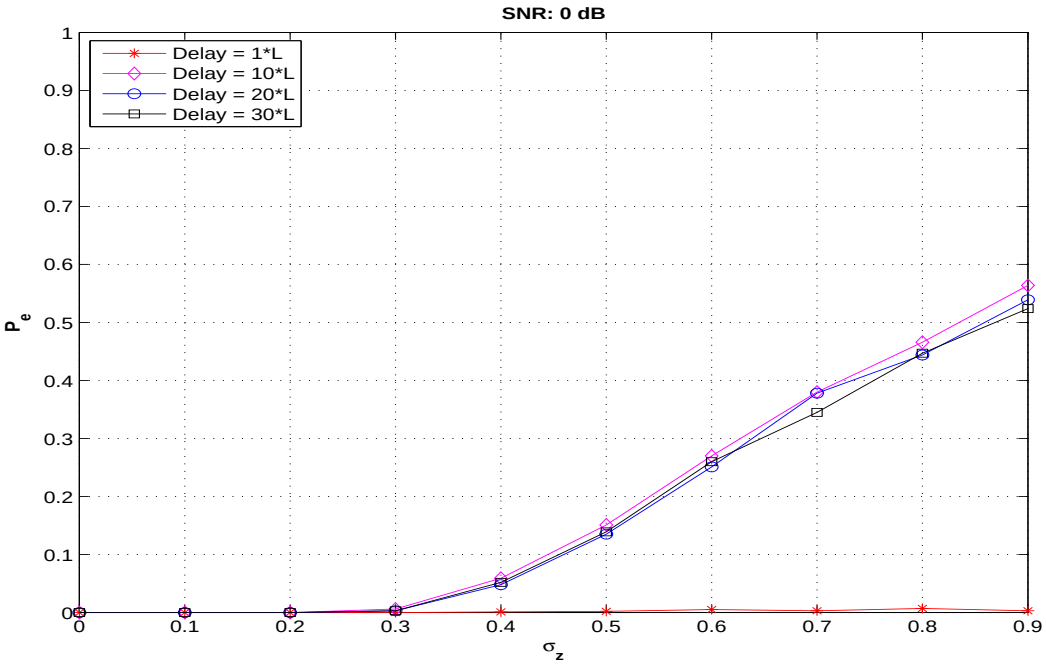

Figure F.3: Graph of $P_{e_{symbol}}$ vs. σ_z with no oversampling and $SNR = 0$ dB for the symbol boundary correlation results.

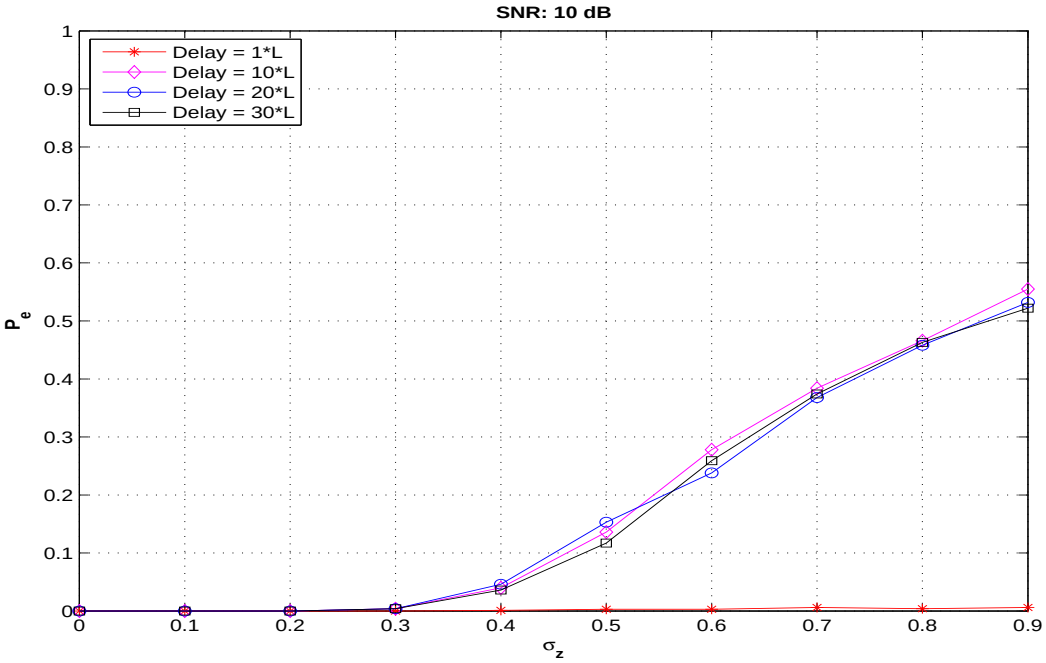

Figure F.4: Graph of $P_{e_{symbol}}$ vs. σ_z with no oversampling and $SNR = 10$ dB for the symbol boundary correlation results.

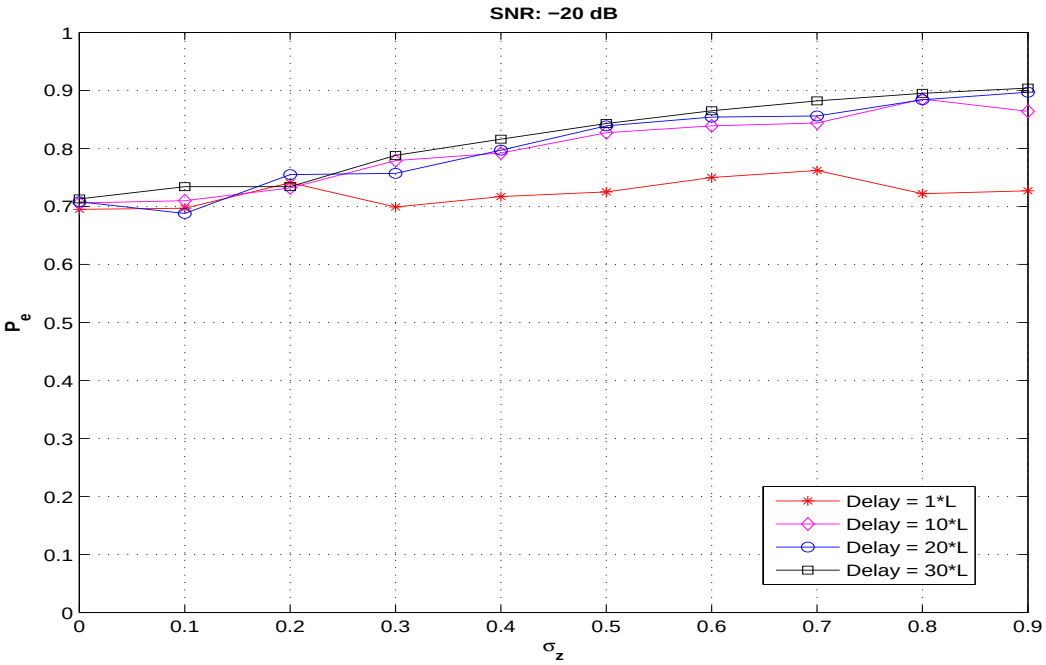

Figure F.5: Graph of $P_{e_{symbol}}$ vs. σ_z with 3× oversampling and $SNR =$ -20 dB for the symbol boundary correlation results.

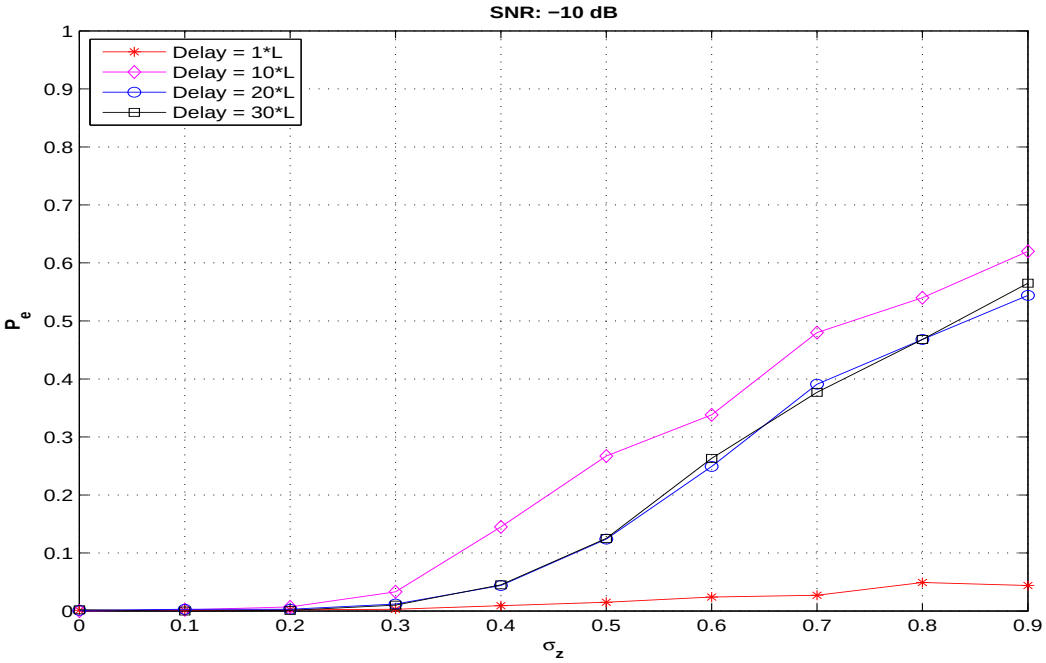

Figure F.6: Graph of $P_{e_{symbol}}$ vs. σ_z with 3× oversampling and SNR = -10 dB for the symbol boundary correlation results.

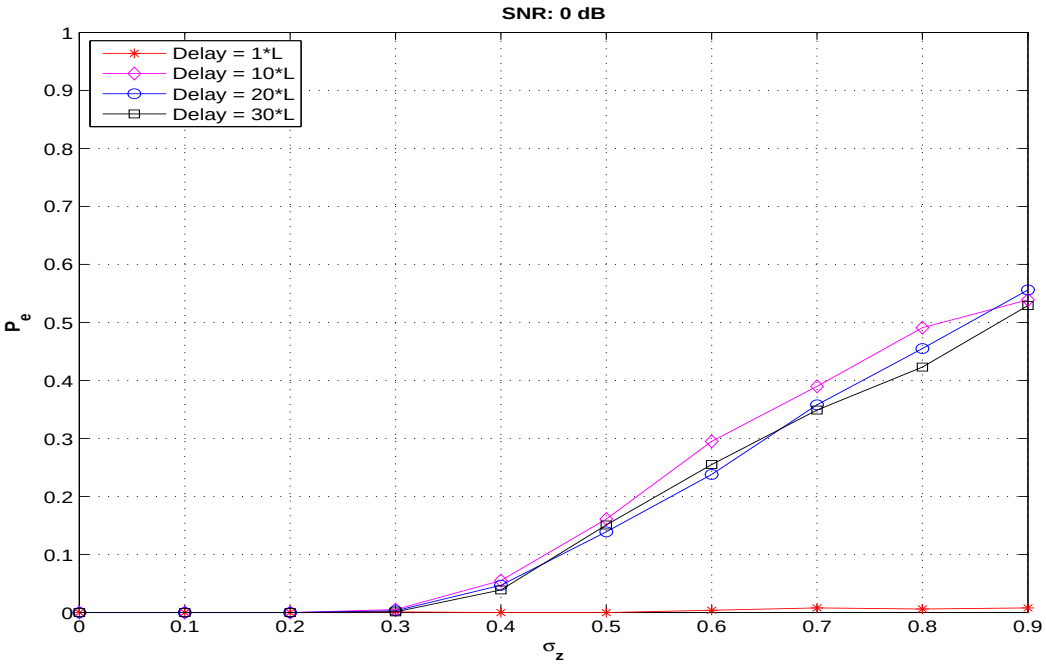

Figure F.7: Graph of $P_{e_{symbol}}$ vs. σ_z with 3× oversampling and $SNR = 0$ dB for the symbol boundary correlation results.

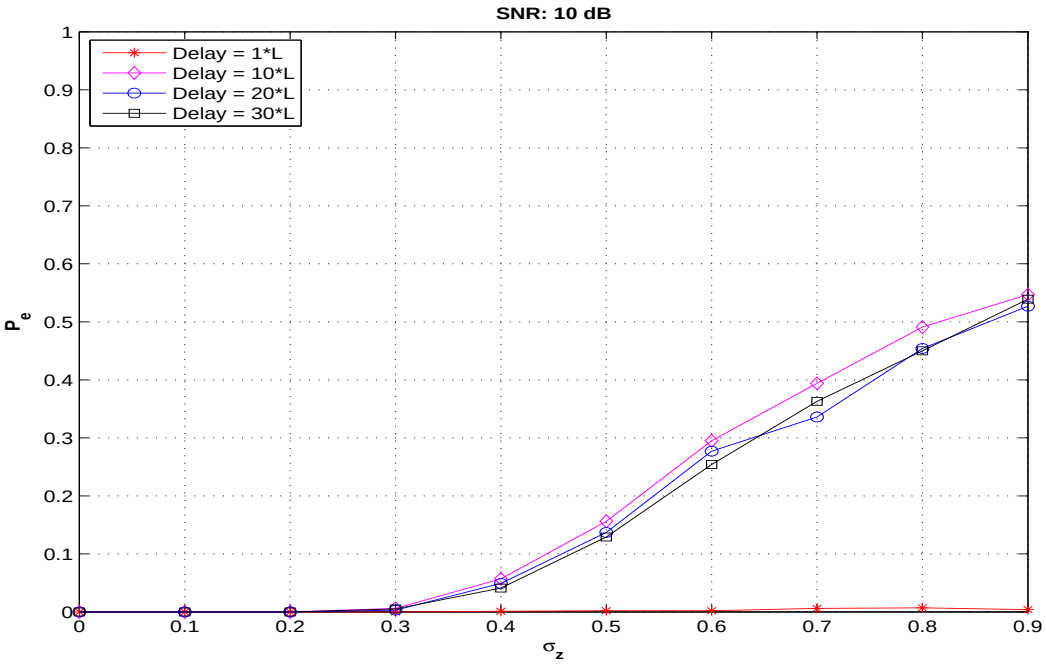

Figure F.8: Graph of $P_{e_{symbol}}$ vs. σ_z with $3\times$ oversampling and $SNR = 10$ dB for the symbol boundary correlation results.

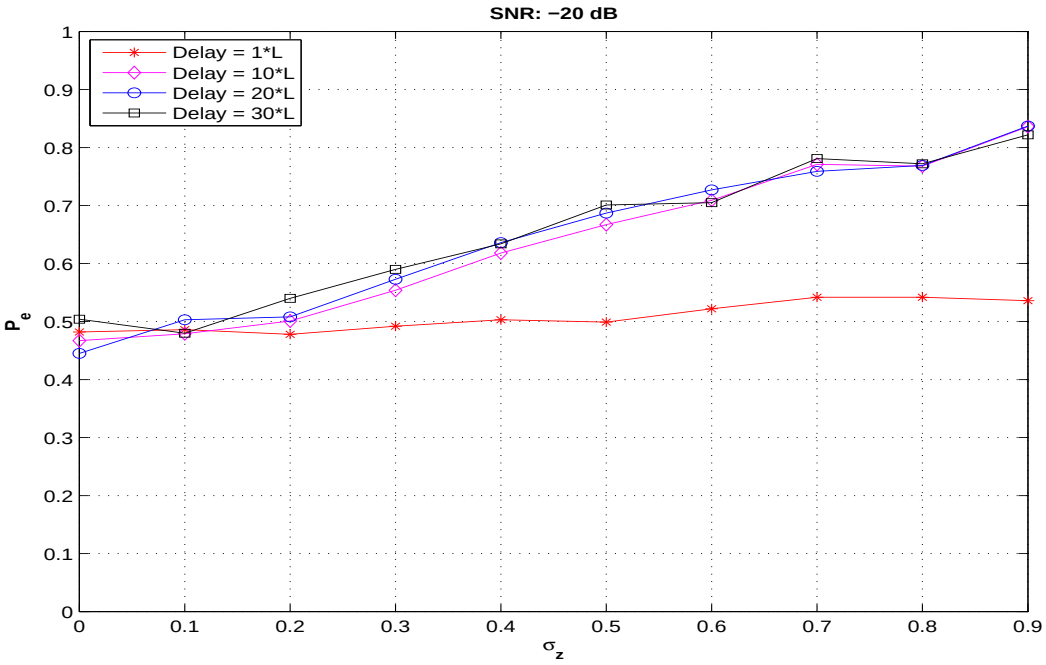

Figure F.9: Graph of $P_{e_{symbol}}$ vs. σ_z with $9\times$ oversampling and $SNR =$ -20 dB for the symbol boundary correlation results.

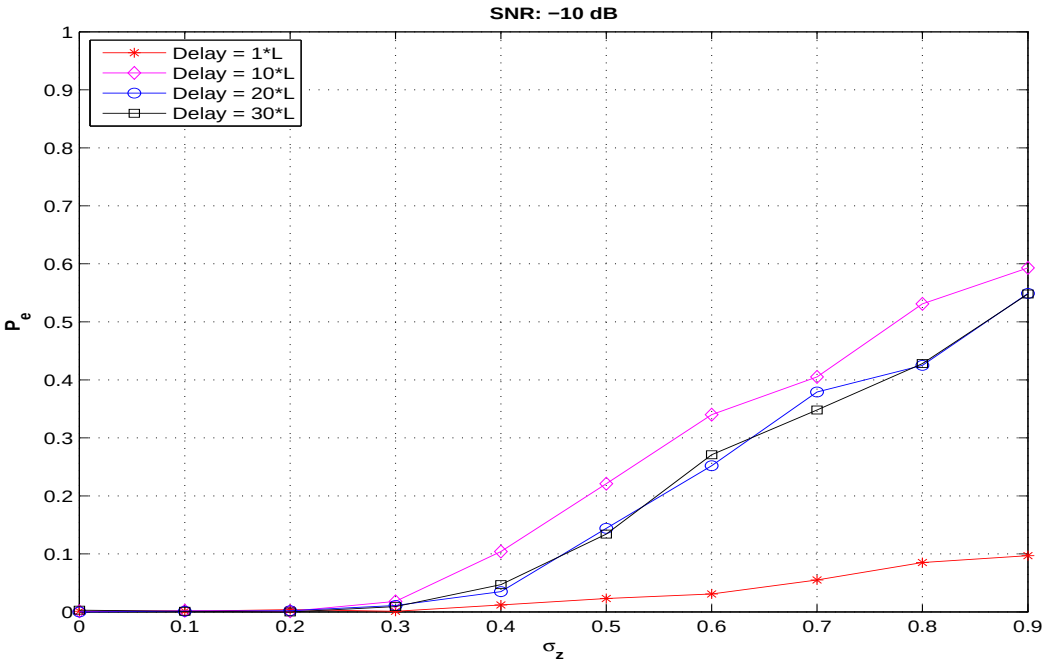

Figure F.10: Graph of $P_{e_{symbol}}$ vs. σ_z with 9× oversampling and SNR = -10 dB for the symbol boundary correlation results.

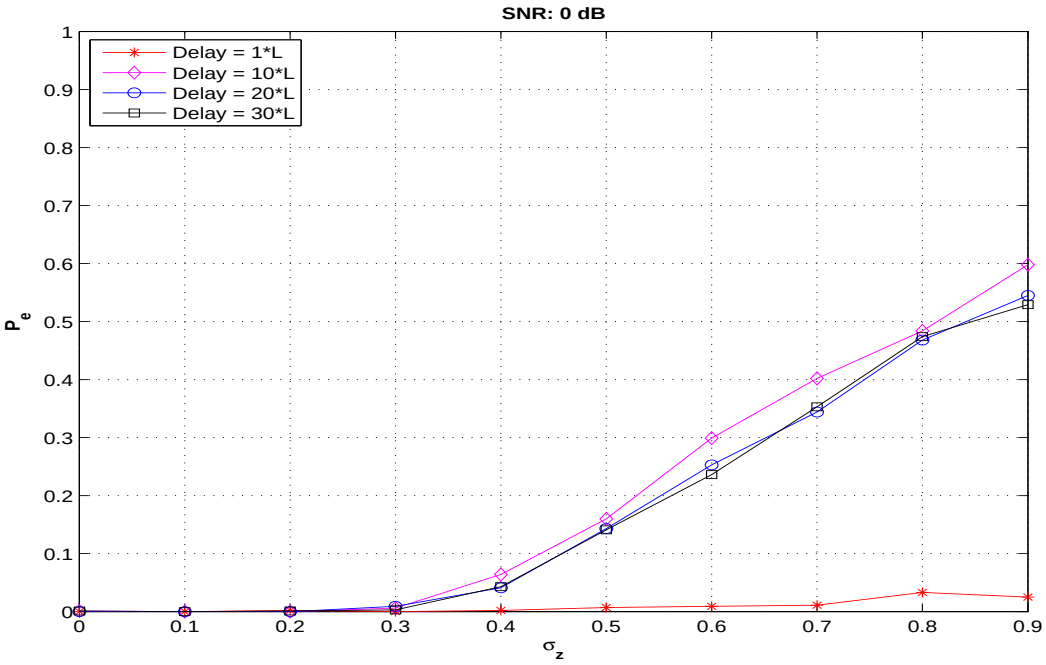

Figure F.11: Graph of $P_{e_{symbol}}$ vs. σ_z with 9× oversampling and $SNR = 0$ dB for the symbol boundary correlation results.

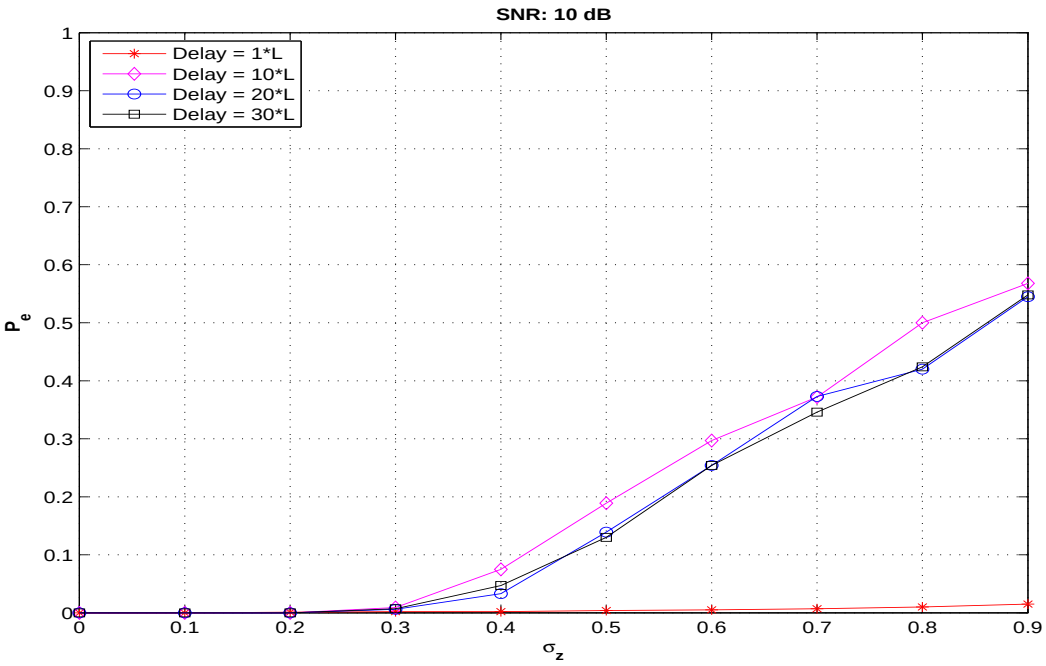

Figure F.12: Graph of $P_{e_{symbol}}$ vs. σ_z with 9× oversampling and $SNR = 10$ dB for the symbol boundary correlation results.

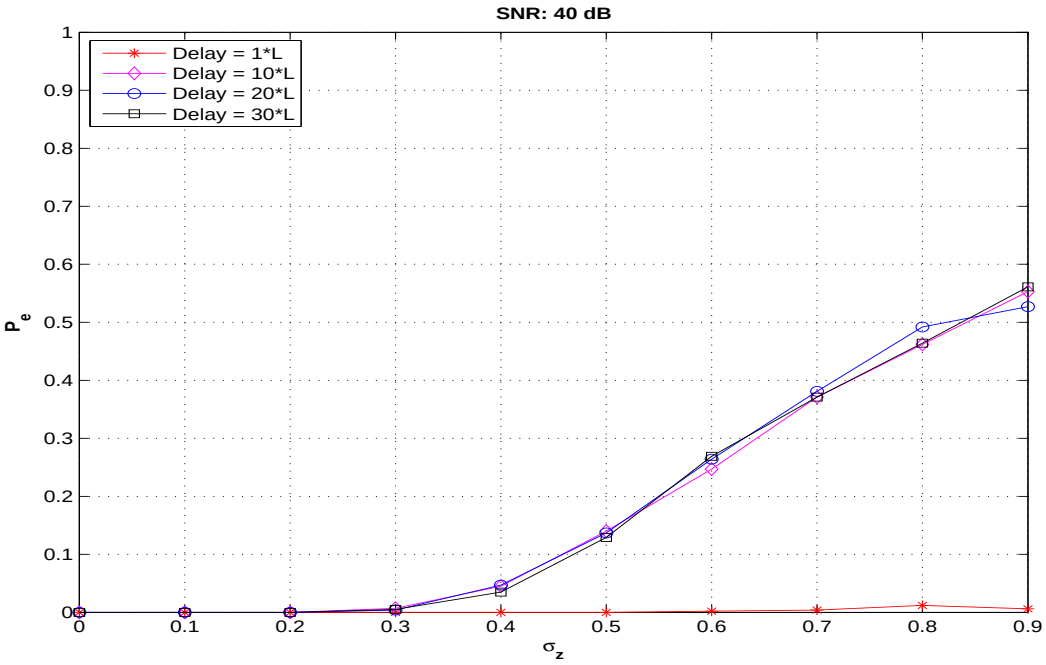

Figure F.13: Graph of $P_{e_{symbol}}$ vs. σ_z with no oversampling and $SNR = 40$ dB for the symbol boundary correlation results.

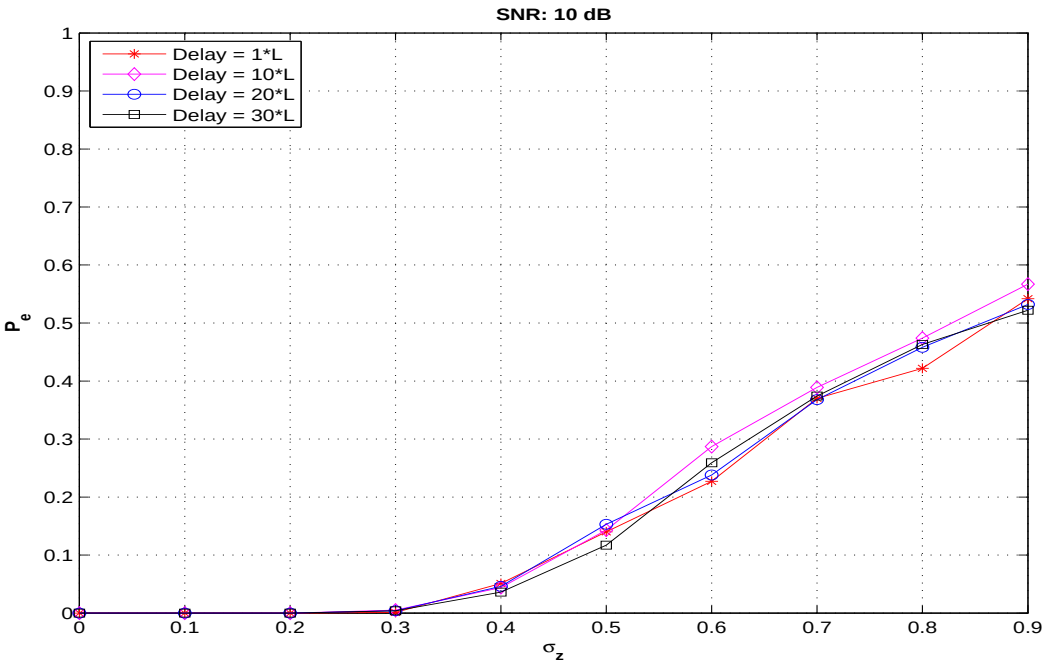

Figure F.14: Graph of $P_{e_{symbol}}$ vs. σ_z without the error threshold for the symbol boundary correlation results. The correlation peak must be exact to avoid registering an error.

Figures F.15 through F.20 show the $P_{e_{feature}}$ for the case of no oversampling and $K = 10$ symbols, Figures F.21 through F.24 show the results for $3\times$ oversampling, and Figures F.25 and F.28 show the results for $9\times$ oversampling. These simulations were run again with the window size increased to 100 symbols and the results are displayed in Figures F.29 through F.40. Also, Figure F.41 shows the performance of the mean compared to the mini-mean with no multipath, no oversampling, and window sizes of 10 and 100 symbols.

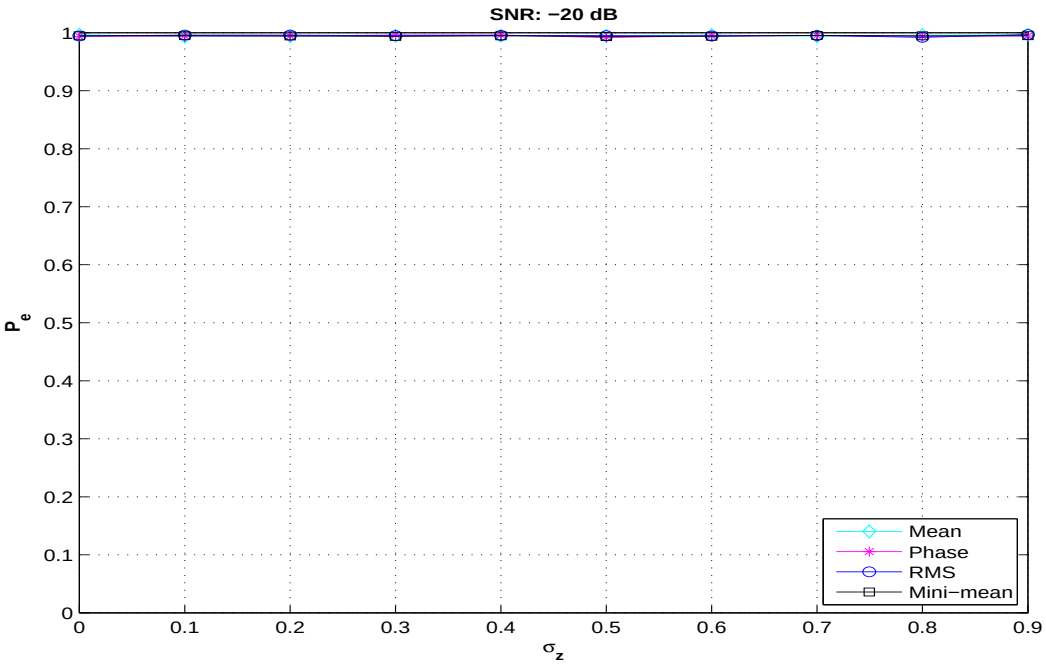

Figure F.15: Graph of $P_{e_{feature}}$ vs. σ_z with no oversampling, SNR = -20 dB, and $K = 10$ symbols for the feature correlation results.

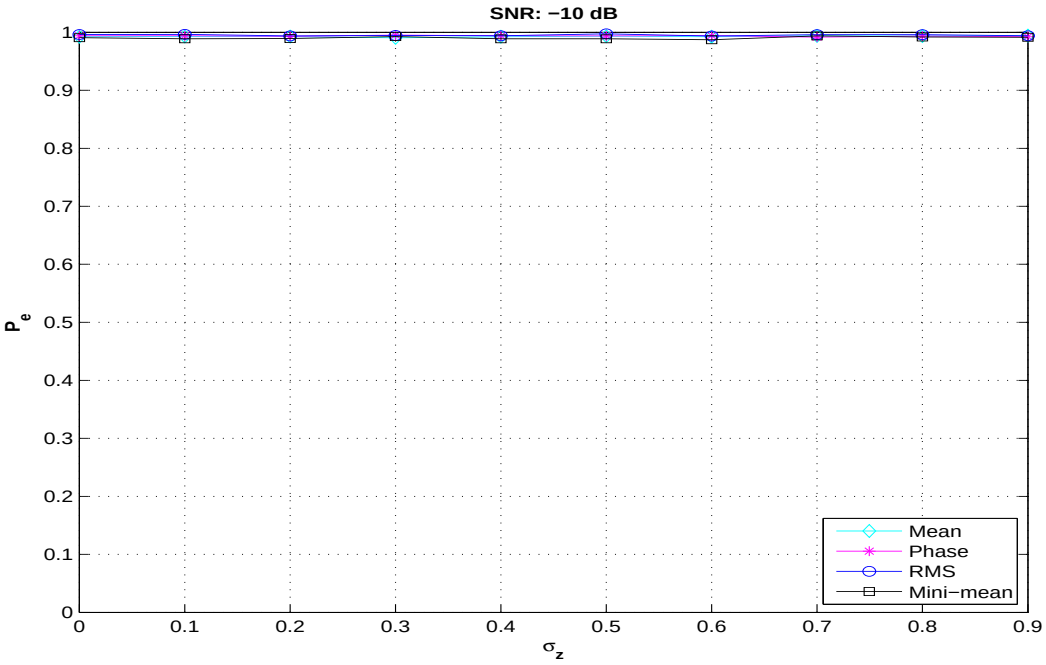

Figure F.16: Graph of $P_{e_{feature}}$ vs. σ_z with no oversampling, SNR = -10 dB, and $K = 10$ symbols for the feature correlation results.

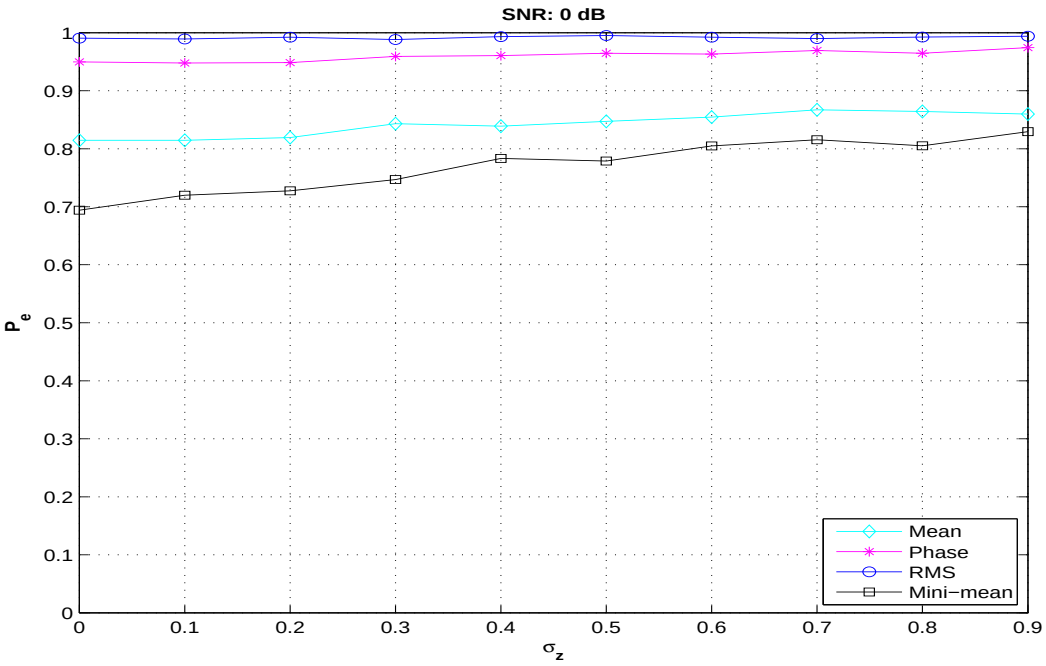

Figure F.17: Graph of $P_{e_{feature}}$ vs. σ_z with no oversampling, $SNR = 0$ dB, and $K = 10$ symbols for the feature correlation results.

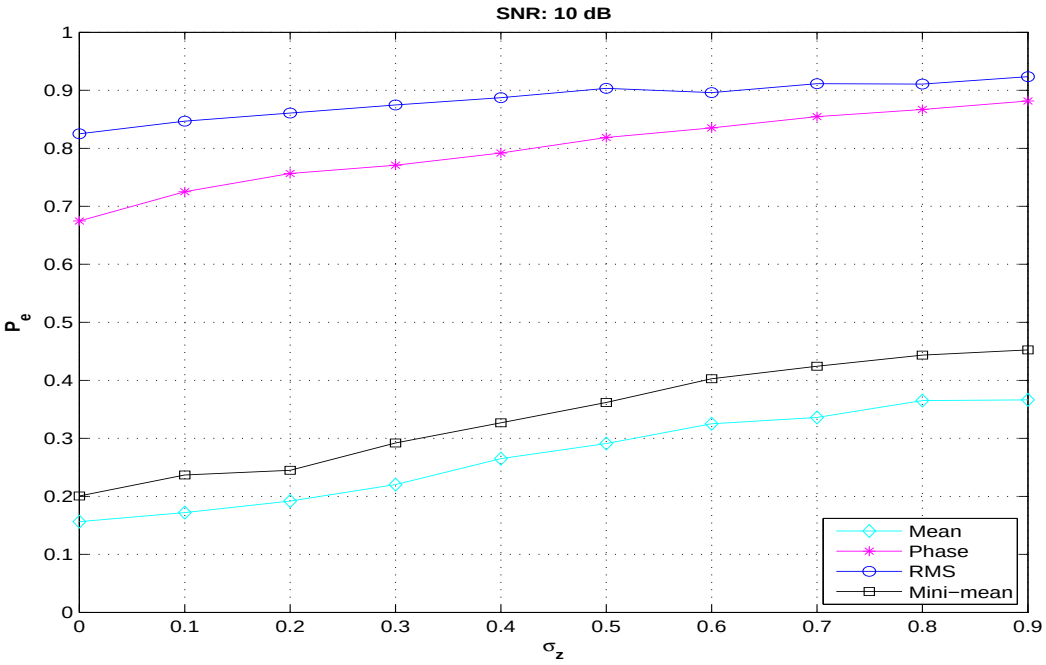

Figure F.18: Graph of $P_{e_{feature}}$ vs. σ_z with no oversampling, $SNR = 10$ dB, and $K = 10$ symbols for the feature correlation results.

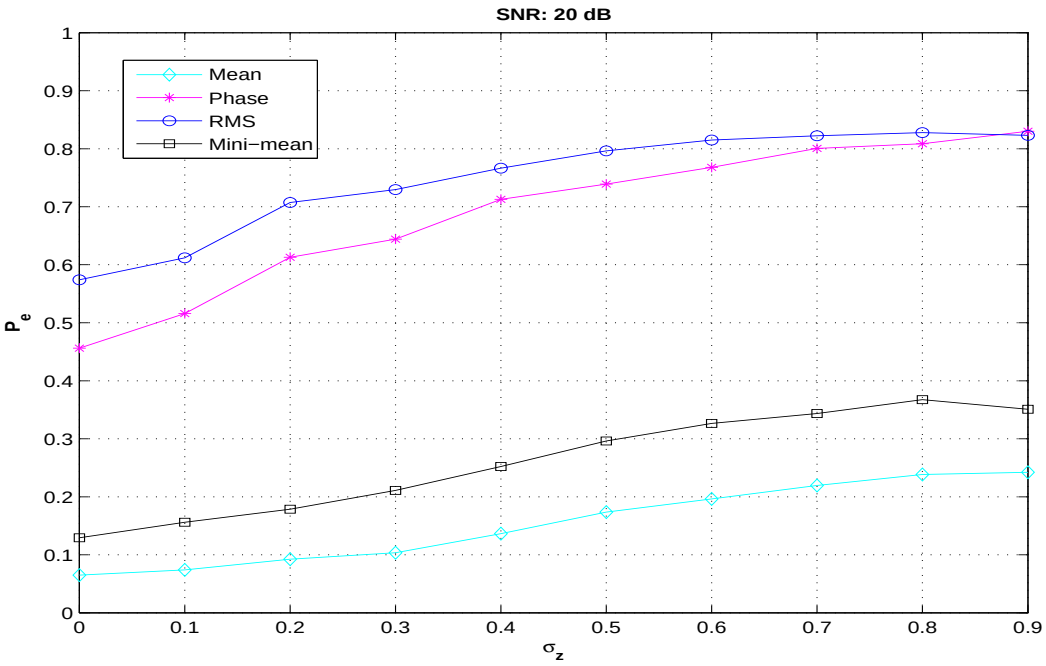

Figure F.19: Graph of $P_{e_{feature}}$ vs. σ_z with no oversampling, $SNR = 20$ dB, and $K = 10$ symbols for the feature correlation results.

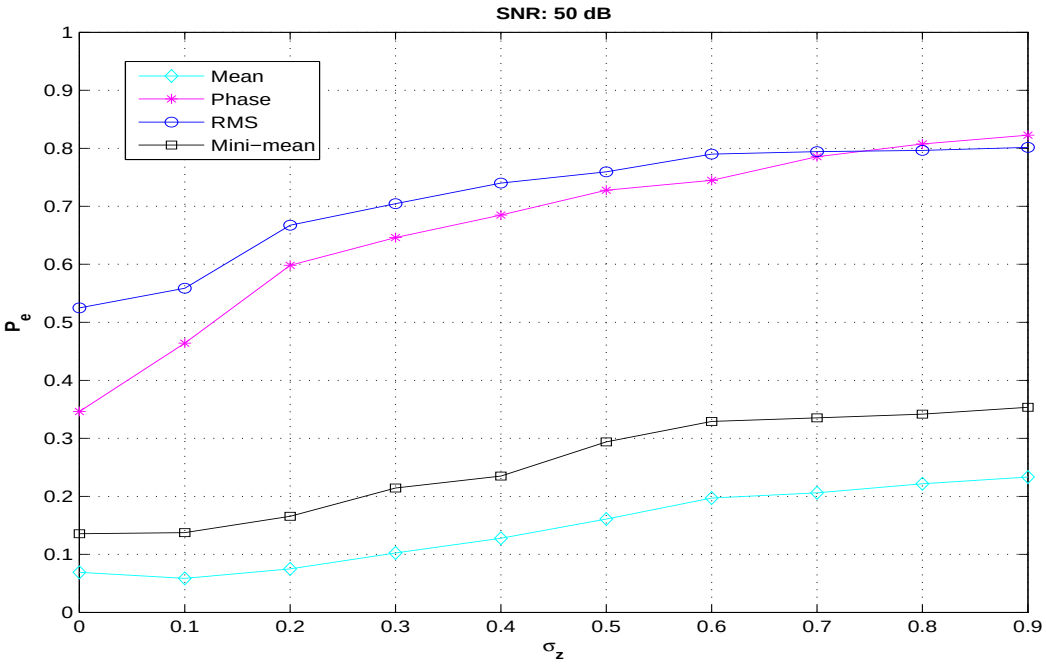

Figure F.20: Graph of $P_{e_{feature}}$ vs. σ_z with no oversampling, $SNR = 50$ dB, and $K = 10$ symbols for the feature correlation results.

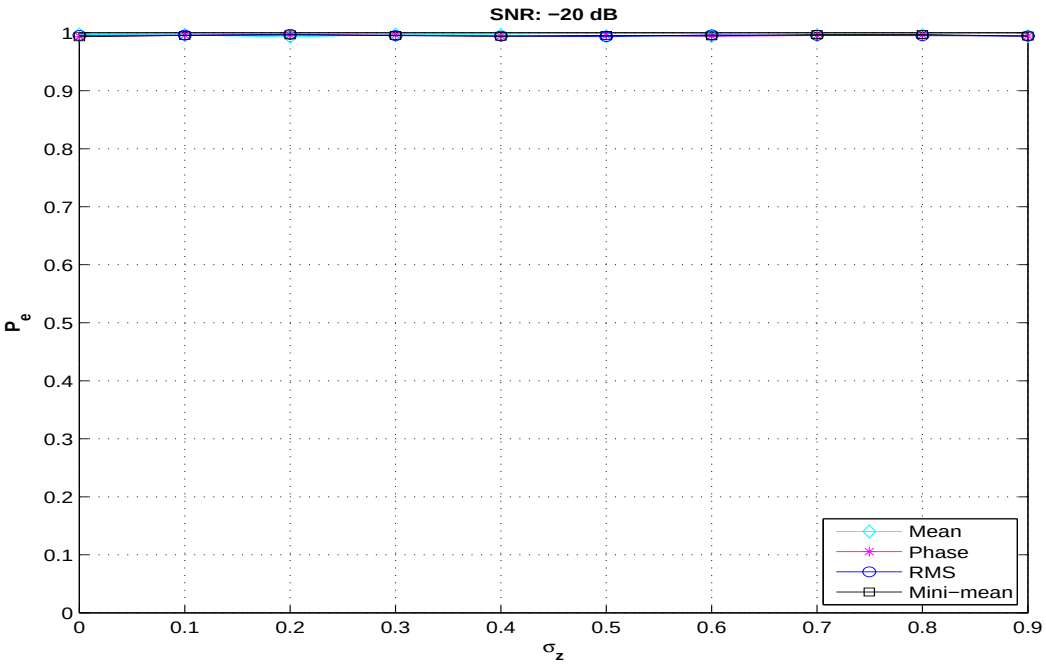

Figure F.21: Graph of $P_{e_{feature}}$ vs. σ_z with 3× oversampling, SNR = -20 dB, and $K = 10$ symbols for the feature correlation results.

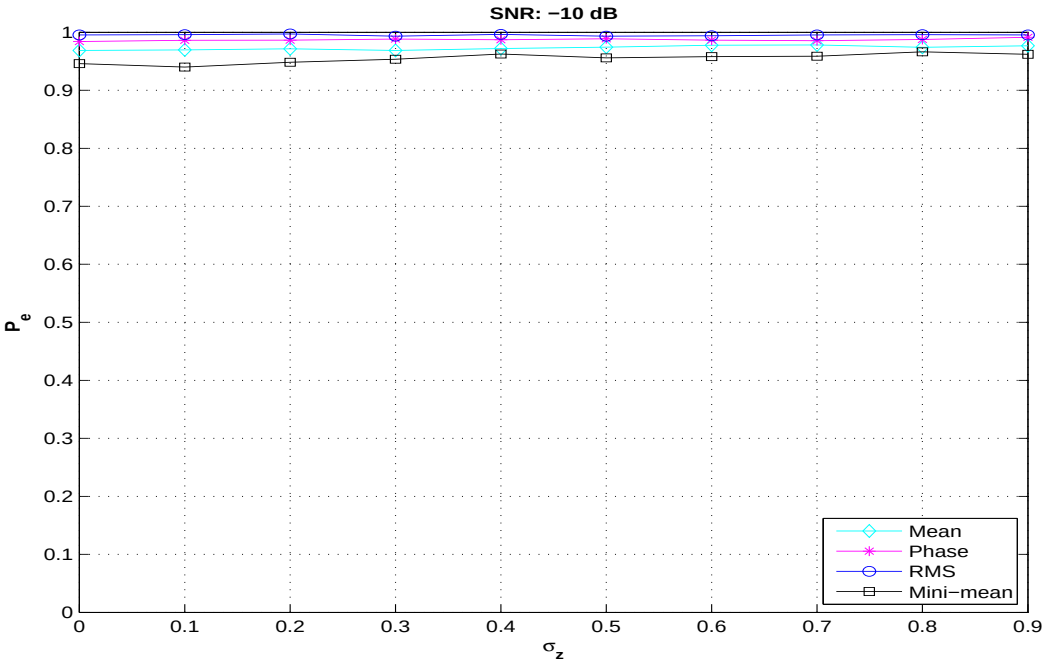

Figure F.22: Graph of $P_{e_{feature}}$ vs. σ_z with 3× oversampling, SNR = -10 dB, and $K = 10$ symbols for the feature correlation results.

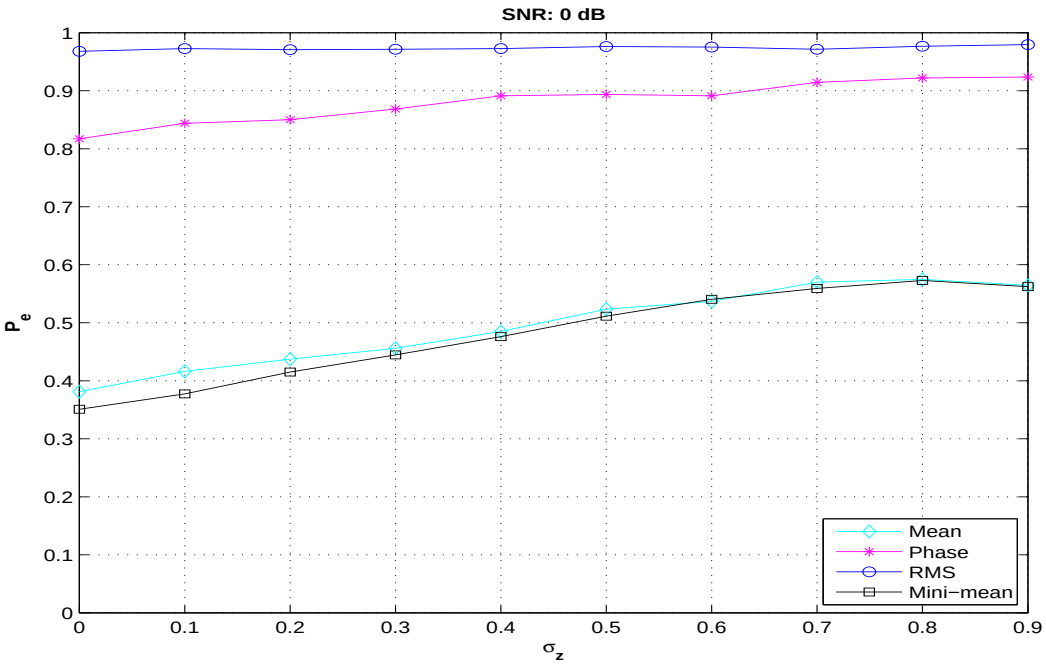

Figure F.23: Graph of $P_{e_{feature}}$ vs. σ_z with 3× oversampling, $SNR = 0$ dB, and $K = 10$ symbols for the feature correlation results.

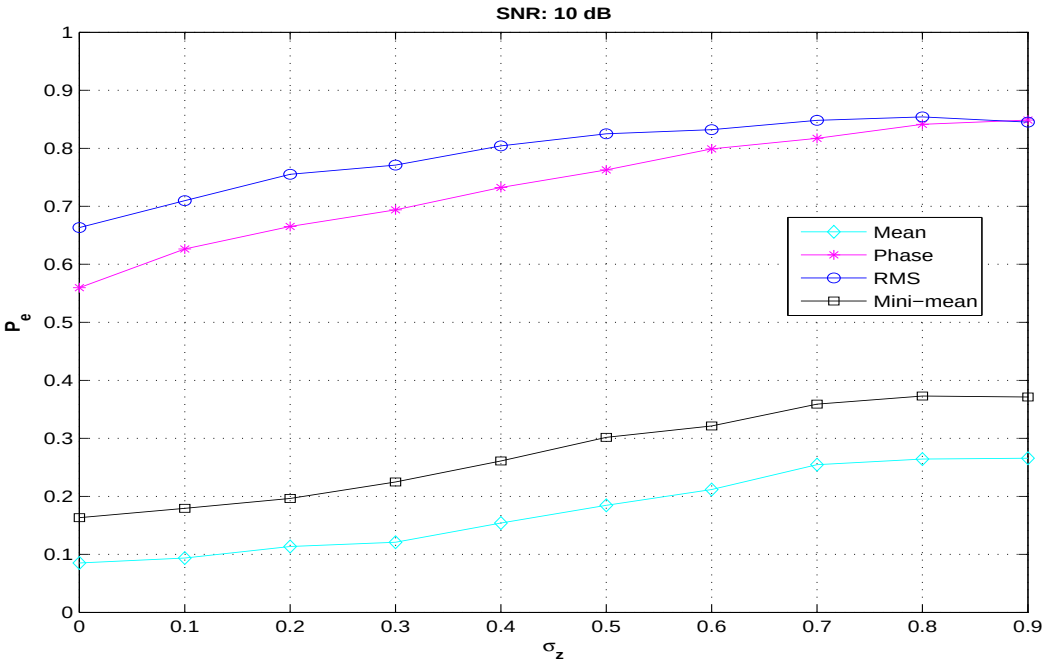

Figure F.24: Graph of $P_{e_{feature}}$ vs. σ_z with 3× oversampling, $SNR = 10$ dB, and $K = 10$ symbols for the feature correlation results.

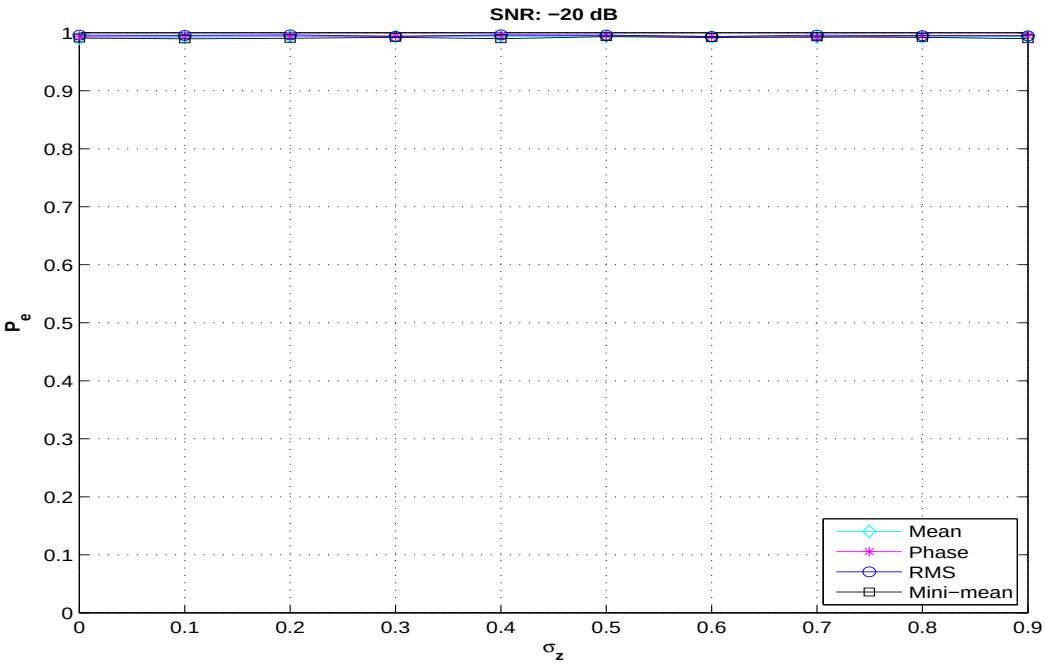

Figure F.25: Graph of $P_{e_{feature}}$ vs. σ_z with 9× oversampling, SNR = -20 dB, and $K = 10$ symbols for the feature correlation results.

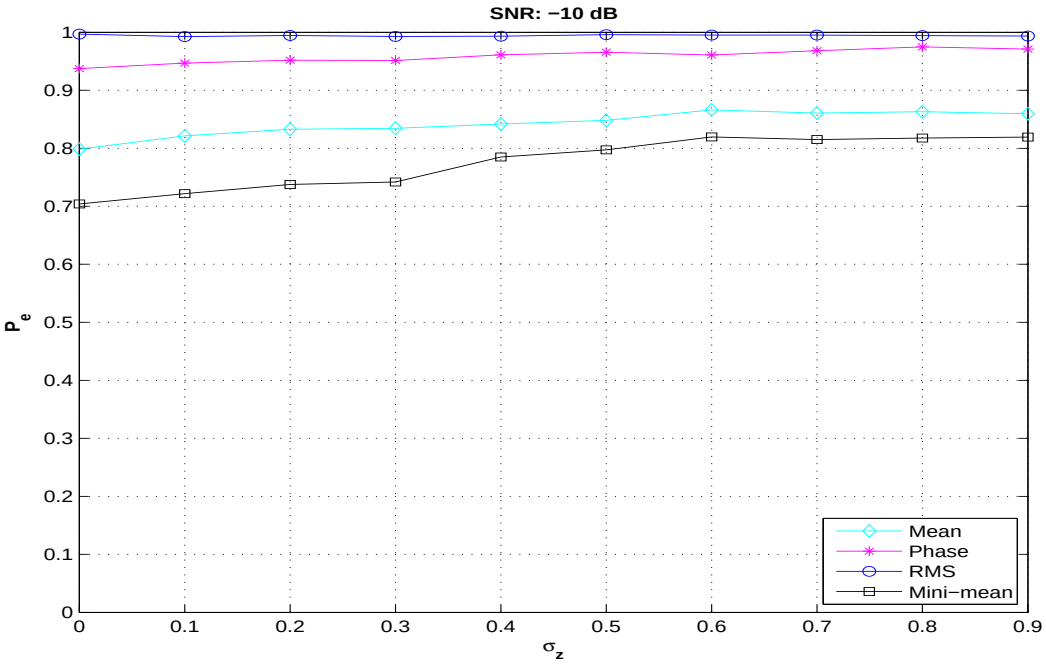

Figure F.26: Graph of $P_{e_{feature}}$ vs. σ_z with 9× oversampling, SNR = -10 dB, and $K = 10$ symbols for the feature correlation results.

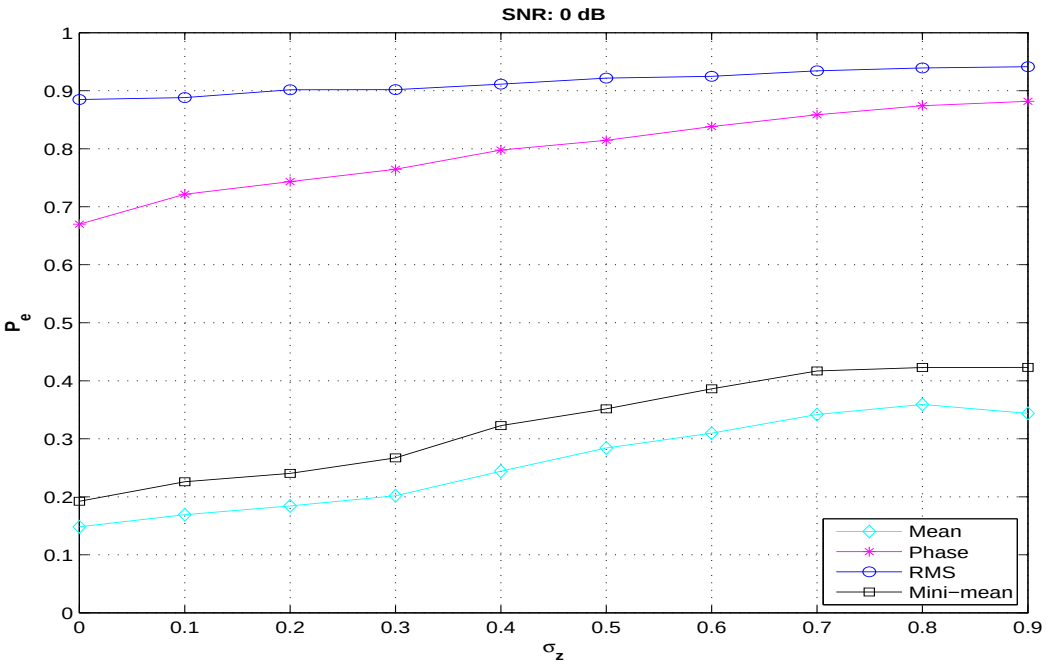

Figure F.27: Graph of $P_{e_{feature}}$ vs. σ_z with 9× oversampling, $SNR = 0$ dB, and $K = 10$ symbols for the feature correlation results.

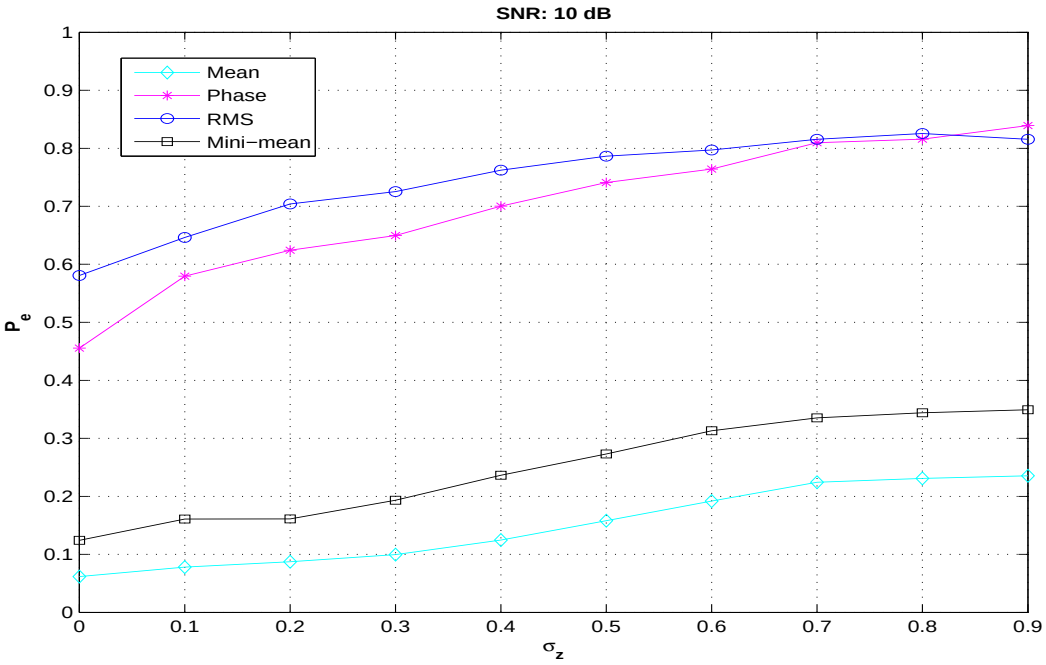

Figure F.28: Graph of $P_{e_{feature}}$ vs. σ_z with 9× oversampling, $SNR = 10$ dB, and $K = 10$ symbols for the feature correlation results.

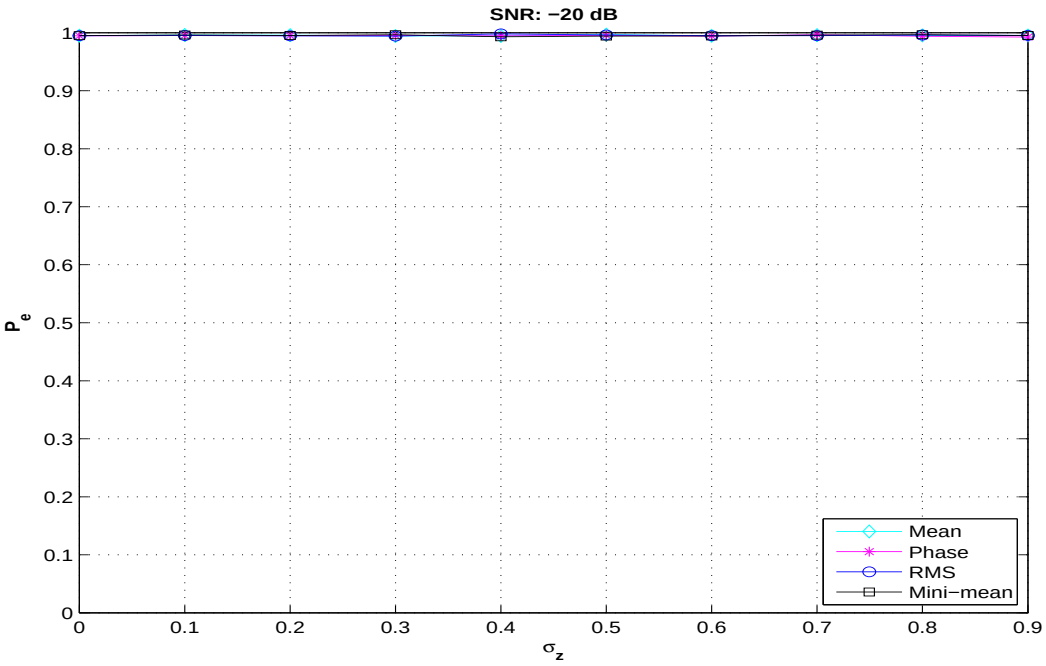

Figure F.29: Graph of $P_{e_{feature}}$ vs. σ_z with no oversampling, SNR = -20 dB, and $K = 100$ symbols for the feature correlation results.

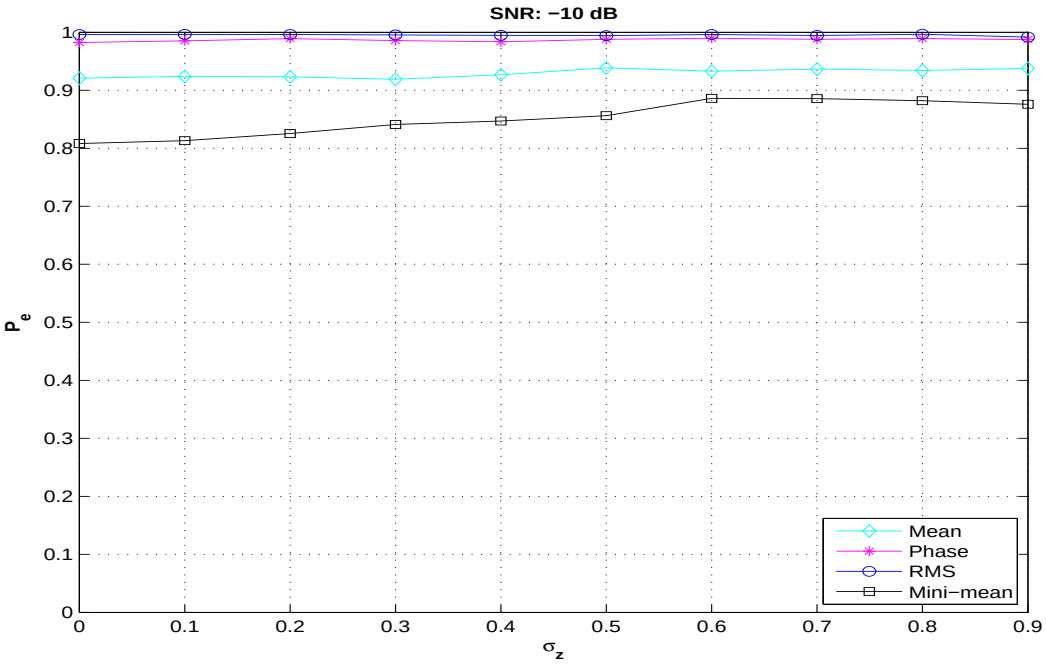

Figure F.30: Graph of $P_{e_{feature}}$ vs. σ_z with no oversampling, SNR = -10 dB, and $K = 100$ symbols for the feature correlation results.

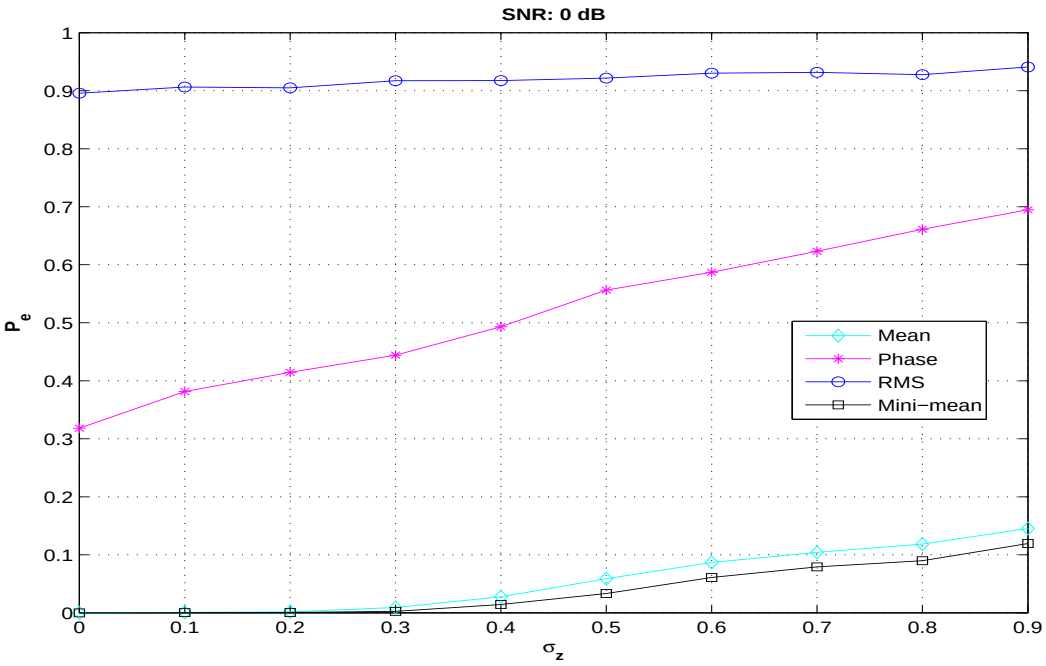

Figure F.31: Graph of $P_{e_{feature}}$ vs. σ_z with no oversampling, $SNR = 0$ dB, and $K = 100$ symbols for the feature correlation results.

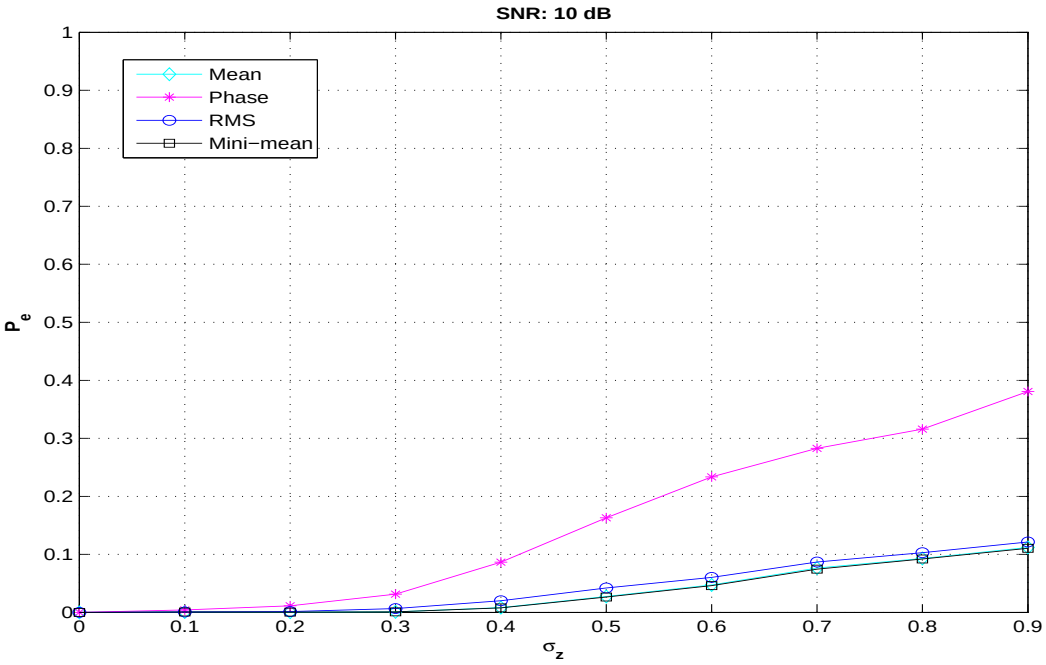

Figure F.32: Graph of $P_{e_{feature}}$ vs. σ_z with no oversampling, $SNR = 10$ dB, and $K = 100$ symbols for the feature correlation results.

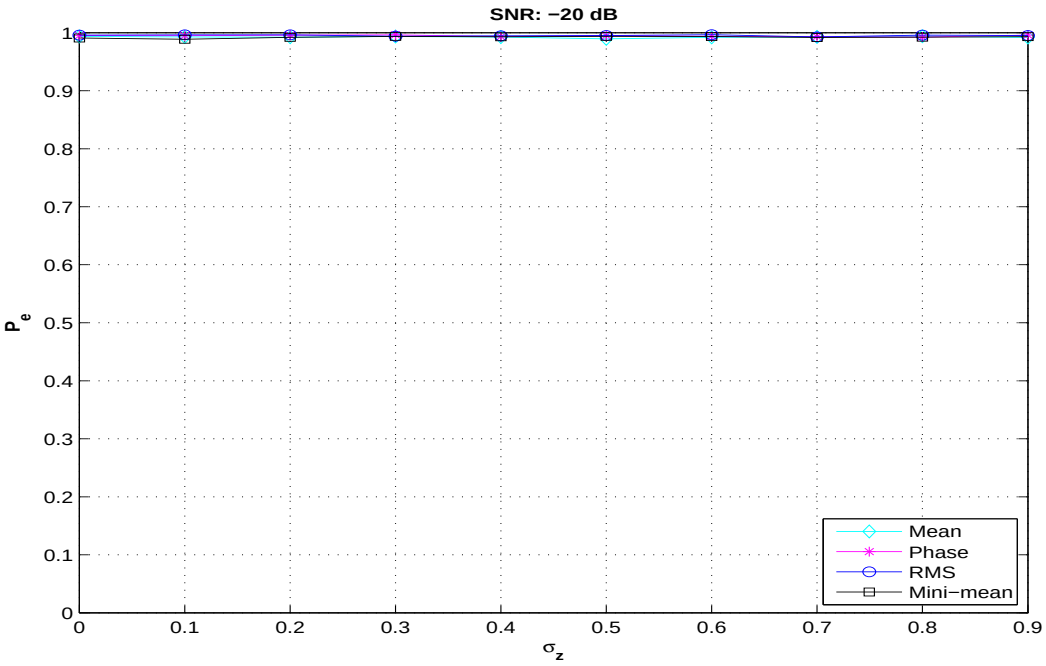

Figure F.33: Graph of $P_{e_{feature}}$ vs. σ_z with 3× oversampling, SNR = -20 dB, and $K = 100$ symbols for the feature correlation results.

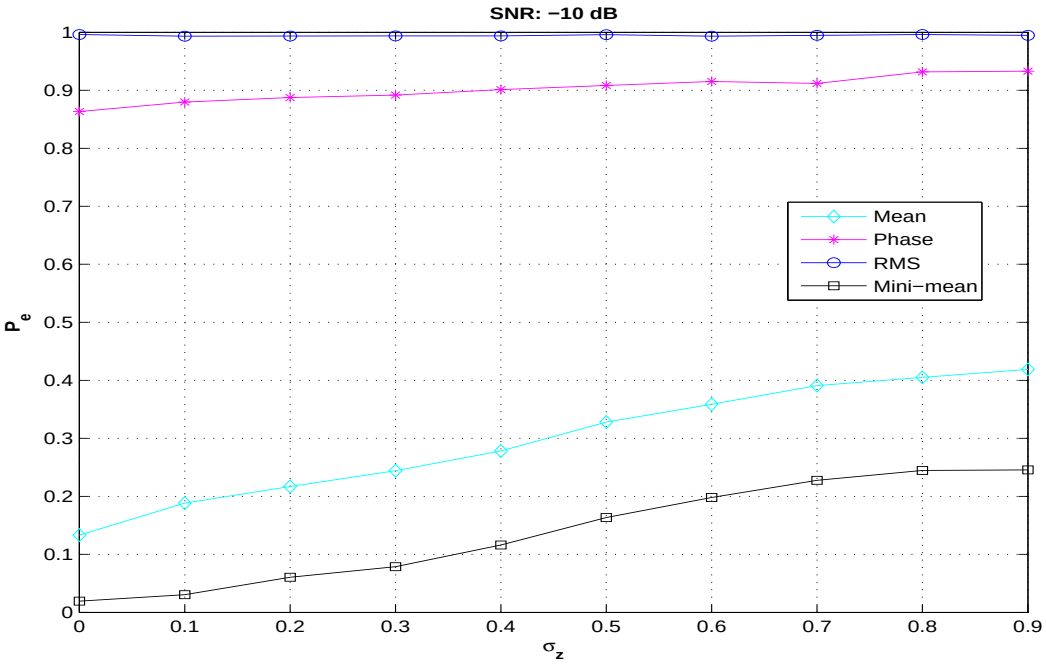

Figure F.34: Graph of $P_{e_{feature}}$ vs. σ_z with 3× oversampling, SNR = -10 dB, and $K = 100$ symbols for the feature correlation results.

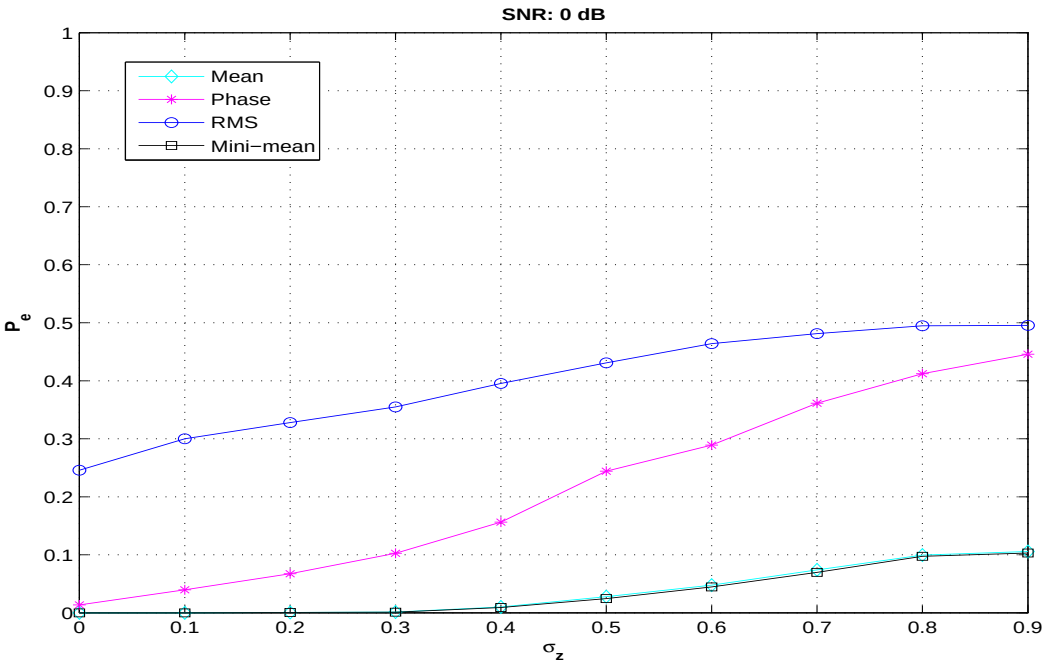

Figure F.35: Graph of $P_{e_{feature}}$ vs. σ_z with 3× oversampling, $SNR = 0$ dB, and $K = 100$ symbols for the feature correlation results.

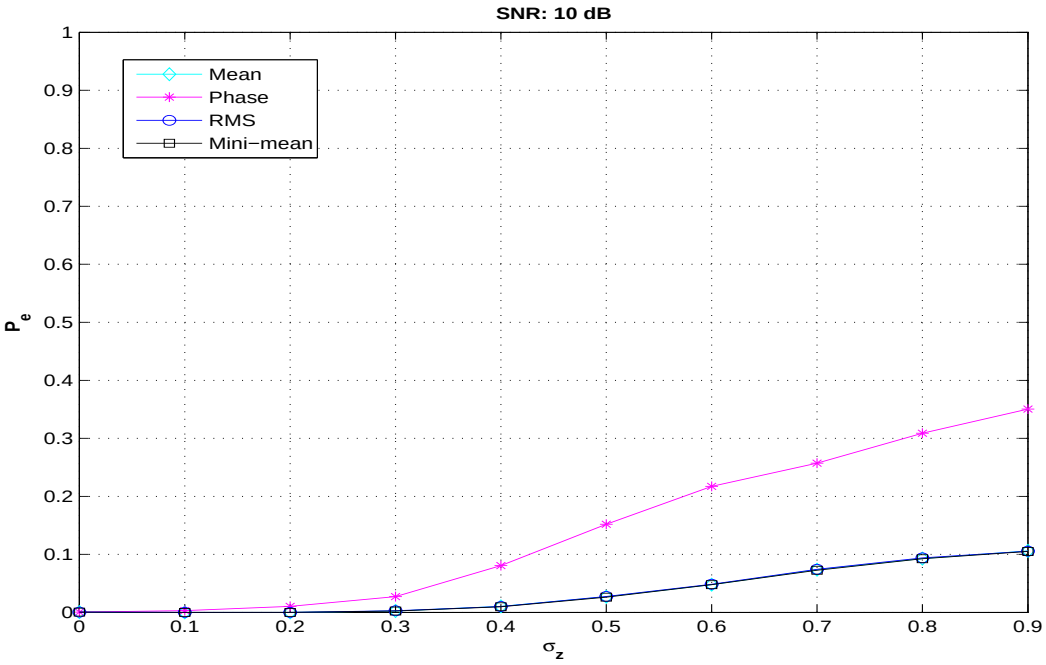

Figure F.36: Graph of $P_{e_{feature}}$ vs. σ_z with 3× oversampling, $SNR = 10$ dB, and $K = 100$ symbols for the feature correlation results.

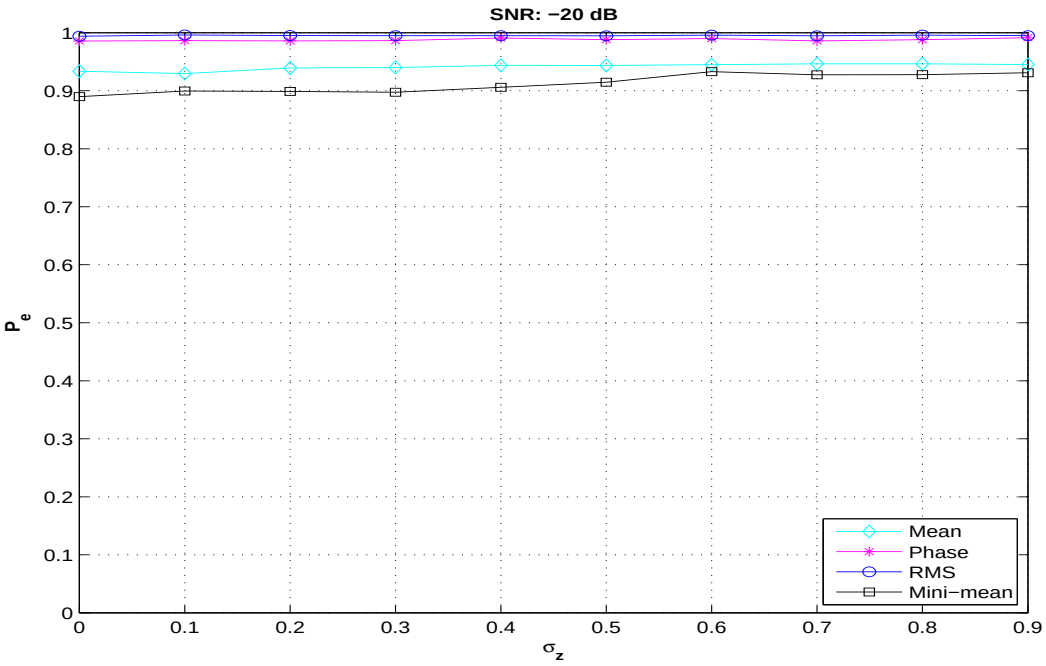

Figure F.37: Graph of $P_{e_{feature}}$ vs. σ_z with 9× oversampling, SNR = -20 dB, and $K = 100$ symbols for the feature correlation results.

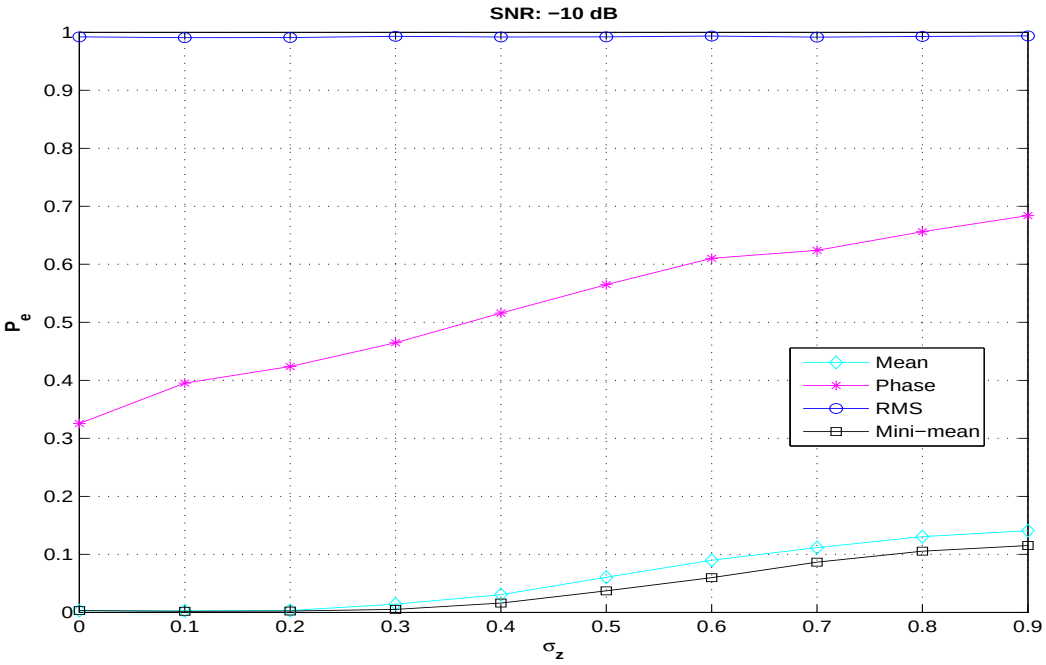

Figure F.38: Graph of $P_{e_{feature}}$ vs. σ_z with 9× oversampling, SNR = -10 dB, and $K = 100$ symbols for the feature correlation results.

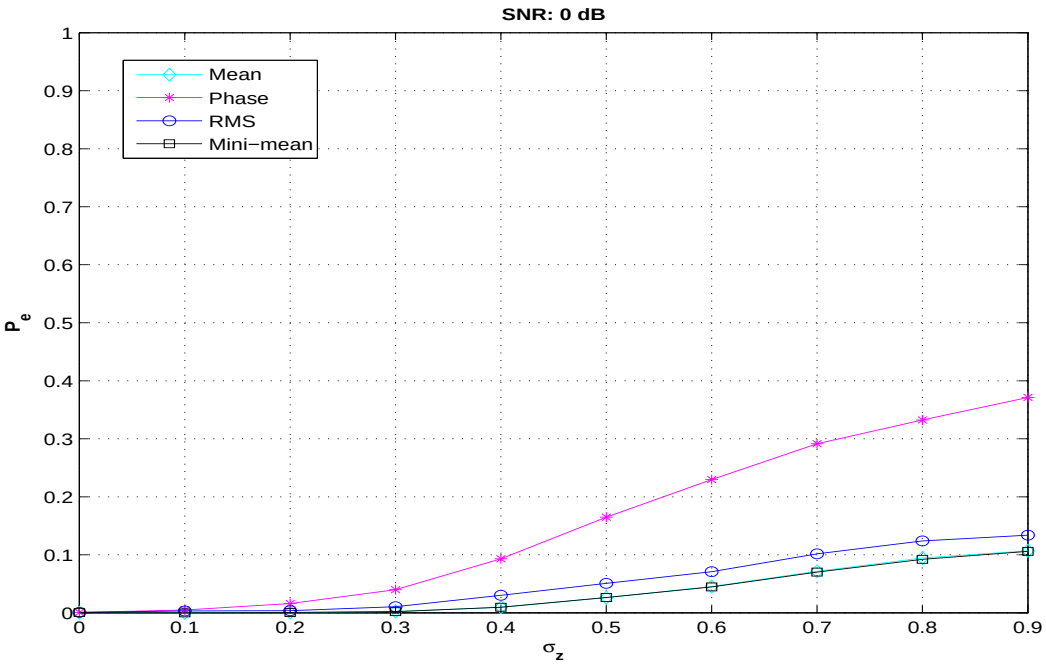

Figure F.39: Graph of $P_{e_{feature}}$ vs. σ_z with 9× oversampling, $SNR = 0$ dB, and $K = 100$ symbols for the feature correlation results.

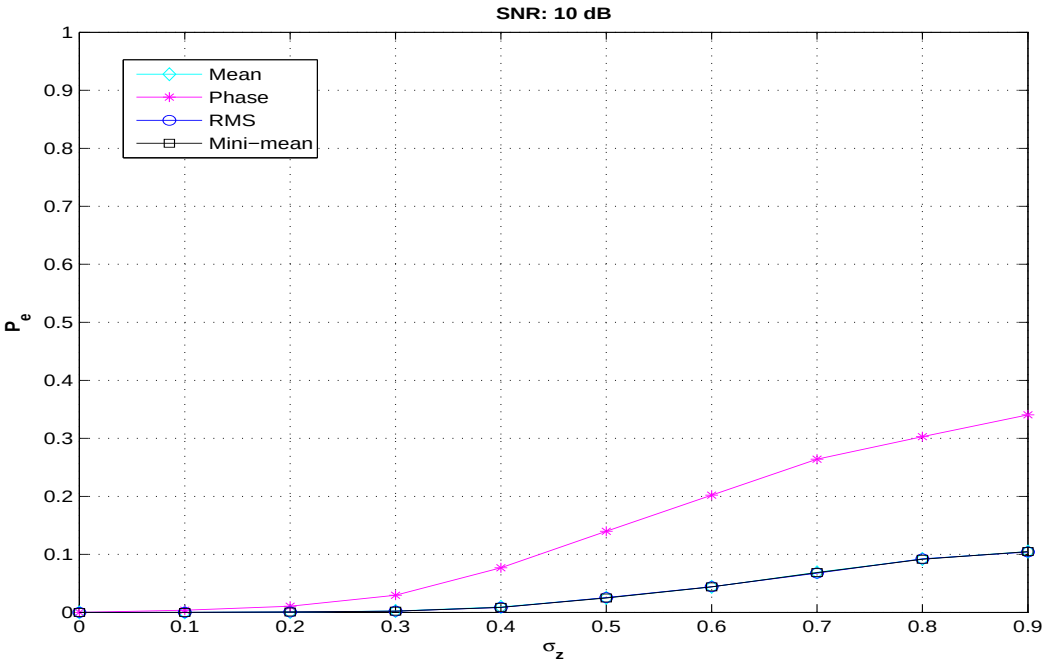

Figure F.40: Graph of $P_{e_{feature}}$ vs. σ_z with 9× oversampling, $SNR = 10$ dB, and $K = 100$ symbols for the feature correlation results.

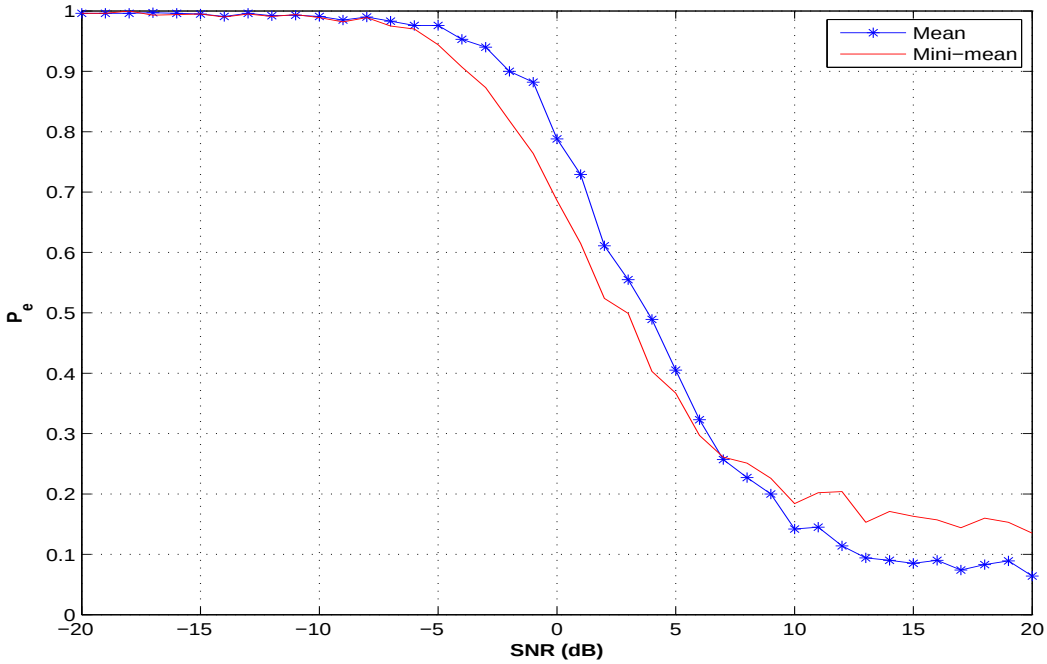

(a) Window Size of 10 Symbols.

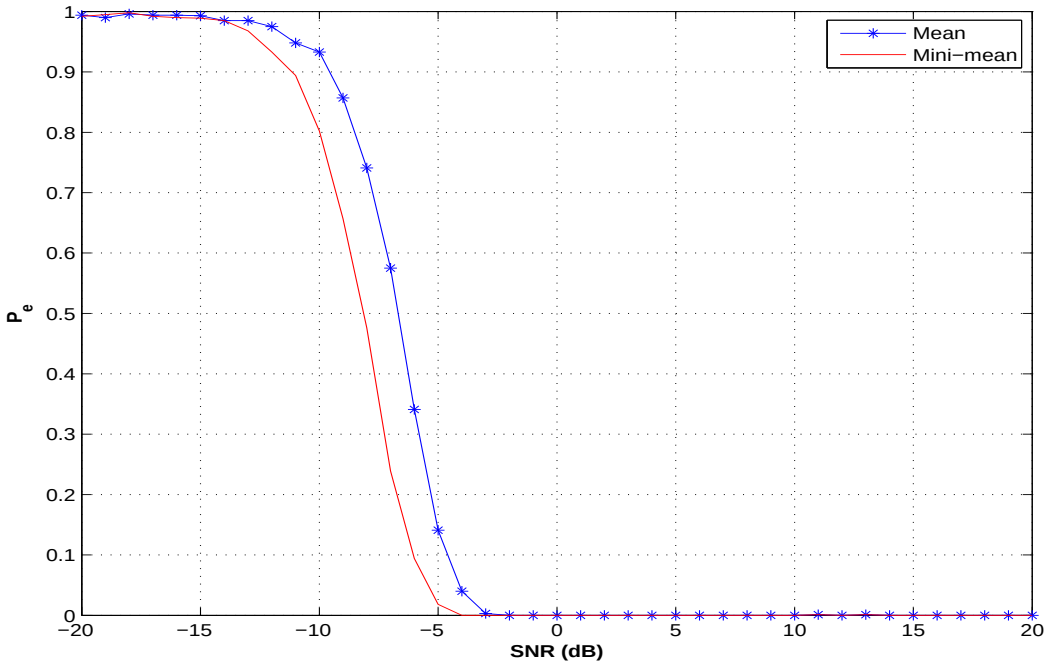

(b) Window Size of 100 Symbols

Figure F.41: Graphs of $P_{e_{feature}}$ vs. SNR comparing Mean vs. Mini-mean with no oversampling, no multipath, and window sizes of: a) 10 symbols and b) 100 symbols.

Bibliography

1. Federation of American Scientists. "Military Space Programs: Navigation". 1997. [Online]. Available at `http://www.fas.org/spp/military/program/nav/overview.htm`. [Accessed 8-November-2007].

2. Raquet, John F. "EENG 533: Navigation Using the GPS", Spring Quarter 2007. Course notes, School of Engineering and Management, Air Force Institute of Technology, Wright-Patterson AFB OH.

3. Velotta, Jamie S. *Navigation Using Orthogonal Frequency Division Multiplexed Signals of Opportunity*. Master's thesis, Graduate School of Engineering, Air Force Institute of Technology (AETC), Wright-Patterson AFB OH, September 2007. AFIT/GE/ENG/07-31.

4. Sandell, Magnus, Jan-Jaap van de Beek, and Per Ola Borjesson. "Timing and Frequency Synchronization in OFDM Systems Using the Cyclic Prefix". *Proceedings of the International Symposium on Synchronization*, 16–19. Essen, Germany, December 1995.

5. Eggert, Ryan J. *Evaluating the Navigation Potential of the National Television System Committee Broadcast Signal*. Master's thesis, Graduate School of Engineering, Air Force Institute of Technology (AETC), Wright-Patterson AFB OH, March 2004. AFIT/GE/ENG/04-08.

6. Misra, Pratap and Per Enge. *GLOBAL POSITIONING SYSTEM: Signals, Measurements and Performance*. Ganga-Jamuna Press, Lincoln, MA, second edition, 2006.

7. Wikipedia. "GEE". Wikimedia Foundation Inc., 2007. `http://en.wikipedia.org/wiki/GEE_(navigation)`.

8. McEllroy, Johnathan A. *Navigation Using Signals of Opportunity in the AM Transmission Band*. Master's thesis, Graduate School of Engineering, Air Force Institute of Technology (AETC), Wright-Patterson AFB OH, March 2006. AFIT/GE/ENG/06-04.

9. Rabinowitz, Matthew and James J. Spilker Jr. "A New Positioning System Using Television Synchronization Signals". *IEEE Transactions on Broadcasting*, volume 51, 51–61. March 2005.

10. Kim, Bryan S. *Evaluating the Correlation Characteristics of Arbitrary AM and FM Radio Signals for the Purpose of Navigation*. Master's thesis, Graduate School of Engineering, Air Force Institute of Technology (AETC), Wright-Patterson AFB OH, March 2006. AFIT/GE/ENG/06-08.

11. Hall, Timothy. *Radiolocation Using AM Broadcast Signals*. Ph.d. dissertation, Massachusetts Institute of Technology, Cambridge, MA, September 2002.

12. Hall, Timothy D. "Radiolocation Using AM Broadcast Signals: The Role of Signal Propagation Irregularities". *Position Location and Navigation Symposium*, 752–761. April 2004.

13. Cyganski, David, John Orr, and William R. Michalson. "A Multi-Carrier Technique for Precision Geolocation for Indoor/Multipath Envrironments". *Proceedings of the Institute of Navigation GPS/GNSS*. Portland, OR, September 2003.

14. Li, X. et al. "Indoor Geolocation using OFDM Signals in HIPERLAN/2 Wireless LANs". *Proceedings of the 11th IEEE International Symposium on Personal, Indoor, and Mobile Radio Communications (PIMRC)*, volume 2, pp. 1449–1453. London, UK, Sept. 18-21 2000.

15. van Nee, Richard and Ramjee Prasad. *OFDM for Wireless Multimedia Communications*. Artech House Publishers, Boston, MA, 2000.

16. Institute of Electrical and Electronics Engineers. Piscataway, NJ. *IEEE Std 802.11a-1999(R2003), IEEE Standard for Information technology-Telecommunication and information exchange between systems-Local and metropolitan area networks-Specific requirements, Part 11: Wireless LAN Medium Access Control (MAC) and Physical Layer (PHY) Specifications: High-speed Physical layer in the 5 GHz Band*. 1999, Revised 2003.

17. Sklar, Bernard. *Digital Communications Fundamentals and Applications*. Prentice Hall PTR, Upper Saddle River, NJ, second edition, 2001.

18. Bahai, Ahmad, Burton Saltzberg and Mustafa Ergen. *Multi-Carrier Digital Communications Theory and Applications of OFDM*. Springer Science+Business Media, Inc., New York, NY, second edition, 2004.

19. European Telecommunications Standards Institute, "Digital Video Broadcasting (DVB): Implementation guidelines for DVB terrestrial services; transmission aspects," European Telecommunications Standards Institute, ETSI TR-101-190, 1997. [Online]. Available at `http://www.etsi.org`. [Accessed 25-September-2007].

20. Oppenheim, Alan V., Ronald W. Schafer, and John R. Buck. *Discrete-Time Signal Processing*. Prentice Hall, New Jersey, second edition edition, 1999.

21. Henkel, Werner et al. "The Cyclic Prefix of OFDM/DMT - An Analysis". *2002 International Zurich Seminar on Broadband Communications. Access, Transmission, Networking.*, 22.1 – 22.3. Institute of Electrical and Electronics Engineers (IEEE), Zurich, Switzerland, February 2002.

22. Proakis, John G. *Digital Communications*. McGraw-Hill, Boston, MA, third edition edition, 1995.

23. Richard Martin, Jamie Velotta and John Raquet. "Bandwidth Efficient Cooperative TDOA Computation for Multicarrier Signals of Opportunity", October 2007. Submitted to IEEE Trans. on Signal Processing.

REPORT DOCUMENTATION PAGE

Form Approved
OMB No. 0704–0188

1. REPORT DATE *(DD–MM–YYYY)*	2. REPORT TYPE	3. DATES COVERED *(From — To)*
27–03–2008	Master's Thesis	Mar 2006 - Mar 2008

4. TITLE AND SUBTITLE

Effects of Multipath and Oversampling on Navigation Using Orthogonal Frequency Division Multiplexed Signals of Opportunity

5a. CONTRACT NUMBER

5b. GRANT NUMBER

5c. PROGRAM ELEMENT NUMBER

6. AUTHOR(S)

Christopher M. Schexnayder

5d. PROJECT NUMBER

5e. TASK NUMBER

5f. WORK UNIT NUMBER

7. PERFORMING ORGANIZATION NAME(S) AND ADDRESS(ES)

Air Force Institute of Technology
Graduate School of Engineering and Management (AFIT/EN)
2950 Hobson Way
WPAFB OH 45433-7765

8. PERFORMING ORGANIZATION REPORT NUMBER

AFIT/GE/ENG/08-25

9. SPONSORING / MONITORING AGENCY NAME(S) AND ADDRESS(ES)

Jacob L. Campbell
AFRL/RYRN, AFMC
2241 Avionics Circle, Bldg 620
Wright-Patterson AFB, OH, 45433-7301
DSN: 785-6127 x4154
jacob.campbell@wpafb.af.mil

10. SPONSOR/MONITOR'S ACRONYM(S)

11. SPONSOR/MONITOR'S REPORT NUMBER(S)

12. DISTRIBUTION / AVAILABILITY STATEMENT

APPROVED FOR PUBLIC RELEASE; DISTRIBUTION UNLIMITED.

13. SUPPLEMENTARY NOTES

14. ABSTRACT

This research exploits the Orthogonal Frequency Division Multiplexed (OFDM) signal for the purpose of navigation. A transmitter and reference receiver, both at known locations, and a mobile receiver at an unknown location were used to conduct simulations of a transmitted OFDM signal in a Rayleigh-distributed multipath environment. The OFDM signal structure was exploited by using the cyclic prefix in a correlation process to find the first symbol boundary in each received signal. Statistical features about each symbol is calculated at both receivers and then correlated to find the difference in arrival times. The simulations were run for varying levels of multipath, and also for oversampling in an effort to gain more accurate results by decreasing the sample period. Results show that oversampling the signal only slightly reduces errors in the symbol boundary correlation process, while multipath has a significant impact on the performance of both correlation processes. It was also found that increasing the window size significantly improved the performance of the feature correlator and yielded promising results even in the presence of high multipath environments.

15. SUBJECT TERMS

Orthogonal Frequency Division Multiplex, Signals of Opportunity, Time Difference of Arrival, Rayleigh Fading, Oversampling

16. SECURITY CLASSIFICATION OF:			17. LIMITATION OF ABSTRACT	18. NUMBER OF PAGES	19a. NAME OF RESPONSIBLE PERSON
a. REPORT	b. ABSTRACT	c. THIS PAGE			John F. Raquet, Civ, USAF (AFIT/ENG)
U	U	U	UU	124	19b. TELEPHONE NUMBER *(include area code)* (937)255–3636 x4580 jraquet@afit.af.mil